UNIVERSITÀ
DEGLI STUDI
DI PADOVA

SCUOLA DI DOTTORATO DI RICERCA IN TERRITORIO AMBIENTE RISORSE E SALUTE

INDIRIZZO: IDRONOMIA AMBIENTALE

CICLO XXV

A FRAMEWORK FOR THE ANALYSIS OF THE INFLUENCE OF RAINFALL SPATIAL ORGANIZATION AND BASIN MORPHOLOGY ON FLOOD RESPONSE

Direttore della Scuola : Ch.mo Prof. Mario Aristide Lenzi

Coordinatore d'indirizzo: Ch.mo Prof. Mario Aristide Lenzi

Supervisore :Ch.mo Prof. Marco Borga

Dottorando : Davide Zoccatelli

Abstract

This work describes the derivation of a set of statistics, termed *spatial moments of catchment rainfall*, that quantify the dependence between rainfall spatial organization, basin morphology and runoff response. These statistics describe the spatial rainfall organisation in terms of concentration and dispersion along the flow distance coordinate. These statistics were derived starting from an analytical framework, and related with the statistical moments of the flood hydrograph. From *spatial moments* we also created an index quantifying *catchment scale storm velocity*. This index measures the overall movement of the rainfall system over the catchment, reflecting the filtering effect of its morphology. We also extended *spatial moments* to the hillslope system, developing a framework to evaluate the relevance of hillslope and channel propagation in the flood response to spatially variable rainfall fields. Data from six flash floods occurred in Europe between 2002 and 2007 are used to evaluate the information provided by the framework. High resolution radar rainfall fields and a distributed hydrologic model are employed to examine how effective are these statistics in describing the degree of spatial rainfall organisation, which is important for runoff modelling. The size of the study catchments ranges between 36 to 2586 km^2. The analysis reported here shows that spatial moments of catchment rainfall can be effectively employed to isolate and describe the features of rainfall spatial organization which have significant impact on runoff simulation. Rainfall distribution was observed to play an important role in catchments as small as 50 km^2. The description timing error was further improved by the inclusion in the framework of hillslope propagation. This development allows to compare scenarios of hillslope conditions, to evaluate the sensitivity of single basins or the effect of catchment scale. The analysis of catchment scale storm velocity showed a nonlinear dependence with basin scale. The values of velocity observed were however rather moderate, in spite of the strong kinematic characteristics of individual storm elements, and did not play a relevant effect on the flood analyzed.

Sommario

Questo lavoro presenta una serie di statistici, denominati "momenti spaziali di pioggia a scala di bacino", che permettono di quantificare la relazione tra l'organizzazione spaziale della pioggia, la morfologia del bacino e la forma dell'idrogramma di piena. Tali statistici descrivono la posizione e la dispersione della pioggia su un assegnato bacino idrografico. La trattazione include la derivazione di una serie di relazioni che consentono di stabilire un rapporto fra detti statistici di pioggia ed i momenti temporali dell'onda di piena. La formulazione complessiva del lavoro consente di isolare e quantificare l'effetto della variabilità spaziale della pioggia sulla struttura della risposta di piena, e di creare un indice di velocità del sistema di pioggia. Questo indice considera l'iterazione tra morfologia del bacino e spostamento della pioggia, quantificando l'influenza sull'idrogramma. I momenti spaziali stati poi ampliati alla propagazione su versante, sviluppando degli statistici per valutare l'importanza della propagazione di canale e di versante sulla risposta nella riposta di un bacino ad una pioggia distribuita. Dati relativi a sei eventi estremi di piena improvvisa verificatisi in diverse regioni Europee sono utilizzati per illustrare il significato degli statistici e le relazioni con la forma dell'idrogramma. Stime di pioggia da radar ed un modello idrologico distribuito sono utilizzati per valutare l'efficacia degli statistici nel cogliere l'organizzazione delle piogge che ha un'influenza sulla simulazione di piena. Lo studio mostra che i *momenti spaziali di pioggia a scala di bacino* possono essere efficaci nel cogliere questa organizzazione. Nelle piene improvvise analizzate la distribuzione della pioggia ha un effetto rilevante anche per bacini di circa 50 km^2. La descrizione dell'errore temporale dell'idrogramma è ulteriormente migliorata dalla considerazione dell'effetto del versante. Questo sviluppo permette inoltre di confrontare condizioni di versante diverse, di valutare la suscettibilità di singoli bacini o l'effetto in relazione alla scala dei bacini. L'analisi della velocità di spostamento a scala di bacino mostra una relazione non lineare con le dimensioni del bacino. I valori di velocità osservati sono comunque moderati, nonostante la forte velocità di spostamento delle singole celle convettive, e non hanno avuto un ruolo rilevante nell'evento analizzato.

TABLE OF CONTENTS

LIST OF FIGURES

LIST OF TABLES

RIASSUNTO

I. Introduzione

L'esame dell'effetto indotto dalla distribuzione spazio-temporale delle piogge sulla risposta di piena riveste un'importanza fondamentale sia nell'analisi fisica dei processi idrologici che in diversi campi dell'idrologia applicata. Tale conoscenza condiziona per esempio le indicazioni relative alla risoluzione con cui è necessario campionare e stimare il campo di pioggia al fine di mantenere un determinato grado di accuratezza nelle predizioni di piena. La trattazione dei campi di pioggia come variabili aleatorie ha permesso di inquadrare il problema di stima in modo rigoroso (Berne *et al.* 2004) per il caso di analisi a scala di bacino, associando la varianza di stima della precipitazione media areale alla estensione del bacino ed all'intervallo di aggregazione temporale. La comprensione del legame fra la organizzazione spaziale di pioggia a scala di bacino e la corrispondente risposta di piena rimane tuttavia piuttosto rudimentale, e le indicazioni fornite dalla letteratura sono spesso contraddittorie (Nicótina *et al.* 2008).

Questo lavoro introduce una metodologia per l'analisi della variabilità spaziale delle precipitazioni a scala di bacino mediante l'impiego di una serie di statistici di pioggia (denominati 'momenti spaziali di pioggia a scala di bacino') che consentono di individuare la relazione tra l'organizzazione spaziale della pioggia, la morfologia del bacino e la forma dell'idrogramma di piena (Zoccatelli *et al.* 2011). In particolare, gli statistici di pioggia vengono formulati tramite l'impiego di una coordinata fondamentale, rappresentata dalla distanza fra il punto generico e la sezione di chiusura del bacino misurata lungo le linee di flusso. L'introduzione di statistici fondati su tale coordinata è motivata dall'osservazione che la risposta di piena di un bacino idrografico tende ad attenuare la variabilità spaziale di pioggia misurata lungo una stessa linea isocorriva, in quanto il deflusso generato su tali punti arriva nello stesso istante alla sezione di chiusura. La componente di variabilità spaziale che può effettivamente influenzare la risposta di piena è quindi quella residua, misurata lungo la linea di deflusso, perpendicolare alla isocorriva. Si noti che tali posizioni sono accurate quando sia possibile considerare la distanza di deflusso come un surrogato del tempo di propagazione, ovvero quando sia possibile trascurare gli effetti della dispersione idrodinamica e la variazione spaziale e temporale delle celerità di propagazione del deflusso (Rinaldo *et al.* 1991). Lo studio evidenzia come i momenti spaziali di pioggia possano essere efficacemente utilizzati per valutare la sensibilità della risposta di piena alla distribuzione delle piogge e per valutare se le scale di monitoraggio della pioggia siano adeguate per catturare l'organizzazione delle piogge rilevanti ai fini idrologici. Dati relativi a cinque eventi estremi di piena improvvisa verificatisi in

diverse regioni Europee sono utilizzati per illustrare il significato degli statistici e delle relazioni fra gli statistici e la forma dell'idrogramma.

II. Momenti spaziali di pioggia a scala di bacino

I momenti spaziali di pioggia a scala di bacino (MSP – momenti spaziali di pioggia) descrivono l'organizzazione della pioggia su un assegnato bacino idrografico in funzione del tasso di pioggia r(x,y,t) [$L\ T^{-1}$] in corrispondenza del punto (x,y) e del tempo t, e della distanza d(x,y) [L] rispetto alla sezione di chiusura, misurata lungo le linee di deflusso. La base concettuale che ha permesso la derivazione dei momenti spaziali di pioggia è rappresentata dai lavori di Woods and Sivapalan (1999) e Viglione *et al.* (2010). Questi contributi sono intesi ad individuare le modalità con cui la distribuzione spaziale del deflusso superficiale (e della precipitazione, nel caso in cui il coefficiente di deflusso locale possa assumersi uniforme nello spazio e nel tempo) influenza la forma dell'idrogramma di piena.

Il generico momento spaziale di pioggia n-ennesimo p_n [$L^{n+1}\ T^{-1}$] è espresso come segue:

$$p_n(t) = A^{-1}\int_A r(x,y,t)d(x,y)^n dA \qquad \textbf{1}$$

dove A [L^2] è l'area del bacino su cui lo statistico viene calcolato. Si può notare che il momento di ordine zero descrive la pioggia media sul bacino all'istante t. In modo analogo è possibile scrivere anche gli statistici relativi alla distribuzione delle distanze di deflusso sul bacino g_n [L^n]:

$$g_n = A^{-1}\int_A d(x,y)^n dA \qquad \textbf{2}$$

dove il momento di primo ordine descrive la distanza media di deflusso del bacino. Una scrittura adimensionale dei momenti spaziali può essere ottenuta combinando (1) e (2) come segue (per i primi due ordini):

$$\delta_1(t) = \frac{p_1(t)}{p_0(t)g_1} \qquad \textbf{3}$$

$$\delta_2(t) = \frac{1}{g_2 - g_1^2}\left[\frac{p_2(t)}{p_0(t)} - \left(\frac{p_1(t)}{p_0(t)}\right)^2\right] \qquad \textbf{4}$$

Il momento di primo ordine, $\delta_1(t)$, rappresenta il rapporto tra il baricentro della distribuzione di pioggia all'istante t, misurata lungo le linee di flusso, e la distanza di deflusso media del bacino. Valori di δ_1 superiori ad 1 indicano pertanto una distribuzione di pioggia concentrata verso la periferia del bacino; valori unitari indicano una distribuzione di pioggia concentrata sul baricentro del bacino oppure spazialmente uniforme; valori inferiori ad 1 descrivono una distribuzione di pioggia concentrata verso la sezione di chiusura. Il momento di secondo ordine, $\delta_2(t)$, rappresenta invece il rapporto tra la dispersione della pioggia attorno al proprio baricentro e la dispersione delle distanze di deflusso attorno al proprio valor medio. Ancora una volta quindi valori prossimi ad 1 indicano una pioggia distribuita uniformemente sul bacino, mentre un valore inferiore ad 1 indica una concentrazione spaziale della precipitazione. Valori superiori ad 1 sono invece più rari, ed indicano una distribuzione multimodale della precipitazione in funzione della distanza di flusso.

L'Eq. (1) può essere estesa per descrivere la distribuzione di pioggia relativa ad un intervallo di tempo finito Ts [T], come segue:

$$P_n = A^{-1}\int_A r_t(x,y)d(x,y)^n dA = \frac{1}{T_s}\int_{T_s} p_n(t)dt \qquad \textbf{5}$$

dove r_t (x,y) indica il valore medio del tasso di pioggia relativo all'intervallo di tempo T_s in corrispondenza del punto (x,y). E' possibile in tal modo scrivere le relazioni corrispondenti ai momenti spaziali di pioggia media sul tempo T_s, come segue:

$$\Delta_1(t) = \frac{P_1(t)}{P_0(t)g_1} \qquad \textbf{6}$$

$$\Delta_2(t) = \frac{1}{g_2 - g_1^2}\left[\frac{P_2(t)}{P_0(t)} - \left(\frac{P_1(t)}{P_0(t)}\right)^2\right] \qquad \textbf{7}$$

III. Relazione fra i momenti spaziali di pioggia e la forma dell'idrogramma

La base teorica che consente di valutare l'influenza della struttura spaziale dei campi di pioggia sulla forma dell'idrogramma è descritta in Woods and Sivapalan (1999), Viglione *et al.* (2010) e Zoccatelli *et al.* (2011). Viene qui presentata la formulazione analitica relativa alla struttura del momento di primo ordine. A tal fine si considera il momento di primo ordine (baricentro) dell'idrogramma di piena, scritto nel modo seguente:

$$E(T_q) = \frac{\int_0^\infty q(t)\, t\, dt}{\int_0^\infty q(t)\, dt} \qquad \textbf{8}$$

che viene espresso in funzione del momento di primo ordine dello ietogramma di bacino:

$$E(T_r) = \frac{\int_A r_t(x,y)\, t\, dt}{\int_A r_t(x,y)\, dt} \qquad \textbf{9}$$

e del momento spaziale di pioggia del primo ordine utilizzando lo schema sviluppato da Zoccatelli et al. (2011):

$$E(T_q) = E(T_r) + \frac{\Delta_1 g_1}{v} \qquad \textbf{10}$$

L'Eq. (10) è valida alla luce delle seguenti posizioni:

- il coefficiente di deflusso è uniforme nello spazio e costante nel tempo;
- il tempo di propagazione del deflusso viene valutato sulla base della distanza di flusso e dell'impiego di un unico valore di celerità, *v*, uniforme nello spazio e costante nel tempo.

Queste assunzioni limitano l'applicazione dell'Eq. (10) ad eventi caratterizzati da elevate intensità di pioggia, per i quali l'intensità del deflusso superficiale rende del tutto irrilevante l'effetto della variabilità spaziale delle perdite di infiltrazione e della celerità del deflusso stesso. In particolare, questa trattazione analitica fondata sull'impiego dei momenti spaziali di pioggia può essere utilmente adottata per lo studio delle piene improvvise, come di seguito illustrato.

IV. Presentazione dei casi di studio

La metodologia di analisi delle precipitazioni è stata applicata a cinque eventi di piena improvvisa verificatisi in corrispondenza dei bacini individuati in Fig.1 e studiati nell'ambito del Progetto EU-FP6 HYDRATE (Borga *et al.* 2011).

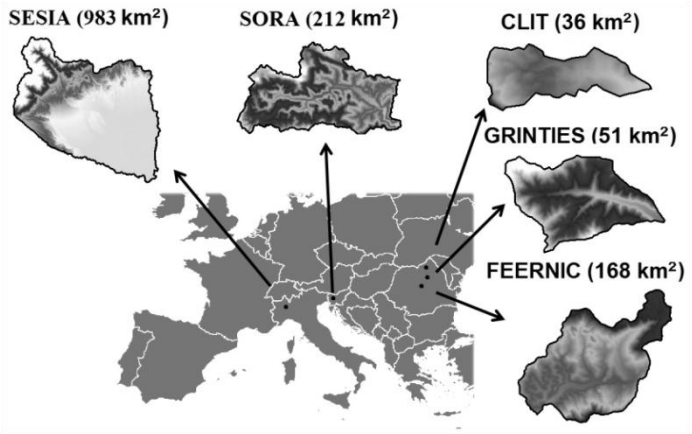

Figura 1. Bacini di studio e la loro posizione in Europa.

Si tratta di tre eventi verificatisi in Romania, uno in Slovenia ed uno in Italia (Marchi *et al.* 2010; Zoccatelli *et al.* 2010). Una sintesi delle caratteristiche principali di questi eventi è riportata in Tab. 1. Per ciascun evento sono disponibili accurate stime di pioggia da radar meteorologico e valutazioni della risposta di piena ottenute sia da misure idrometriche che da rilievi post-evento (Borga *et al.* 2008; Marchi *et al.* 2010).

Tabella 1. Riassunto delle caratteristiche dei cinque eventi analizzati e conseguenti piene improvvise.

Paese	**Bacino idrografico**	**Data**	**No. bacini analizzati**	**Dimensione bacini [km^2]**	**Durata pioggia [h]**	**Pioggia cumulata [mm]**
Italia	Sesia (Po)	05.06.2002	9	75 - 983	22	126
Slovenia	Selška Sora	18.09.2002	4	31.9 - 212	16.5	157
Romania	Feernic	23.08.2005	9	5 - 168	5.5	76
Romania	Clit	30.06.2006	2	12 - 36	4	81
Romania	Grinties	04.08.2007	3	11 - 51	4	67

La risposta di piena è stata simulata per ognuno dei casi di studio utilizzando un modello idrologico distribuito. La simulazione della formazione del deflusso è fondata sull'impiego del modello di Green-Ampt e su una descrizione semplificata del deflusso sottosuperficiale. La propagazione del deflusso superficiale viene rappresentata utilizzando uno schema basato sulla discretizzazione dell'albero drenante in elementi di versante e di canale, caratterizzati da diverse celerità di propagazione, nel seguito denominate rispettivamente celerità di versante e di canale. Il modello è stato applicato per ciascun evento, esaminando una serie di sottobacini (Tab. 1) per i quali sono disponibili osservazioni relative alla portata ed al tempo di picco.

Al fine di isolare l'effetto della variabilità spaziale delle precipitazioni, le simulazioni idrologiche sono state ripetute per ciascun sottobacino, con precipitazioni prima distribuite e poi uniformi. La Fig. 2 riporta le due simulazioni ottenute per il caso della piena del 5 Giugno 2002 sul bacino del Sesia a Quinto (983 km^2). Il valore dello statistico Δ_1 calcolato per tale evento è pari a 0.4, evidenziando un'importante concentrazione della precipitazione nella parte più a monte del bacino. A tale organizzazione di pioggia corrisponde una struttura dell'idrogramma di piena che viene completamente deformata allorché la simulazione di piena non considera la reale distribuzione di pioggia. In particolare, come atteso, la simulazione di piena ottenuta a partire da piogge spazialmente uniformi viene anticipata di diverse ore rispetto alla simulazione di piena conseguita sulla base delle piogge spazialmente distribuite.

L'errore che si viene a determinare fra i due idrogrammi di piena è stato esaminato utilizzando lo statistico dTn, ottenuto normalizzando la differenza fra i baricentri dei due idrogrammi conseguiti, per il tempo medio di deflusso T_c, come segue:

$$dTn = \frac{E(T_{q\_Dist}) - E(T_{q\_Unif})}{T_c} \qquad \textbf{11}$$

dove $E(T_{q\_Dist})$ ed $E(T_{q\_Unif})$ indicano i baricentri degli idrogrammi generati rispettivamente da piogge distribuite ed uniformi. L'impiego dell'Eq. 10 consente di riscrivere la relazione 11 come segue:

$$dTn = \Delta_1 - 1 \qquad \textbf{12}$$

L'Eq. 12 indica che lo statistico di primo ordine adimensionale equivale (a meno della sottrazione del valore unitario) all'errore relativo, evidenziando così l'efficacia del metodo fondato sui momenti spaziali della pioggia ai fini dell'analisi dell'effetto delle caratteristiche

spaziali di variabilità del campo di pioggia sui momenti primi temporali dell'idrogramma di piena.

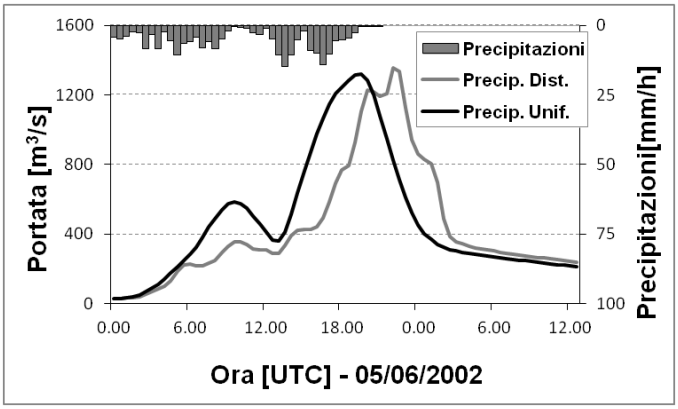

Figura 2. Idrogrammi di piena simulati ottenuti sulla base di piogge spazialmente distribuite oppure uniformi per il caso della piena del 05.06.2002 sul Sesia a Quinto (983 km^2).

V. Applicazione dei momenti spaziali di pioggia ai casi di studio

L'Eq. 12 è formalmente valida quando le assunzioni su cui si basa possano considerarsi verificate. E' importante quindi verificare sperimentalmente l'accettabilità del modello teorico con riferimento a possibili condizioni di applicazione del metodo nei diversi casi di studio. A tale scopo sono stati considerati 3 diversi Scenari di applicazione.

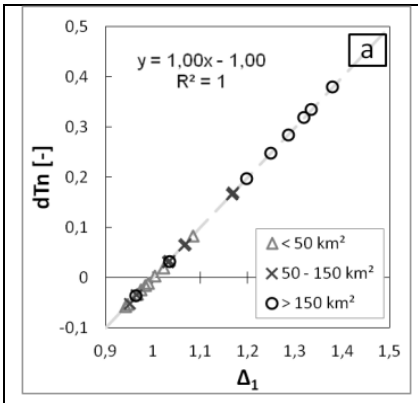	Scenario 1: Suoli impermeabili; Celerità di versante e di canale uguali fra loro;
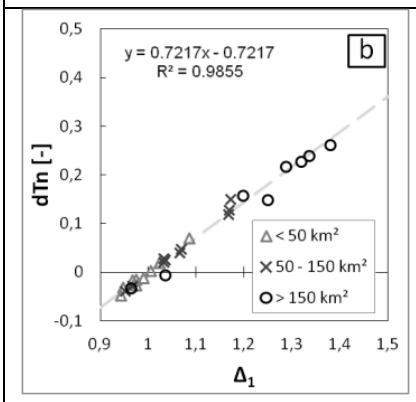	Scenario 2: Suoli impermeabili; Celerità di versante e di canale diverse fra loro e pari ai valori ottenuti nella fase di calibrazione del modello idrologico.
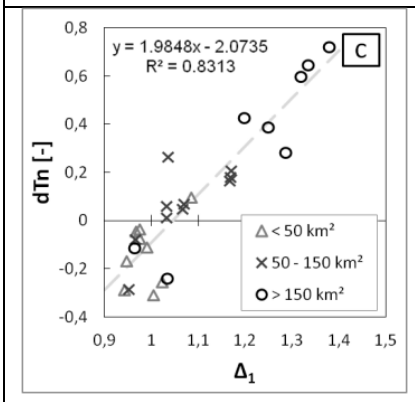	Scenario 3: Suoli permeabili, caratterizzati dai valori di conducibilità idraulica identificati e validati nella fase di calibrazione; Celerità di versante e di canale diverse fra loro e pari ai valori ottenuti nella fase di calibrazione del modello idrologico.

Figura 3. Relazione fra il parametro dTn e lo statistico Δ_1 per tre diversi scenari di implementazione del modello idrologico.

Con lo Scenario 1, i suoli sono stati considerati impermeabili e la celerità di versante uguale a quella di canale. Questo Scenario riproduce le ipotesi alla base del metodo, e ci si attende quindi che l'Eq. 12 descriva i risultati sperimentali senza errore apprezzabile. Con la Scenario 2, i suoli vengono considerati impermeabili, mentre le celerità di versante e di canale sono diverse fra loro e assunte pari ai valori ottenuti nella fase di calibrazione del modello idrologico. Con lo Scenario 3, i suoli vengono considerati come permeabili, caratterizzati dai valori di conducibilità idraulica identificati e validati nella fase di calibrazione del modello. La fase di propagazione è strutturata come nello Scenario 2. Tali Scenari rappresentano quindi condizioni di applicazione del metodo progressivamente più realistiche.

I risultati sono riportati in Fig 3, dove emerge piuttosto chiaramente come la distribuzione dei valori di Δ_1 sia asimmetrica, con una prevalenza dei valori maggiori di 1, corrispondenti a condizioni di concentrazione delle piogge verso la periferia del bacino. E' evidente in questa distribuzione l'effetto dell'orografia nella organizzazione della precipitazione a scala di bacino. Come ci si attende, i valori più elevati di Δ_1 (1.2-1.4) corrispondono ai bacini di dimensione maggiore (> 150 km^2), mentre i bacini più piccoli (< 50 km^2) sono caratterizzati da valori di Δ_1 piuttosto modesti compresi fra 0.95 e 1.15.

I risultati riportati per lo Scenario 1 (Fig. 3a) mostrano che il ritardo dell'idrogramma è perfettamente predetto da Δ_1, come atteso. I valori dell'errore relativo, compresi fra -0.07 e 0.4, sono piuttosto significativi, indicando che l'errore nella posizione temporale del baricentro dei deflussi può rappresentare una percentuale cospicua del tempo medio di deflusso.

Nel caso dello Scenario 2 (Fig. 3b) la simulazione idrologica include la funzione del versante. Tale inserimento ha l'effetto evidente di attenuare l'influenza della variabilità spaziale di pioggia sugli errori negli idrogrammi simulati: la pendenza della relazione si abbassa a 0.72, conservando comunque una buona capacità predittiva (R^2 = 0.98). Corrispondentemente, i valori di errore relativo risultano compresi fra -0.05 e 0.28.

Il terzo ed ultimo Scenario considera condizioni del tutto realistiche di implementazione del modello idrologico. In questa situazione le non-linearità dei processi di formazione del deflusso concentrano il deflusso in aree ad elevata precipitazione, aumentando notevolmente il ritardo dell'idrogramma rispetto al valore atteso. Questo processo risulta in un incremento notevole della pendenza della relazione, che si porta a 1.98 (R^2 = 0.83), accompagnato da una maggiore dispersione dei risultati e quindi da una minore capacità predittiva del modello. Nonostante questo effetto, la relazione fra dTn e Δ_1 si mantiene lineare, mostrando che i valori di Δ_1 sono comunque informativi circa l'errore atteso nella simulazione idrologica quando si trascura la variabilità spaziale della precipitazione.

VI. Ruolo del trasporto in versante sulla sensibilità dell'idrogramma di piena alla variabilità spaziale del campo di pioggia

In questa sezione estendiamo il concetto di MSP alla propagazione su versante, rielaborando i termini di covarianza utilizzati in Viglione et al. (2010) per descrivere la media e la varianza del tempo di deflusso. La propagazione di flusso all'interno del bacino è qui rappresentata con due velocità, v_c e v_h $[L\,T^{-1}]$, che rappresentano rispettivamente la velocità di propagazione su canale e versante. Indichiamo con $d_h(x,y)$ la distanza da un punto qualsiasi del bacino alla rete idrografica lungo il percorso di massima pendenza, mentre indichiamo con $d_c(x,y)$ la lunghezza del tratto seguente attraverso il reticolo idrografico fino alla sezione di chiusura. I MSP di ordine *n* per canale e versante sono definiti come segue:

$$p_{n,c}(t) = A^{-1}\int_A r(x,y,t)d_c(x,y)^n dA \qquad 13$$

$$p_{n,h}(t) = A^{-1}\int_A r(x,y,t)d_h(x,y)^n dA$$

Il momento di ordine 0 sia per il canale che versante equivale alla pioggia media areale at tempo t. Analogamente a quanto fatto in equazione 5, possiamo mediare il valore di $\mathrm{p_{n,c}}$ e $\mathrm{p_{n,h}}$ su un intervallo $\mathrm{T_s}$, uguale alla durata della precipitazione, per ottenere i valori medi $P_{n,c}$ e $P_{n,h}$.

Possiamo scrivere separatamente anche gli statistici relativi alla distribuzione delle distanze di deflusso lungo canale e versante:

$$g_{n,c}(t) = A^{-1}\int_A d_c(x,y)^n dA \qquad 14$$

$$g_{n,h}(t) = A^{-1}\int_A d_h(x,y)^n dA$$

I momenti di primo ordine $g_{1,h}$ e $g_{1,c}$ corrispondono rispettivamente alla distanza media di deflusso lungo il versante e lungo il canale. Una scrittura adimensionale dei momenti spaziali su versante e su reticolo idrografico può essere ottenuta in modo simile ad eq. 3 e 4 per i primi due ordini:

$$\delta_{1,c}(t) = \frac{p_{1,c}(t)}{p_0(t)g_{1,c}} \qquad 15$$

$$\delta_{1,h}(t) = \frac{p_{1,h}(t)}{p_0(t)g_{1,h}}$$

$$\delta_{2,c}(t) = \frac{A^{-1}\int_A r(x,y,t)\left[d_c(x,y)-\delta_{1,c}(t)g_{1,c}\right]^2 dA}{A^{-1}\int_A r(x,y,t)dA\; A^{-1}\int_A\left[d_c(x,y)-g_{1,c}\right]^2 dA} = \frac{1}{g_{2,c}-g_{1,c}^2}\left[\frac{p_{2,c}(t)}{p_0(t)} - \left(\frac{p_{1,c}(t)}{p_0(t)}\right)^2\right]$$

$$\delta_{2,h}(t) = \frac{A^{-1}\int_A r(x,y,t)\left[d_h(x,y)-\delta_{1,h}(t)g_{1,h}\right]^2 dA}{A^{-1}\int_A r(x,y,t)dA\, A^{-1}\int_A\left[d_h(x,y)-g_{1,h}\right]^2 dA} = \frac{1}{g_{2,h}-g_{1,h}^2}\left[\frac{p_{2,h}(t)}{p_0(t)} - \left(\frac{p_{1,h}(t)}{p_0(t)}\right)^2\right]$$

L'indice di primo ordine $\delta_{1,c}$ descrive il rapporto tra la distanza su canale pesata con la distribuzione di pioggia e la distanza su canale media del bacino. Una distribuzione di pioggia uniforme o concentrata sui valori medi di d_c, risulterebbe in $\delta_{1,c}$ con valori prossimi ad 1. Valori inferiori ad 1 indicano una pioggia concentrata vicino alla sezione di chiusura e valori più alti indicano maggiore pioggia nella parte più lontana del reticolo idrografico. Il momento di secondo ordine indica la dispersione delle distanze su canale pesate con la distribuzione di pioggia rispetto al loro baricentro, ed è normalizzato rispetto alla dispersione delle distanze su canale sul bacino. La scrittura adimensionale di $\delta_{1,h}$ e $\delta_{2,h}$ segue il concetto appena espresso, ma rispetto alla distanza su versante.

Analogamente ad equazione 6 e 7 definiamo con $\Delta_{n,h}$ e $\Delta_{n,c}$ i momenti spaziali di pioggia media sul tempo T_s rispettivamente per versante e canale. Per il primo ordine possiamo scrivere:

$$\Delta_{1,c} = \frac{P_{1,c}}{P_0 g_{1,c}} \qquad 16$$

$$\Delta_{1,h} = \frac{P_{1,h}}{P_0 g_{1,h}}$$

Il valore complessivo Δ_1 riportato in eq. 6 è essere espresso in funzione della distanza $d(x,y)$, che equivale alla somma di $d_h(x,y)$ e $d_c(x,y)$. Possiamo quindi scrivere Δ_1 in funzione di $\Delta_{1,c}$ e $\Delta_{1,h}$ come segue:

$$\Delta_1 = \frac{\Delta_{1,c}g_{1,c}+\Delta_{1,h}g_{1,h}}{g_{1,c}+g_{1,h}} \qquad 17$$

Mantenendo esplicito il tempo di trattenuta su versante possiamo riscrivere eq. 10 come:

$$E(T_q) = E(T_r) + \frac{\Delta_{1,c}g_{1,c}}{v_c} + \frac{\Delta_{1,h}g_{1,h}}{v_h} \qquad 18$$

Come fatto in precedenza, rispetto alla formulazione originale di Viglione *et al.* (2010) la distribuzione della pioggia e del deflusso sono equiparate. Definendo il tempo medio di residenza su versante come $\tau_h = g_{1,h}v_h^{-1}$, e il tempo medio di residenza in canale come $\tau_c = g_{1,c}v_c^{-1}$, possiamo riscrivere equazione 18 come:

$$E(T_q) = E(T_r) + \Delta_{1,c}\tau_c + \Delta_{1,h}\tau_h \qquad 19$$

Definiamo quindi con Θ_1 un indice adimensionale direttamente collegato al tempo medio di risposta del bacino:

$$\Theta_1 = \frac{\Delta_{1,c}\tau_c + \Delta_{1,h}\tau_h}{\tau_{tot}} \quad (20)$$

Dove $\tau_{tot} = \tau_c + \tau_h$. L'indice Θ_1 rappresenta il rapporto tra $E(T_h) + E(T_c)$ e il tempo medio di propagazione del bacino. Valori di Θ_1 uguali ad 1 rappresentano pioggia distribuita uniformemente o concentrata in aree con un tempo medio di deflusso. Valori di Θ_1 inferiori (superiori) ad 1 indicano una pioggia concentrata in aree con tempo medio di deflusso inferiore (superiore) alla media. Da equazione 18 ci aspettiamo che con valori di Θ_1 inferiori (superiori) all'unità avremo un anticipo (ritardo) dell'idrogramma generato con piogge spazialmente distribuite rispetto ad un idrogramma generato con piogge spazialmente uniformi.

Combinando equazione 19 e 11 possiamo trovare la relazione tra Θ_1 e l'errore atteso sull'idrogramma:

$$dT_n = \frac{E(T_{q\,Dist}) - E(T_{q\,Unif})}{E(T_c) + E(T_h)} = \frac{E(T_r) + \frac{\Delta_{1,c} g_{1,c}}{v_c} + \frac{\Delta_{1,h} g_{1,h}}{v_h} - E(T_r) - \frac{g_{1,c}}{v_c} - \frac{g_{1,h}}{v_h}}{\frac{g_{1,c}}{v_c} + \frac{g_{1,h}}{v_h}} = \Theta_1 - 1 \quad (21)$$

La relazione è simile a quella di eq. 12, ma qui viene incluso anche l'effetto che il versante ha sulla tempistica di piena.

Vista la diversa dimensione caratteristica di versanti, nell'ordine di grandezza del centinaio di metri, e della distribuzione cumulata della pioggia, con ordine di grandezza di chilometri, possiamo assumere che non ci sia correlazione tra la pioggia $r_t(x, y)$ e la distanza su versante $d_h(x, y)$. Una conseguenza di questa assunzione è che $\Delta_{1,h}$ abbia valori prossimi all'unità, e da equazione 19 possiamo quindi definire un indice semplificato Θ_1^*:

$$\Theta_1^* = \Delta_1 \frac{\tau_c + \frac{g_{1,h}}{v_c}}{\tau_{tot}} + \frac{\tau_h - \frac{g_{1,h}}{v_c}}{\tau_{tot}} \quad (22)$$

Equazione 22 permette di separare ed identificare l'effetto dell'organizzazione della pioggia sul bacino (Δ_1) con l'effetto dei singoli parametri geomorfologici $g_{1,c}$, $g_{1,h}$ e dei parametri dinamici τ_c e τ_h. Grazie a questo si può, ad esempio, analizzare la variazione di tempistica sull'idrogramma al variare dei singoli parametri di propagazione. L'assunzione su cui si basa equazione 22 può essere verificata nei 27 sottobacini analizzati calcolando $\Delta_{1,c}$ e $\Delta_{1,h}$, come mostrato in figura 4. Il valore contenuto di $\Delta_{1,h}$ porta a validare l'ipotesi di non-correlazione tra pioggia e distanza su versante.

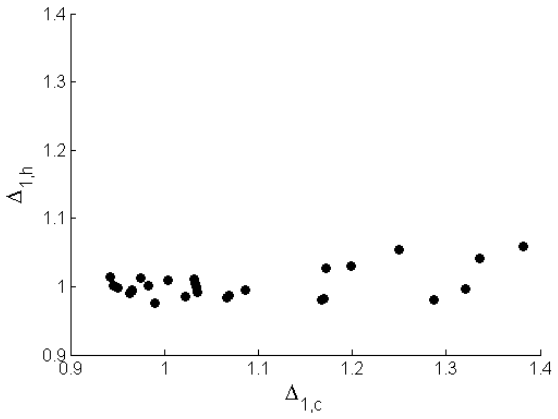

Figura 4: Relazione tra i valori di $\Delta_{1,c}$ e $\Delta_{1,h}$.

In modo simile a quanto fatto per figura 3, possiamo rapportare l'errore temporale sull'idrogramma con il valore degli statistici per diversi scenari.

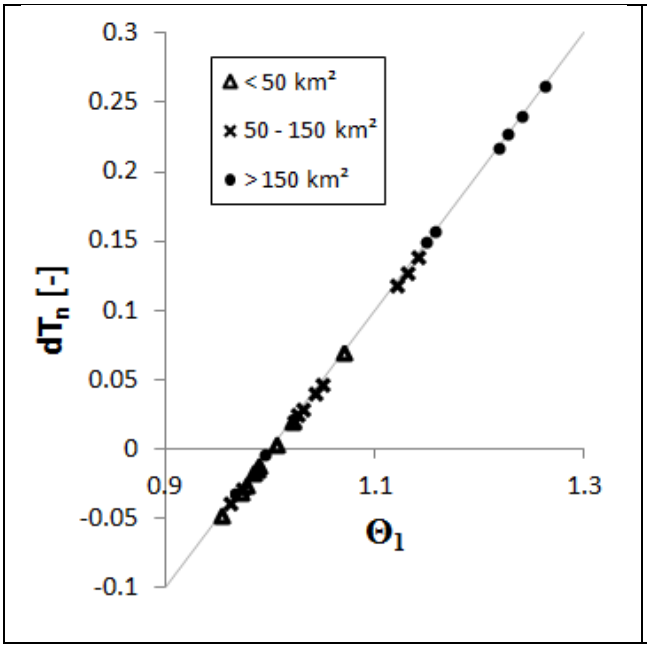

Scenario 1:

Suoli impermeabili;

Celerità di versante e di canale diverse fra loro e pari ai valori ottenuti nella fase di calibrazione del modello idrologico.

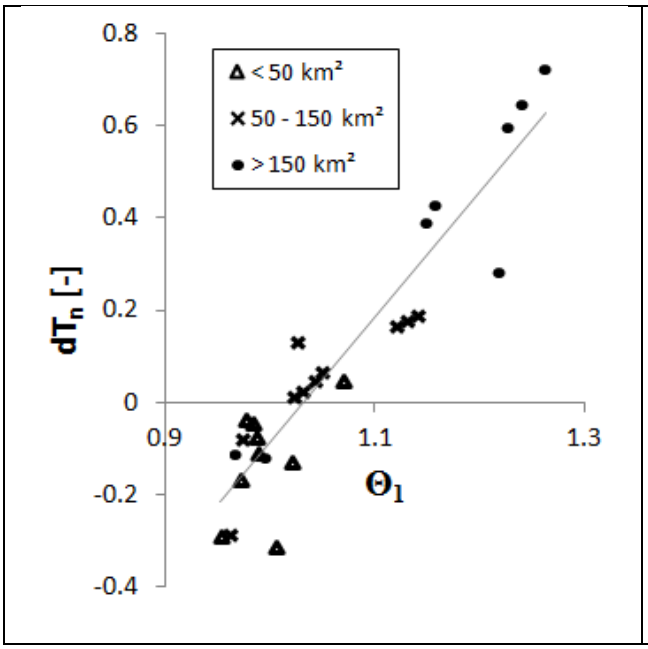

Scenario 2:

Suoli permeabili, caratterizzati dai valori di conducibilità idraulica identificati e validati nella fase di calibrazione;

Celerità di versante e di canale diverse fra loro e pari ai valori ottenuti nella fase di calibrazione del modello idrologico.

Figura 5. Relazione fra il parametro dT_n e lo statistico Θ_1 per due diversi scenari di implementazione del modello idrologico. La linea grigia rappresenta la regressione dei punti, ed è uguale a $dT_n = \Theta_1 - 1$ per il primo scenario ($r^2 = 1$) e $dT_n = 2.71\,\Theta_1 - 2.8$ per il secondo ($r^2 = 0.83$).

In figura 5, scenario 1 il modello ha le stesse caratteristiche di figura 3b, ma possiamo vedere come lo statistico Θ_1 sia in grado di rappresentare l'andamento teorico riportato in equazione 21. In figura 5, scenario 2 invece le nonlinearità nella generazione del deflusso aumentano l'errore temporale, come avevamo visto per figura 3c. Il valore di Θ_1 calcolato è quindi una soglia minima di errore temporale sull'idrogramma.

VII. Effetto del movimento della pioggia sull'idrogramma

Partendo dalla formulazione analitica di Viglione *et al.* (2010) relativa alla varianza dell'idrogramma, possiamo scrivere che:

$$var(T_q) = var(T_r) + var(T_c) + 2cov(T_r, T_c) \qquad 23$$

Il termine $cov(T_r, T_c)$ rappresenta l'effetto del movimento del sistema di precipitazione sulla varianza dell'idrogramma. Riscrivendo questo termine attraverso i momenti spaziali otteniamo un indice di velocità della precipitazione:

$$V_s(t) = \underbrace{g_1 \frac{cov_t[T, \delta_1(t)w(t)]}{var[T]}}_{V_s1} - \underbrace{g_1 \frac{cov_t[T, w(t)]}{var[T]}}_{V_s2} \Delta_1 \qquad 24$$

Dove $w(t) = p_0(t)P_0^{-1}$. Questo indice di velocità di spostamento include la variazione temporale della posizione, descritta come $\delta_1(t)g_1$, e dell'intensità di pioggia $w(t)$. La struttura è composta dalla differenza tra la pendenza di due regressioni temporali: V_s1 e V_s2. Per il caso di pioggia media areale costante nel tempo l'indice diventa una pura variazione della posizione nel tempo. Per il caso di pioggia stazionaria ma con intensità variabile nel tempo, le due regressioni assumono lo stesso valore, e V_s diventa uguale a 0. Valori positivi (negativi) di velocità indicano uno spostamento verso monte (valle) del sistema di precipitazione.

La velocità di spostamento del sistema di precipitazione è applicato alla piena del 27 Agosto 2003 sul bacino del Fella a Moggio, un bacino di 623 km^2 nelle Alpi Carniche e Giulie (Figura 6). La pioggia è durata per 12 ore, generando precipitazioni cumulate superiori ai 400 mm e intensità superiori ai 130 $mm\ h^{-1}$. Le condizioni iniziali particolarmente secche hanno limitato i coefficienti di deflusso nei sottobacini (Borga *et al.* 2007), ma nonostante questo sono stati registrati picchi unitari sopra gli 8 $m^3 s^{-1} km^{-2}$.

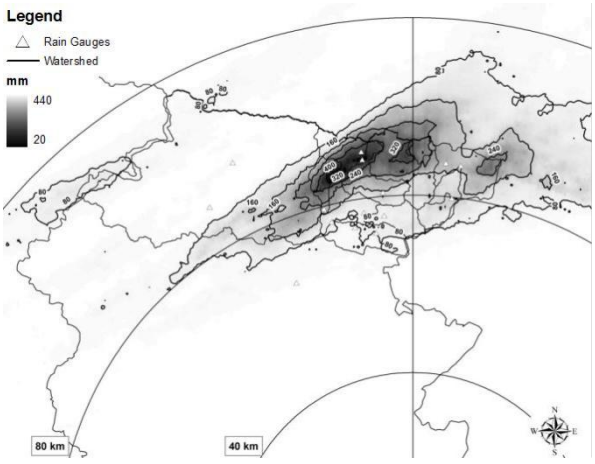

Figura 6: pioggia cumulata per l'evento del 29 Agosto 2003 in Friuli Venezia Giulia. Il cerchio rappresenta la distanza dal radar.

Un'analisi completa dell'evento è stata svolta all'interno del progetto HYDRATE (Borga *et al.* 2011), consistentemente con gli eventi presentati al capitolo IV. Anche per questo evento sono disponibili accurate stime di pioggia da radar meteorologico e valutazioni della risposta di piena ottenute sia da misure idrometriche che da rilievi post-evento (Borga *et al.* 2007).

Il bacino a Moggio è stato suddiviso in 21 sottobacini per analizzare la relazione tra l'effetto della velocità di spostamento della precipitazione e la scala dei bacini. I sottobacini hanno un'area compresa tra 7.7 e 623 km^2. La velocità euclidea di spostamento delle celle di precipitazione è stata quantificata tra 6 e 10 $m\ s^{-1}$.

Per limitare la dipendenza dei risultati dalla struttura del modello idrologico, oltre al modello presentato al capitolo IV (KLEM), l'analisi è stata ripetuta utilizzando anche un secondo modello. Il secondo modello, tRIBS, è basato su vertici geodetici (Ivanov *et al.* 2004). Tre simulazioni sono ripetute per ogni bacino: oltre alle due simulazioni descritte al capitolo IV, *distribuite* e *uniformi,* se ne aggiunge una terza con *variabilità costante*. Questa terza simulazione utilizza precipitazioni con una distribuzione spaziale costante nel tempo, e uguale alla distribuzione spaziale delle piogge cumulate su tutto l'evento. Con questa distribuzione gli statistici Δ_1 e Δ_2 risultano uguali a quelli della simulazione distribuita, ma senza spostamento temporale.

Per ogni sottobacino l'equazione 24 è applicata su due finestre temporali diverse, che descrivono informazioni diverse e complementari. Una velocità istantanea V è rilevata su un intervallo temporale mobile di un'ora. Questa grandezza descrive la velocità istantanea di spostamento del sistema di precipitazione, filtrata attraverso la morfologia di bacino. Nella seconda velocità, V_s, la finestra di calcolo è invece diversa tra i bacini, e corrisponde al tempo di risposta del bacino stesso. Dal momento che il tempo di risposta cresce con l'area, anche la finestra di calcolo aumenta con l'area. Un movimento continuo in questo intervallo è probabile che abbia un effetto sulla forma dell'idrogramma risultante. Mentre V descrive una velocità istantanea filtrata attraverso la morfologia del bacino, la velocità V_s è scelta per l'influenza sulla risposta idrologica del bacino.

Le simulazioni idrologiche per 3 bacini, scelti per rappresentare un intervallo ampio di scale, è riportata in figura 7.

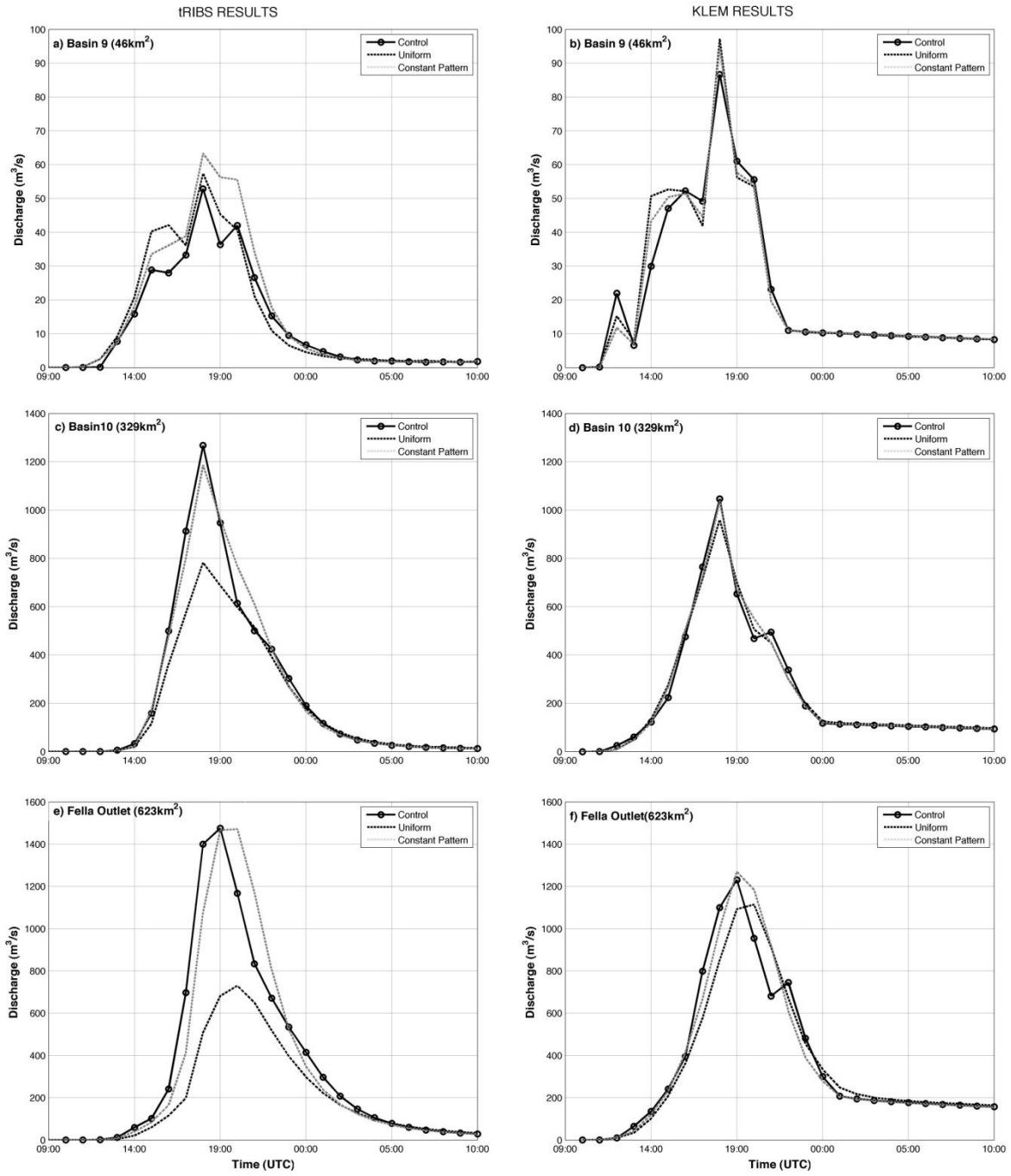

Figura 7: Idrogrammi simulati con i modelli tRIBS (sinistra) e KLEM (destra) per i tre bacini selezionati. Per ogni bacino sono riportati i risultati per pioggia distribuita (Control), uniforme (Uniform) e a variabilità costante (Constant Pattern).

Da figura 7 possiamo notare che la differenza tra simulazione distribuita e uniforme aumenta con l'area del bacino. Questo perché nei bacini piccoli la distribuzione della pioggia è più vicina a valori uniformi. Una differenza sostanziale tra queste due simulazioni è nel volume di deflusso. Questa differenza è dovuta alle nonlinearità nella generazione del deflusso, dove una precipitazione media areale genera meno deflusso di una concentrata. Questa differenza è notevolmente attenuata nella simulazione a variabilità costante.

Per analizzare la dipendenza della scala con la velocità del sistema di pioggia, l'intero insieme di valori della velocità V e V_s sono riportati assieme all'area dei bacini (figura 8).

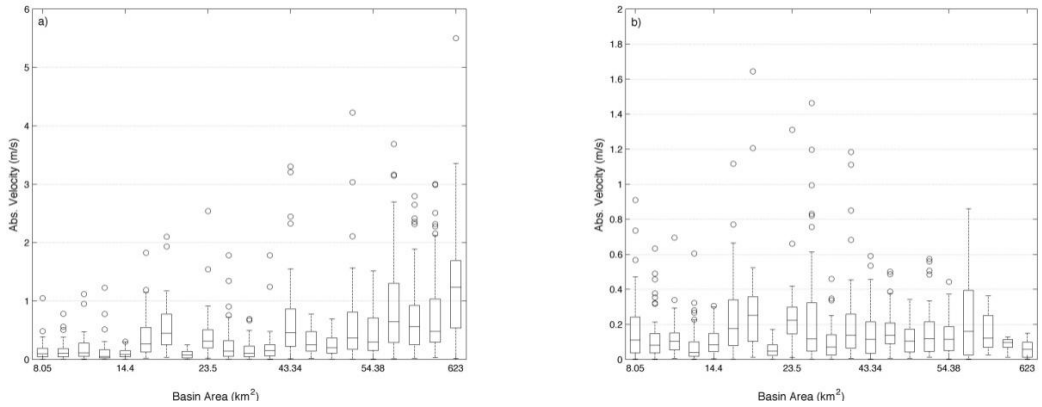

Figura 8: boxplot con la distribuzione di (a) V e (b) V_s in relazione dell'area di ogni sottobacino. I cerchi corrispondono a valori oltre una volta e mezza lo scarto interquantile della distribuzione.

Se riportiamo il valore medio della distribuzione di V e V_s rispetto all'area invece otteniamo quanto mostrato in figura 9.

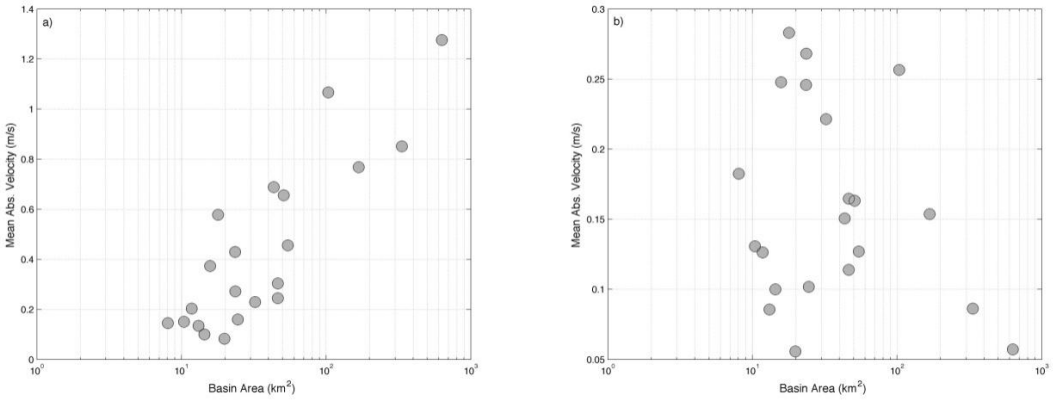

Figura 9: Valore medio di (a) V e (b) V_s in relazione con l'area dei bacini.

Figura 9a mostra come al crescere dell'area dei bacini il valore di velocità istantaneo filtrato dall'area dei bacini cresca. Questo significa che in bacini più grandi in media lo spostamento del sistema di precipitazione è maggiore. Un'interpretazione per questo dato è che più i bacini sono grandi più riescono a contenere il sistema di pioggia e rappresentare la continuità del suo movimento. In figura 9b invece vediamo come, se utilizziamo finestre di calcolo più ampie su bacini più grandi, questa dipendenza con la scala sia persa. Mentre i bacini piccoli hanno basse velocità istantanee, i bacini più grandi non mostrano uno spostamento continuo per un periodo abbastanza lungo. Come risultato l'effetto massimo sull'idrogramma è simile per tutte le scale di bacini analizzati.

VIII. Conclusioni

Questo lavoro illustra la derivazione di una serie di statistici di pioggia (denominati 'momenti spaziali di pioggia a scala di bacino') che consentono di individuare la relazione tra l'organizzazione spaziale della pioggia, la morfologia del bacino e la forma dell'idrogramma di piena. Tali statistici descrivono la posizione e la dispersione della pioggia su un assegnato bacino idrografico in funzione della distanza di flusso. La trattazione include la derivazione di una serie di relazioni che consentono di stabilire, alla luce di ipotesi relativamente comuni nella modellistica idrologica di piena, un rapporto fra detti statistici di pioggia ed i momenti temporali dell'onda di piena. Viene mostrato come il momento spaziale adimensionale di primo ordine Δ_1 sia direttamente proporzionale all'errore medio relativo che si viene a conseguire nel momento in cui si trascura la variabilità spaziale della pioggia nella modellazione idrologica di piena.

Le assunzioni fatte durante la derivazione limitano l'utilizzo a piene composte principalmente da deflusso superficiale. Dati di eccellente qualità relativi a cinque eventi estremi di piena improvvisa osservati in diverse regioni Europee sono utilizzati per illustrare il significato degli statistici e per verificare l'accuratezza dell'approccio qui descritto. I risultati indicano che la metodologia di analisi delle piogge qui illustrata può essere utilizzata efficacemente per valutare l'errore che si viene a determinare nella modellazione idrologica di piena quando la distribuzione spaziale delle piogge viene trascurata. Di converso, la metodologia può essere utilizzata per progettare i sistemi di monitoraggio di pioggia più idonei per la modellazione e previsione di assegnati eventi di piena, tenendo conto della struttura morfologica del bacino di studio.

È quindi analizzato l'effetto che la propagazione in canale e versante ha sulla relazione tra distribuzione della pioggia e tempistica dell'idrogramma di piena. La struttura analitica presentata può essere utilizzata per valutare l'effetto di diversi parametri che caratterizzano la propagazione su canale e versante, valutando scenari diversi e identificando i fattori dominanti. L'ipotesi di non-correlazione tra pioggia e versanti, che consente una semplificazione degli statistici di distribuzione, è stata verificata per le cinque piene improvvise. Questa assunzione permette una relazione diretta tra la distribuzione di pioggia su bacino Δ_1 e l'indice Θ_1, che descrive l'errore nella tempistica dell'idrogramma al netto del tempo di trattenuta su versante. Questo metodo può essere utilizzato ad esempio per valutare la sensibilità di bacini alla distribuzione delle piogge al variare delle condizioni dei versanti. I parametri geomorfologici e dinamici di propagazione possono essere a loro volta collegati con fattori ambientali quali le condizioni di umidità del bacino.

Un indice che collega lo spostamento del sistema di precipitazione con il suo effetto sull'idrogramma è stato calcolato per 21 sottobacini tra 7 e 623 km^2. Due approcci sono stati analizzati, che mirano a valutare la velocità istantanea V filtrata dalla morfologia di bacino e una velocità rilevante per la risposta idrologica V_s. I valori istantanei Vsi sono mostrati un ordine di grandezza più elevati di V_s, che non eccede mai 1 $m\ s^{-1}$. Inoltre è stato osservato che V aumenta linearmente all'aumentare del logaritmo dell'area del bacino. Questo fatto è probabilmente legato all'aumentare della variabilità della pioggia con l'area del bacino. Lo statistico V_s invece maschera l'aumento della velocità istantanea con un aumento della finestra di regressione. Nonostante la notevole velocità di spostamento delle celle convettive osservato durante questo evento, l'effetto sull'idrogramma è stato limitato dalla struttura del bacino. È stata anche sviluppata una metodologia per isolare l'effetto dello spostamento della pioggia sull'idrogramma a partire da simulazioni idrologiche. Nei casi analizzati l'idrogramma distribuito e a variabilità costante sono praticamente identici (Nash-Suttcliffe > 0.9), segno che la variabilità non ha rivestito un ruolo importante, come rilevato dai bassi valori di V_s (in media sotto i 0.4 $m\ s^{-1}$). Il risultato è in contrasto con il forte spostamento della pioggia durante la piena osservato da Borga *et al.* (2007). Le simulazioni idrologiche mostrano anche che un ruolo notevole nella sensibilità rilevata alla distribuzione di precipitazione è svolto dal modello idrologico utilizzato, soprattutto nei processi generazione di deflusso. L'applicazione degli statistici di velocità ad una sola piena limitano la generalizzazione dei risultati osservati, ma mostrano un caso applicativo concreto e possono essere indicativi per ulteriori approfondimenti.

1. Introduction

The growing of concerns about environmental and climate change issues, and the emergence of the concept of sustainable development, has modified the requirements towards hydrological predictions. In the past decades, the focus was mostly on the prediction of the water stream flow at a few locations. The demand has now moved to the prediction of the water balance components (rainfall, runoff, water storage, transpiration, evaporation, groundwater levels etc.) at every point within a catchment. The consideration of land-use and human-induced modifications of landscapes is a major concern for flood risk and water management problems such as flood forecasting, the study of the impact of land use evolution on stream flow, pollutants or sediments transport. For many of these questions, the knowledge of the water balance components at specific river locations is not sufficient and fluxes throughout the landscape are required as well as a proper handling of water pathways. For such questions, a representation of the relevant spatial and temporal variability is necessary.

The quality of hydrologic predictions, and specifically those required at ungauged locations (Sivapalan *et al.* 2003), largely depends on how well we can conceptualize the hydrologic system under study, and on the quantity and quality of the data we have available to force the model, e.g. precipitation. While the fundamental physics of water movement are well understood, it is nonetheless very difficult to conceptualize and parameterize hydrological models. Hydrology is in this sense different from fundamental physics, meteorology or hydraulics, which can largely rely on basic principles to predict system behavior. Hydrology, in this regard, is essentially a big boundary problem (Savenije 2009). In hydrology, the equations that drive water motion are known, but what is missing is the accurate knowledge of the atmospheric input and of the characteristics of the medium through which the water flows and that fully determine the process of water partitioning, storage and release (Beven 2006).

The quantification of rainfall variability in space and time and the analysis of its effect on flood predictions (by models), plays a fundamental role in the above discussion and, at the same time, exemplifies the main issues.

Precipitation is one of the main forcings driving the hydrological cycle. Precipitation phenomena range from cells (associated with cumulus convection) at scales of 1 km and several minutes, to synoptic areas (frontal systems) at scales of 1000 km and more than a day (Orlanski 1975; Bloschl and Sivapalan 1995). Runoff generation and soil moisture (as well as other hydrological processes) are non-linearly linked to precipitation, for instance through the effect of threshold processes. This means that some aspects of precipitation variability are

magnified in the rainfall-runoff transformation, whereas others are filtered out. Because precipitation exhibits a strong spatial and temporal variability over a large range of scales, the hydrological research and operational communities have developed different methodologies for precipitation estimation, ranging from weather radar to raingauge networks to meteorological remote sensing platforms (Berne and Krajewski 2012).

On the other hand, the aforementioned uncertainties in the knowledge of rainfall input and in the dynamics of the hydrological system make appealing the use of hydrological model calibration, when runoff data are available for this purpose. The use of model calibration forces the changes in the model parameters to adjust for uncertainties both in the input data and in the model structure. As a result, the model predictive capability can be improved in the range of conditions which are similar to those encountered in the model calibration process. However, transferring the model parameters and structure to different conditions (more extreme floods, or different basins) may lead to a worsening in predictive performance.

The above mentioned issues in hydrological modeling are partially responsible for the lack of consensus regarding the effect of spatial variability in rainfall on the streamflow prediction during floods. In spite of the large amounts of case studies and model applications which have considered the impact of spatial rainfall variability on flood hydrographc (see the Section on State of the Art), results from these studies are mixed. Whereas it is well known that the role of rainfall spatial variability is important for basins above 1000-5000 km^2 (Nicótina *et al.* 2008), or for urban catchments (Berne *et al.* 2004), for other situations results vary and no general framework is available. On the one hand, there are multiple indicators and parameters (mostly based on geostatistics, Berne *et al.* 2004) available to summarize information on the spatial rainfall variability at certain temporal aggregations and for certain catchment sizes; on the other hand, very poor knowledge is available on how the rainfall spatial variability interacts with the catchment properties (for instance, with the morphological properties) to filter out certain spatial variability components and to influence the flood response. As such, it is difficult to predict the role of spatial rainfall variability for new floods and for ungauged catchments, to distinguish the role of rainfall variability on the various processes, and to identify a priory the needs in term of rainfall sampling and monitoring.

This study aims to develop and test a new framework for understanding the role of rainfall spatial variability on flood hydrographs. As a way to develop a framework which can provide general insight into the problem, we need to avoid the use of a specific simulation model, which would limit the conclusions to a specific model setting. As an alternative to the use of an hydrological simulation model, an analytical approach is appealing. This allows one to specify the assumptions concerning the various hydrological processes, the form of the input,

and the type of inference (for instance, based on statistics). The analytical framework which is used in this work to describe the flood-generation hydrological processes is based on the contribution by Woods and Sivapalan (1999) and later developed by Viglione *et al.* (2010). The framework developed by Woods and Sivapalan (1999) quantifies the effects of flood event space–time variability on catchment storm response using several assumptions concerning the space–time structure of the hydrological patterns and runoff routing. This framework is generally applicable to any simulated or observed data-set and defines the effects of hydrological variability by a set of statistics. Viglione *et al.* (2010) significantly extended the theory proposed by Woods and Sivapalan (1999) by relaxing some of their most restrictive assumptions.

This work develops upon this earlier work by defining a number of statistical indices of clear physical meaning which summaries the interaction of the rainfall space and time organization with those morphological and hydrological catchment properties which influence the flood hydrograph. The rainfall statistical indexes are termed in this work as '*spatial moment of catchment rainfall*'. The flood hydrograph shape is summarized into two fundamental statistics: the mean runoff time (i.e., the time of the center of mass of the flood hydrograph at the basin outlet), and the variance of the timing of runoff (i.e., the temporal dispersion of the flood hydrograph). The statistical indexes developed in this work show how rainfall statistical and geometrical properties (concentration, dispersion, and motion) interact with the river network and the hillslope system to compose the two fundamental statistics of the flood hydrograph.

The conceptual meaning of the statistics is illustrated by application to a number of extreme flash floods occurred in various European regions for which high resolution rainfall fields and basin morphological properties are available. Focus on flash floods allows one to examine cases where the rainfall fields are characterized by marked space time variability. At the same time, it permits to consider a range of basin size, from 10 km^2 to 1000 km^2, which is of high interest for hydrological modeling and where past research provided mixed results. Results obtained in terms of statistical indexes are compared with those obtained based on the application of a distributed hydrological model.

With a focus on the analysis of the interaction between rainfall and catchment properties, this study aims to:

- Characterize the distribution of rainfall over a basin, for temporal scales relevant to flood events. The development of statistical indexes that measure the patterns of rainfall over a basin can be useful for a variety of purposes: for example it can be used to identify recurrent patterns of rainfall in the generation of floods or it can improve the planning of rainfall

monitoring network, overlaying rainfall patterns with the gauging network to define the space-time scales of monitoring.

- Develop a set of simple indexes directly relating rainfall with basin response to predict the features of flood hydrographs avoiding the complexities of hydrological models. These indexes can be used to estimate the potential effects of different rainfall scenarios, just quantifying the indexes. The assumption stated during the derivation of the indexes are important to define the limits of applicability.

- Compare basins and storms. In the field of comparative hydrology it is often emphasized the need for methods that capture hydrological similarities (Sivapalan *et al.* 1987; McDonnell and Woods 2004; Bloschl 2006). The development of statistical indexes like the 'spatial moments of catchment rainfall' can provide a rational basis to identify similarities both across basins and across storms. These statistics can help to examine the dynamics of physically complex systems, without looking at specific hydrological models.

- Lastly, this work aims to develop a methodology that isolates the effect of rainfall space-time distribution on hydrological model simulations of flash flood events. Through the application of the statistical indexes, this work will specify the role of single factors on runoff response. Identifying and ranking sources of variability can help to provide information on the required rainfall information avoiding the application of complex hydrological models.

The work done will be presented with the following structure:

- Derivation of the statistics and application to a set of extreme flash floods;
- Analysis of the role of hillslope processes in the response to variable rainfall fields;
- Quantification of catchment scale storm motion and its effect on flood response;
- Effect of direction and duration of storm movement on planar flow by using the presented framework.

2. State of the art

The aim of this work is to examine and predict the combined effects of rainfall space-time distribution and catchment properties on the shape of the flood hydrograph. Rainfall is the primary input to most hydrological systems, particularly under flood conditions, and a key issue for hydrological science and practice is to assess the importance of the spatial structure of rainfall and its representation for flood runoff generation. This generally depends on complex interactions between the type of event, the nature of the catchment and the spatial scale (i.e. catchment area) of the problem. The rainfall structure may influence the flood hydrograph both in terms of runoff generation and in terms of runoff propagation. The first effect, which will be only partially analyzed in this work, corresponds to the change in runoff generation processes due to spatially and temporally variable rainfall intensities. The second effect is due to the added variability that rainfall space-time distribution may have on the distribution of runoff timing. Indeed, the mean time that water takes to route to the outlet depends on the position of rainfall, and not only on morphological basin properties. To exemplify this effect, we may contrast the case of a storm which is spatially concentrated in the lower part of the catchment with one characterized by spatially uniform rainfall. In the first case, the runoff will take less time to reach the outlet and the flood hydrograph will be likely anticipated with respect to one generated by uniform precipitation. The focus of this work is placed on the analysis of this second effect, by considering the rainfall space-time distribution and the basin morphology. To this end, this work builds upon the development of an analytical framework by Woods and Sivapalan (1999) and later by Viglione *et al.* (2010a,b). The framework developed by Woods and Sivapalan (1999) quantifies the effects of flood event space–time variability on catchment storm response using several assumptions concerning the space–time structure of the hydrological patterns and runoff routing. This framework is generally applicable to any simulated or observed data-set and defines the effects of hydrological variability by a set of statistics. Viglione *et al.* (2010) significantly extended the theory proposed by Woods and Sivapalan (1999) by relaxing some of their most restrictive assumptions.

The state of the art is examined as follows:

- Influence of rainfall distribution on flood hydrograph;
- Influence of storm movement on the hydrograph;
- Studies based on development of analytical frameworks.

2.1.Influence of rainfall distribution on flood hydrograph

Given the key importance of the hydrological significance of rainfall space-time distribution, the relevant literature is extensive. As a first indication, it is interesting to note that the effects of rainfall spatial variability are usually assessed indirectly, via a watershed model. Only a few studies have attempted to isolate the effects of rainfall variability based on hydrological data alone (Smith *et al.* 2004). This explains why many conclusions are by design model- and application- specific. Moreover, this partially explains why the literature on this topic fails to provide general indications. While hydrological models provide a powerful tool to test the sensitivity of the catchment to various rainfall patterns, their calibration at a fixed spatial scale and with reference to a specific rainfall information introduces uncertainties in relating the rainfall input to the simulated flow (Koren *et al.* 1999; Smith *et al.* 2004). As reported above, several hydrological modeling studies have analyzed the impact of spatial rainfall variability on flood hydrograph to quantify the effect of rainfall space-time aggregations on model simulations (Dawdy and Bergmann 1969; Wood *et al.* 1988; Krajewski *et al.* 1991; Beven and Wood 1993; Ogden and Julien 1993; Blöschl *et al.* 1995). General results indicate that spatial rainfall patterns have a strong effect on the hydrograph for large rural catchments (> 1000-5000 km^2) or in urban (even small) catchments. These findings clearly point to different explanations: i) scale effects and ii) runoff generation effects.

As reported by Nicótina *et al.* (2008), the spatial distribution of rainfall does play an important role in the case of large catchments because the transport paths sampled by rainfall are in this case very heterogeneous due to the importance of channel residence times. Similar observations were reported by Arnaud *et al.* (2002).

For smaller basins, Obled *et al.* (1994) observed that accurate estimation of the mean areal rainfall is enough for the model-based flood simulation. In a study conducted on a 71 km^2 catchment in France, they found that spatially-uniform rainfall estimated from five raingauges was enough to estimate the streamflow hydrograph because of the large damping behavior of the basin. They argued that because the runoff generation mechanism is predominantly of the Dunne type in this study area, the water infiltrates and local variation of the rainfall input is smoothed and delayed within the soil. Similar observations are reported for small and medium size basins by several investigations (Beven and Hornberger 1982; Naden 1992; Obled *et al.* 1994; Andreassian *et al.* 2001; Smith *et al.* 2004; Smith *et al.* 2004). Nevertheless, some works showed the significance of rainfall distribution even in catchments as small as 4 hectares (Michaud and Sorooshian 1994; Faurès *et al.* 1995; Lopes 1996). Michaud and Sorooshian (1994) recommended a spatial resolution of 2 km to model catchments between 50 and 500 km^2.

As reported by Obled *et al.* (1994), the lack of consensus about the significance of rainfall spatial variability on the flood response is partially due to the complexity of the runoff generation processes. Winchell *et al.* (1998), in a review of past studies, concluded that runoff-generation is highly sensitive to the spatial and temporal variability of rainfall. In their review, however, they identified a strong bias in the use of the infiltration-excess runoff generation mechanism in these sensitivity studies. Generally, arid or urban catchments susceptible to Hortonian runoff generation show an higher sensitivity than humid areas to rain variability (Michaud and Sorooshian 1994; Faurès *et al.* 1995; Lopes 1996; Arnaud *et al.* 2002). In humid areas soils are deeper and are able to store more water, while in semi arid regions soil crusting is favoring the generation of Hortonian surface runoff. Similarly, the underlying geology is important and can mask the impact of spatial rainfall. Naden (1992) concluded that a lumped approach is appropriate to model the 7000 km^2 Thames catchment; the hillslope component of runoff has a much longer residence time than the channel routing, due to the large proportion of limestone and chalk. Dodov and Foufoula-Georgiou (2005) found that including information on rainfall spatial distribution improves the prediction performance of streamflow, but less for a catchment with presence of limestone aquifer.

In urban catchments, a large fraction of soil is waterproofed with buildings or has a reduced permeability due to soil compaction. The runoff produced is quickly routed through the large number of preferential runoff paths, such as sewage systems or roads, generating runoff peaks higher than other landuses (Smith *et al.* 2002). Many studies demonstrated that urban hydrology requires rainfall measurements with high spatial and temporal resolution in order to describe rainfall volume within the short response time (Berndtsson and Niemczynowicz 1988; Niemczynowicz 1999; Ogden *et al.* 2000; Berne *et al.* 2004). However the structure of the hydrological network can be enough to smooth rainfall variability (Smith *et al.* 2005) and the variation in routing times due to rainfall position may be disregarded even in this conditions.

For similar reasons, in temperate climates the most favourable conditions to high hydrological sensitivity are strong convective rainfall, impervious soils and mountainous basins (Ajami *et al.* 2004). Still the heterogeneity of the catchment smoothes rainfall variability, and the effect depends also on whether rainfall variability is enough to overcome the damping and filtering effect of the basin (Obled *et al.* 1994; Smith *et al.* 2004).

Floods and their sensitivity to rain variability have been observed to be largely influenced by antecedent soil moisture conditions (AMC) (Sturdevant-Rees *et al.* 2001; Gaume *et al.* 2004; Smith *et al.* 2005; Borga *et al.* 2007; Le Lay and Saulnier 2007; Merz and Bloschl 2009) . Again, this sensitivity is nevertheless largely controlled by climates and flood types (Castillo *et al.* 2003; Merz

and Bloschl 2003; Marchi *et al.* 2010). Generally in temperate climates wet antecedent conditions translate into higher runoff coefficients (Norbiato *et al.* 2009) and a larger amount of surface runoff. The main factor influencing AMC is the amount of antecedent rainfall. However moisture is influenced also by the draining capacities of the soil, by the amount of evapotranspiration or by other water inputs such as snow melt. A possible approach to study the effect of AMC on floods isolates all the parameters depending on the catchment properties into a variable called *soil moisture memory (Pathiraja et al. 2012)*. This variable describes the amount of time in which a catchment runoff is influenced by a given antecedent rainfall and can be useful for catchment classification.

2.2. Influence of storm movement on the hydrograph

The influence of storm movement on flood hydrographs has been investigated for nearly four decades (Maksimov 1964; Niemczynowicz 1984; Singh 1998; De Lima and Singh 2002). Relevant factors of storm motion which may influence the shape of the flood hydrograph are i) the direction with respect to the catchment shape (e.g., upstream, downstream, transverse, or angular), ii) the areal coverage over the basin (e.g., full or partial), the storm duration (e.g., duration leading to equilibrium hydrograph in which the whole basin is contributing to the peak discharge, or partial equilibrium hydrograph, in which the above condition is not met). Maksimov (1964) was probably the first to investigate the influence of the movement of rain storms on surface runoff and demonstrated that it modified peak discharge. Marcus (1968) undertook laboratory studies to demonstrate the importance of rainstorm movement to the time distribution of surface runoff. Roberts and Klingeman (1970) found that the direction of storm movement might augment or reduce flood peaks and modify the hydrograph recession. Surkan (1974) observed that peak flow rates and average flow rates were most sensitive to changes in the direction and speed of the rainstorms. This last factor is particularly important in relation with the flood propagation velocity (Lee and Huang 2007), and in downstream storm motion if the two are comparable the peak discharge is likely to be maximized (Ogden *et al.* 1995).

Overall, the investigations of the past decades have shown that storm movement may have an influence on flood peak, modifying the hydrograph shape. For the same storm duration a storm moving downstream tend to generate a greater peak relative to storms moving upstream (Ogden *et al.* 1995). The impact on flood hydrograph is expected to depend on the catchment area, on the structure of the drainage system and its directional orientation relative to the main storm movement. For example, the runoff response from a long and narrow basin parallel to the storm motion vector is expected to show more dependence on storm velocity than a short, wide basin (Woods and Sivapalan 1999; Smith *et al.* 2000). Small basins have also been demonstrated to be

more sensitive to storm movement (Ngirane-Katashaya and Wheater 1985; Michaud and Sorooshian 1994; Faurès *et al.* 1995; Michaelides and Wainwright 2002; Schuurmans and Bierkens 2007).

2.3. Studies based on the development of analytical frameworks

An analytical approach can be used as alternative to the numerical simulations to study the influence of rainfall distribution on the hydrograph. The catchment is represented with some simplification, allowing to identify the relations between single factors (Wooding 1965; Kirkby 1976; Beven and Wood 1993; Robinson *et al.* 1995; Robinson and Sivapalan 1997; Robinson and Sivapalan 1997). With this approach we are able to define the order of magnitude of the processes involved. This information can be used to search for hydrological similarities between events, and this in turn can be useful for the synthesis invoked in the introduction. In this section we start presenting the analytical framework developed by Woods and Sivapalan (1999). Then we discuss the modifications produced by Viglione *et al.* (2010) and the possible application. Finally we are going to discuss a branch of literature that, to describe the effect of hillslope variability, uses indicators with a structure similar to Woods and Sivapalan (1999).

Woods and Sivapalan (1999) (termed WS1999 elsewhere) proposed an analytical method to identify the importance of different components on the shape of the flood hydrograph for humid temperate catchments. In their conceptualization, the fraction of rainfall that is transformed into runoff is routed through hillslope and then through the hydrological network until the catchment outlet. We can divide the total catchment runoff time, defined as the time from the start of the event until the centroid of runoff, into three parts:

$$T_q = T_r + T_c + T_h \qquad \textbf{2.1}$$

Where T_r, T_c and T_h are the holding times for rainfall excess, channel network travel and hillslope travel respectively. In this framework runoff generation processes are represented by the application of a runoff coefficient, variable in space and time. The function of hillslope routing is instead invariant in space and time. After passing through hillslopes the water goes to the channel network, where it is propagated with a constant velocity v_c $[L\,T^{-1}]$ along the flow distance coordinate. This metric is employed because rainfall spatial organisation measured along the river network by using the flow distance coordinate is considered to be a significant property of rainfall spatial variability when considering flood response modelling. Runoff routing through branched channel networks imposes an effective averaging of spatial rainfall excess across locations with equal routing time, in spite of the inherent spatial variability. Flow distance may be used as a surrogate for travel time, when the hydrograph response is determined mainly by the distribution of travel times, neglecting hydrodynamic dispersion, and variations in runoff propagation

celerities may be disregarded. We distinguish here between rainfall spatial variability and organization. By spatial organization we mean systematic spatial variation of rainfall with respect to certain basin geomorphic properties which directly control the runoff response, such as the flow distance.

WS1999 characterized storm response with three quantities: the mean rainfall excess rate, surrogate for flood magnitude; the mean runoff time, surrogate for the time to peak; the variance of the runoff time that, together with flood magnitude, describes the hydrograph peakness. For a given rainfall excess and timing, the hydrograph peak is higher with lower variance of runoff times (Woods 1997). In this framework the factors describing the influence that rainfall position has over the hydrograph timing and dispersion are explicit. This allows for example to compare the role that rainfall position has on runoff timing with the role of storm duration.

We can now examine the assumptions done in the development of the analytical framework and the relevant limits of application:

- Since the method was built as event-based, it does not include subsurface flow and evapotranspiration. The method is best suited to represent short and intense storms with low subsurface flow.
- Infiltration processes are neglected also along the path to the outlet, limiting the use to conditions where the connectivity of soil moisture patterns is developed (Western *et al.* 2001).
- The hydrodynamic dispersion of flood propagation is neglected, as the effect on the hydrograph is much smaller than the geomorphological dispersion described by the distribution of flow distances (Rinaldo *et al.* 1991).
- The use of a channel velocity constant in space and time limits the application to extreme storms, when the channel velocity reaches an asymptotic value (Pilgrim 1976; Beven 1979).
- The assumption of multiplicative space-time separability for both rainfall and runoff generation processes implies that the storm event is stationary, i.e., it does not move over the catchment.

Besides these simplifications, to apply the model to real cases we need the distribution of runoff coefficients. Since we can have no direct observations we need an hydrological model to describe the runoff distribution, introducing more assumptions and calibrations to describe the hydrological processes. On the other hand, the advantage of such an analytical model is to quantify the order of magnitude of processes involved in catchment flood response across events.

For example we can analyze the relative importance of components with increasing basin size. In larger basins the importance of channel travel time is increasing compared to hillslope and storm duration, and with an application of the framework the effect of this relation on the hydrograph can be quantified. Capturing and quantifying the most important processes that shape runoff response allows also to transfer knowledge obtained in similar basins. Other analytical frameworks have been presented before, but they usually neglect spatial variability of rainfall (Wooding 1965; Kirkby 1976).

The WS1999 framework has been further developed by Viglione *et al.* (2010), who relaxed two of its main assumptions. The first assumption relaxed is the space invariability of hillslope routing, retaining the invariability in time. The second one is the assumption of multiplicative space-time separability. With the introduction of new terms in the analytical expressions we can relax this last assumption allowing the examination of the effect of storm movement on hydrograph shape. V2010 proved, based on four schematic storms, that the two components introduced can be extremely relevant to shape basin response. The functionality and applications of the analytical framework remained the same explained for W1999.

According to both the W1999 and V2010 frameworks, the mean catchment runoff time is equal to the sum of the expected times for the three factors in equation 2.1:

$$E(T_q) = E(T_r) + E(T_c) + E(T_h) \qquad 2.2$$

The variance of catchment runoff time instead changes its formulation in V2010, and it is expressed as:

$$var(T_q) = var(T_r) + var(T_c) + var(T_h) + 2cov(T_r, T_h) + 2cov(T_r, T_c) + 2cov(T_h, T_c) \qquad 2.3$$

The three space covariances between holding times come from the relaxation of the two assumptions done in V2010. Viglione *et al.* (2010) applied the framework to four different flood types in Austria: long rain; short rain; rain on snow and snowmelt. The framework was able to capture the order of magnitude of the processes influencing the flood hydrograph in the different cases. A dimensionless statistic that combines the storm averaged rainfall excess and the dispersion of the runoff times is introduced. The clear relation between this statistic and the relative magnitude (peak discharge) of single floods demonstrates one of the possible applications for the framework.

Various measures of rainfall organisation based on the flow distance coordinate have been introduced in the last decade. Smith *et al.* (2005),Smith *et al.* (2002), Zhang *et al.* (2001) and

Borga *et al.* (2007), in a series of monographs on extreme floods and flash floods, systematically employed a scaled measure of distance from the storm centroid and scaled measures of rainfall variability to quantify the storm spatial organisation and variability from the perspective of a distance metric imposed by the river network.

Smith *et al.* (2002) analyzed the distribution of rainfall spatial variability with the application of indexes of normalized distance similar to one presented in this work. The index was used to describe the storm, and to draw conclusions on the effects of rainfall distribution and motion. Smith *et al.* (2005) described rainfall distribution with the same position index plus an index of flow distance dispersion. This last index has the same structure as the one employed in our work. They analyzed a 14.3 km^2 urban catchment and showed that the spatial variability of rainfall is much less when analyzed through the flow distance metric, which is reflected in a small effect on the flood hydrograph.

Smith *et al.* (2004) examined basin outflow response to observed spatial variability of rainfall for several basins in the Distributed Model Intercomparison Project (Smith *et al.* 2004), by using, among other indexes, a rainfall location index based on the distance from the centroid of the catchment to the centroid of the rainfall pattern. They found that all basins except one had a very limited range of rainfall location index, with the rainfall centroid close to the catchment centroid. Interestingly, the catchment displaying the largest range of rainfall location index was also the one characterised by such complexities to suggest the use of a distributed model approach. A similar approach was taken by Syed *et al.* (2003) who evaluated the ability of simple geometric measures of thunderstorm rainfall to explain the runoff response from a 148 km^2 watershed. They also used a location index similar to that introduced by Smith *et al.* (2004). They observed that the position of the storm core relative to the watershed outlet becomes more important as the catchment size increases, with storms positioned in the central portion of the watershed producing more runoff than those positioned near the outlet or near the head of the watershed.

3. Data and hydrological modeling

To test the statistics describing rainfall spatial organization we used data from six flash floods occurred in Europe between 2002 and 2007. The data concerning the events have been selected from the database developed under the EU project HYDRATE (www.hydrate.tesaf.unipd.it) (Borga *et al.* 2010). For each of these events an high-resolution rainfall pattern from radar and rain gauges is available, together with information on the type of processes (whether an hyperconcentrated flow or debris flow occurred), on the flood timing and peak. Most of these information are collected with *Intensive Post Event Campaigns* (IPECs). The database includes also information on climate, morphology and landuse of the region. The storms were selected based on catchment size, storm duration and space-time variability of rainfall. These data were used to calibrate an hydrological model. Simulations with this model have been used to understand the spatio-temporal development of floods and the relation between generating factors. We need to note that, as observed by Obled *et al.* (1994), the sensitivity of hydrological models to spatial variability of inputs is not necessarily the same of the basin sensitivity. To analyze the role of rainfall distribution the effect of the model should be kept to a minimum.

3.1. Events analyzed

The geographical position of the six flash floods is shown in figure 3.1. The main characteristics of the single storms, the ensuing floods and references to more specific studies are reported in table 3.1.

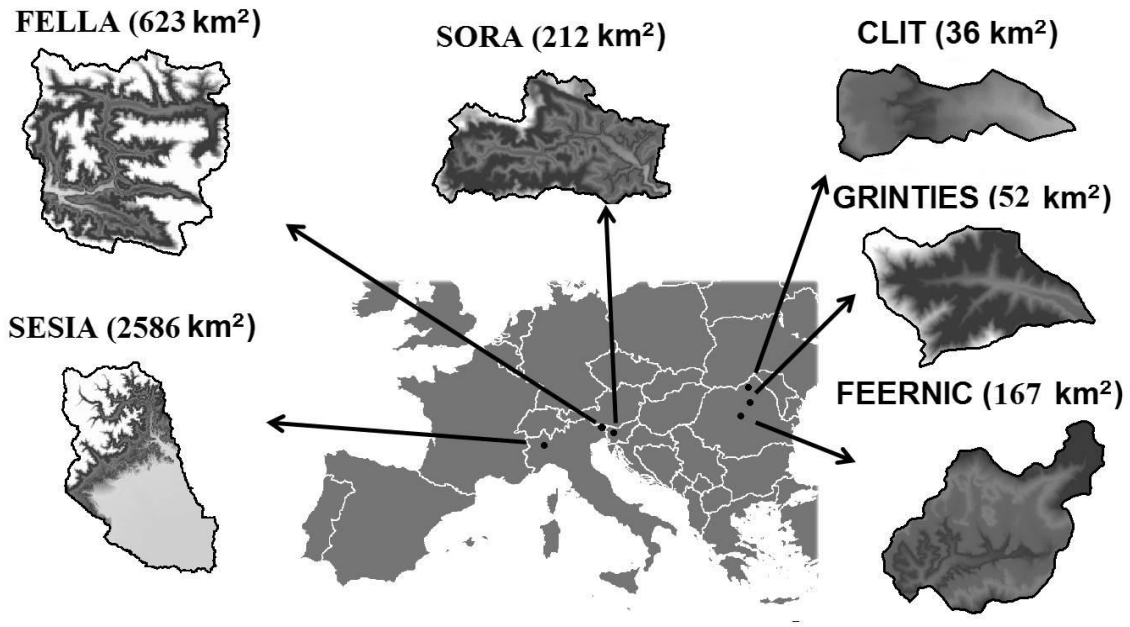

Figure 3.1: Study catchments and their location in Europe

Table 3.1: Details on the floods considered for the study

Event	Date	Rainfall aggregation time	Area [km^2]	Duration [hh:mm]	Rain cum. [mm]	Peak flow [m^3/s]	References
Sesia at Palestro	04/06/2002	30’	2586	21:30	113	3944	Sangati *et al.* (2009)
Feernic at Simonesti	23/08/2005	15’	167	5:30	76	357	Zoccatelli *et al.* (2010)
Clit at Arbore	30/06/2006	15’	36	7:00	81	156	Zoccatelli *et al.* (2010)
Grinties at Grinties	04/08/2007	15’	52	7:00	67	89.5	Zoccatelli *et al.* (2010)
Sora at Vester	18/09/2007	30’	212	17:45	157	351	Zanon *et al.* (2010)
Fella at Moggio	29/08/2003	30'	623	12:00	293	1290	(Borga *et al.* 2007)

A first distinction can be made between the tree floods in the Carpathian range and the three in the Alps. The different position denotes a difference in climate, with the Romanian basins having a much stronger continental climate, with more intense convective rainfall that lasted for a shorter time in comparison with Alpine floods. The climatic forcing influences also the seasonality of floods, with continental areas more subject to floods in summer months compared to the alpine areas.

Rainfall

Rainfall estimation is based on data both from raw radar reflectivity values and from raingauge measurements. Because of the small scales involved in this kind of storms, the estimation of precipitation is a crucial problem (Krajewski and Smith 2002; Bouilloud *et al.* 2010). Physically based correction procedures were used to correct raw radar reflectivity values. The steps of the correction method, that was applied consistently across all the events, are:

- Collection of data and metadata from the radar system and the raingauge network;
- Analysis of the detection domain and correction for ground/anthropic clutters (Pellarin *et al.* 2002)
- Implementation of corrections for range-dependent errors (e.g. screening, attenuation, vertical profiles of reflectivity)
- Optimization of the rainfall estimation procedure by comparison between radar and raingauges at the event scale (Bouilloud *et al.* 2010)

Additional information on the methods employed in the correction of radar reflectivity can be found in Bouilloud *et al.* (2009).

Discharge

To analyze the floods we used discharge estimates both from stream gauges and intensive post event campaigns (IPECs). Stream gauge data from monitoring and private networks contributed to estimate the timing and the extent of the flood. Higher discharges were estimated though extrapolation from rating curves of smaller observed floods. Because of the intensity and the scarce frequency of Flash Floods, we note that the measures from stream gauges are also affected by considerable uncertainty. Other factors reduce the quality of discharge data during floods, such as the modifications in river cross section or damages to the measuring gauges.

Another issue with stream gauge measurements is the extent of basins monitored. Marchi *et al.* (2010) showed how stream gauges are placed in basins larger than the ones where the flood develops. It is important, in order to catalog flash floods, to integrate these data with additional surveys. Intensive Post Event Campaigns were carried out after each flood to collect data on the flood type, intensity and timing. The methods used for this campaigns were standardized for all the events presented here (Borga *et al.* 2008; Gaume and Borga 2008; Marchi *et al.* 2009) and include:

- identification of the flow processes (liquid flow, hyperconcentrated flow, debris flow);
- identification of high water marks (HWMs);
- survey of post flood river geometry;

- application of hydraulic methods for flood computation (Costa and Jarrett 2008);

The slope conveyance method (Gaume 2006) was used to estimate the discharge at the peak. This method requires: the description of a cross section; the identification of different HWMs to accurately define the maximum water depth; local water slope (often approximated with the channel slope); an estimation of the roughness coefficient for the channel. The one-dimensional Manning-Strickler equation is then used for the computation of velocity. For this method to be accurate, the cross section has to be representative of the reach, and the channel slope, water-surface slope and energy slope should be parallel. A range of roughness parameter was applied to account for the uncertainty in its estimation, resulting in a range of possible discharges. This range however does not account for other sources of uncertainty, such as the change in channel section during the flood, and may underestimate the actual uncertainty.

Important information is also collected on the site from different sources, such as official reports of fire brigades, police, civil protection, interviews with eyewitnesses, photos or movies of the flood. Velocity of floating objects for example was computed taking the time of passage between two landmarks (Marchi *et al.* 2009). This information was integrated with the other to reconstruct the time of raising flow as well as the time of flood peak and the rate of recession. The number of subbasins analyzed in each event together with their area is presented in table 3.2.

Table 3.2: Number of subbasins and range of areas for each flood event

Event	Date	Number of sub-basins	Range of subbasin areas [km^2]
Sesia at Quinto	04/06/2002	9	75-982
Feernic at Simonesti	23/08/2005	9	5-167
Clit at Arbore	30/06/2006	2	12-36
Grinties at Grinties	04/08/2007	3	11-52
Sora at Vester	18/09/2007	4	32-212
Fella at Moggio	29/08/2003	10	10-623

Climate, annual water balance, land use and geology

For each site data have been collected on potential evapotranspiration, mean annual precipitation and runoff. In order to understand the conditions of the soil before the flood, the annual data were compared with precipitation from the month before the event. An index was derived (Marchi *et al.* 2010) that was used as an indication for the hydrological simulations. The flood analysis included thematic maps on land use, lithology, soil as well as the digital elevation model (DEM) for each case. The DEM we use in our study for the derivation of the flood paths has a resolution between 12.5 to 80 meters depending on the event. An important feature of the

Alpine catchments is that at higher elevations they have portions of bare rock which can contribute greatly to floods. Lakes and artificial reservoirs are sometimes present, but because of their relatively small drainage areas, we considered their attenuation on flood hydrograph to be of minor effect.

Sesia at Quinto

The Sesia river is a tributary of the Po river, in the Piedmont region of Italy. The area covered is characterized by three pluviometric regimes: the plane, where the mean annual precipitation (MAP) ranges from 900 to 1100 mm; the pre-alpine area, with MAP up to 2000 mm; the inner alpine area, with a decrease in MAP to 1400-1600 mm. The mountain part of the basin has steep slopes, with thin soils and a large portion cover by forests. In the plain there are agricultural cultivations, mainly rice, and urban areas, the largest being Biella with a population of 45000 people. The rain gauge network is pretty dense, with approximately o gauge every 100 km^2, while the discharge was measured by 6 stream gauges within the 2586 km^2 catchment (Fig. 3.2).

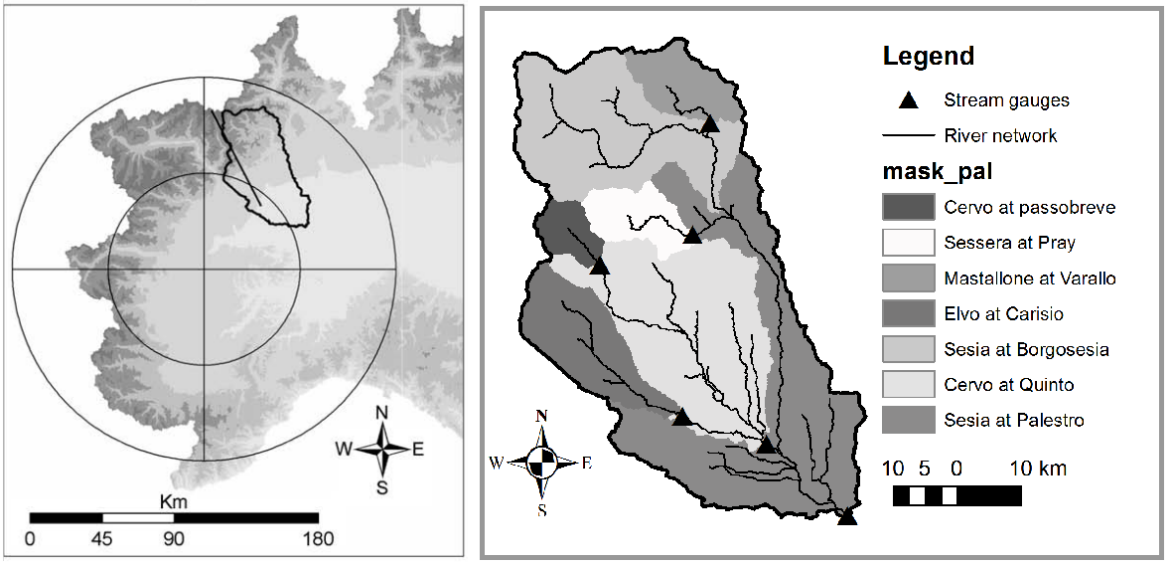

Figure 3.2: **Position of the basin in North-West Italy and subdivision of the study catchment into nested sub-basins.**

As we can see from figure 3.3 during the 4-5 June 2002 storm locally we had over 400 mm of cumulated precipitation over 22 hours and intensities exceeding 80 mm/h (Sangati *et al.* 2009).

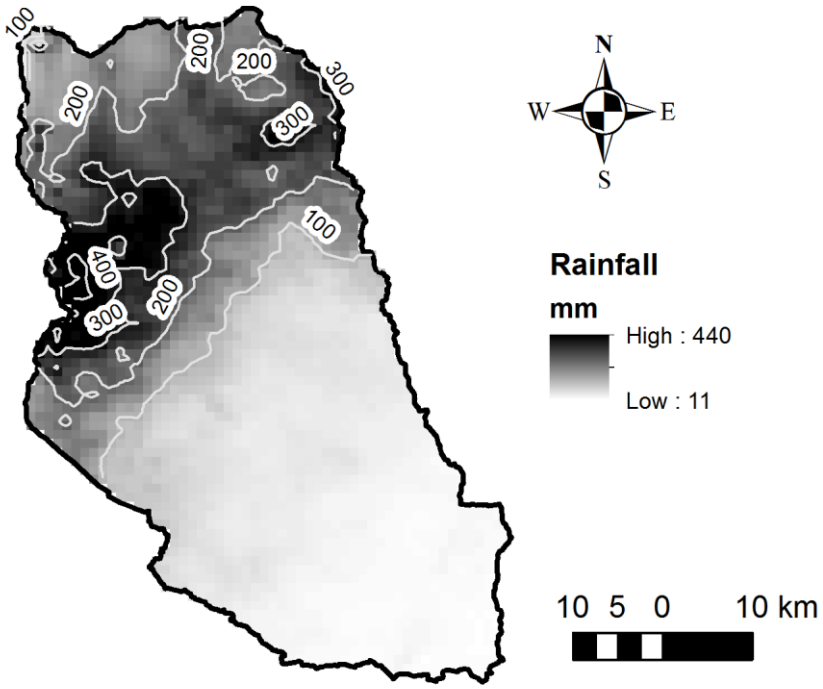

Figure 3.3: rainfall distribution above the Sesia catchment for the June 2002 flood.

The storm produced record flood peaks of 3944 $m^3 s^{-1}$ over the 2586 km^2 basin, and a large number of landslides. The observed flood hydrograph, and the hydrographs simulated by the calibrated hydrological model, are reported in figure 3.4.

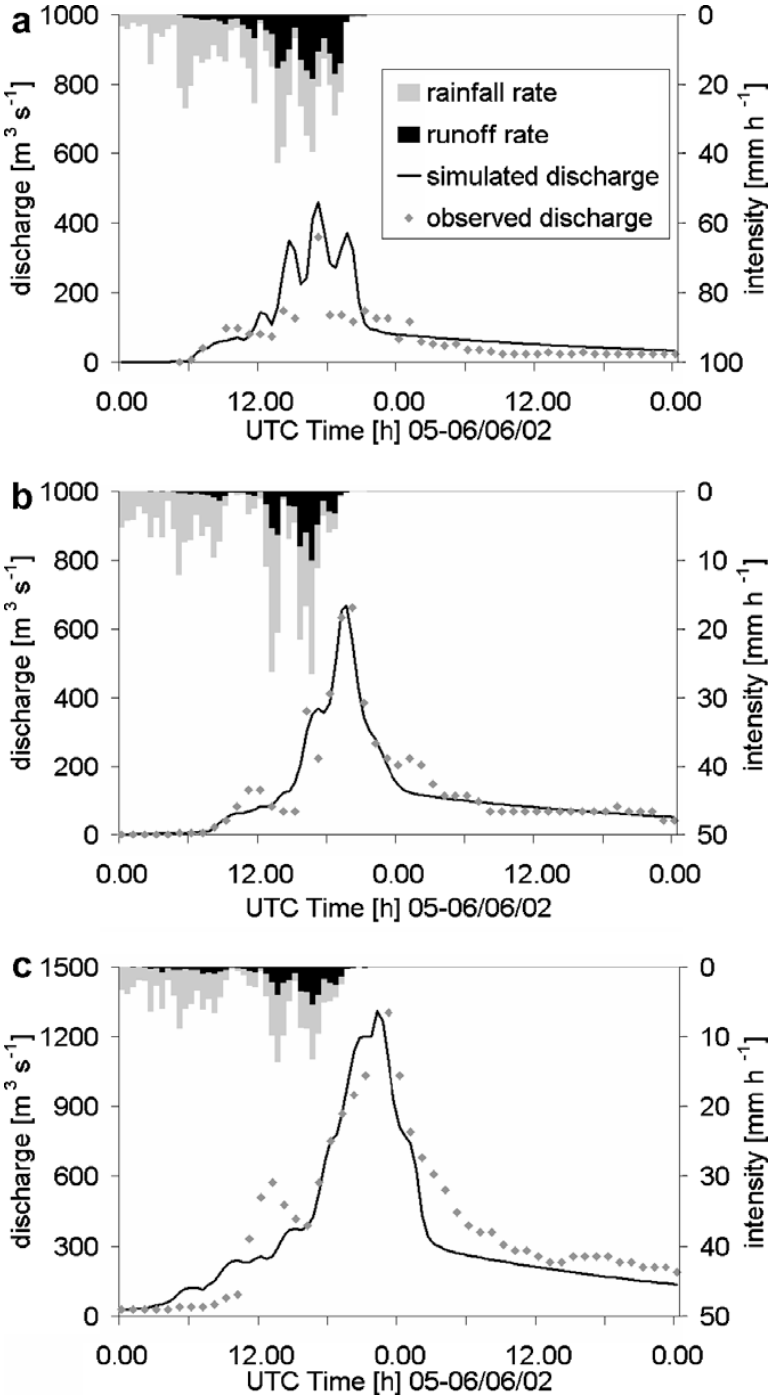

Figure 3.4: Observed and simulated discharge for three stream gauges: (a) Cervo at Passobreve [75 km2]; (b) Elvo at Carisio [261 km2]; (c) Cervo at Quinto [982 km2].

Soil at the begin of the event was wet, with up to 805 mm of rainfall recorded in the 30 days before the flood. This factor is likely to have an influence on the exceptional discharges, as other storms with higher mean cumulated rainfall over the same catchment were not able to produce a flood of this intensity (Sangati *et al.* 2009).

Feernic at Simonesti

The Feernic River at Simonesti (167 km^2) is a small stream in the Mures River catchment, with elevations ranging from 432 to 1049 m a.s.l. (mean elevation 637 m a.s.l.) and mean basin slope 23.5%. The mean annual precipitation ranges between 610 and 650 mm, while the 100-year 24-h rainfall slightly exceeds 100 mm. The geological properties are quite varied, with the upper part of the basin characterized by the volcanic lava and pyroclastic rocks of Harghita Mountains, and the lower by the flysch (marls and clays) of the Transylvanian Subcarpathians. Forests (about 20% of the basin surface) are composed by conifers and beeches on the mountain part of the basin; beeches and chestnut oaks on the hilly part. The percentage of arable soils is 20‑25% and the rest of the land is used as pastures and meadows. Two small towns (Lupeni and Simonesti, with 4600 and 3600 inhabitants, respectively) are located in the floodplain. A streamgauge station is in operation in Simonesti since 1961. The highest peak discharge recorded before the 2005 event amounts to 131 $m^3 s^{-1}$ measured in 1975, while the average discharge is 1.11 $m^3 s^{-1}$. During the flood event, the station was partially damaged and it went out of order for 2 h; however, loss of information was relatively minor, and the combination of observed data and of data from a post-event survey carried out in the weeks following the event afforded the reconstruction of the flood hydrograph. The post-event survey enables also estimation of the peak in other two upstream river sections (Fig. 3.5).

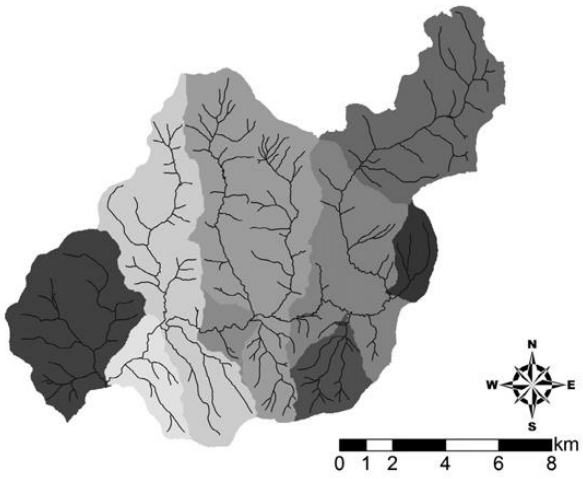

Figure 3.5: Subdivision of the Feernic at Simonesti catchments into nine nested sub-basins.

Only daily raingauge stations are available in the catchment; hence, the rainfall estimation is based on the processing of radar reflectivity values in combination with the daily raingauges and the hourly raingauges of the neighboring basins. As a consequence of the flood, 16 people died in Lupeni and Simonesti, and a large portion of the urban area in the floodplain was flooded and damaged. The storm lasted for 5 h, starting at 12:00 UTC, with a catchment average depth of 76

mm. The time series of basin-averaged rain rate shows a steady increase from 12:00 UTC to the precipitation peak at 15:30 UTC, followed by a period of lower intensity, until around 17:00 UTC. The period of extreme rainfall began at 14:00 and lasted until 15:30. This chronology of storm evolution corresponds with eyewitnesses accounts placing the beginning of extreme rainfall and its rapid transformation to extreme rain rates between 14:00 and 15:00 UTC. The storm exhibited a striking spatial variability, with the precipitation concentrated in the medium and upper part of the catchment, where rainfall accumulation in some places exceeded 190 mm (figure 3.6).

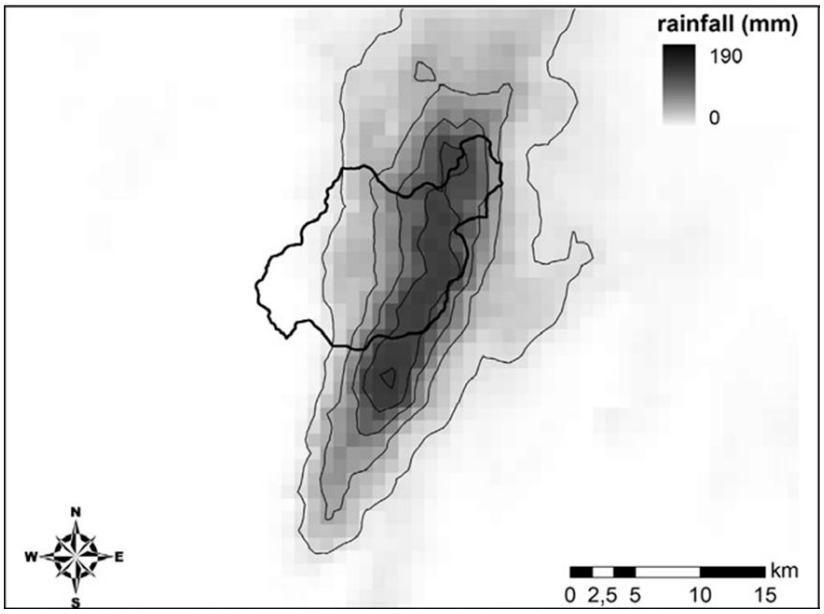

Figure 3.6: rainfall distribution above the Feernic catchment for the 23 August 2005 flood.

The high spatial variability is a consequence of a significant orographic effect, which played an important role in regulating of atmospheric moisture inflow to the storm and in controlling storm motion and evolution. Small catchments in this area had specific contribution reaching 7-8 $m^3 s^{-1} km^{-2}$, as confirmed by the post-event analysis. Rainfall was much less close to the catchment outlet. The flood peak at Simonesti was estimated around 370 $m^3 s^{-1}$, corresponding to 2.2 $m^3 s^{-1} km^{-2}$ (fig. 3.7).

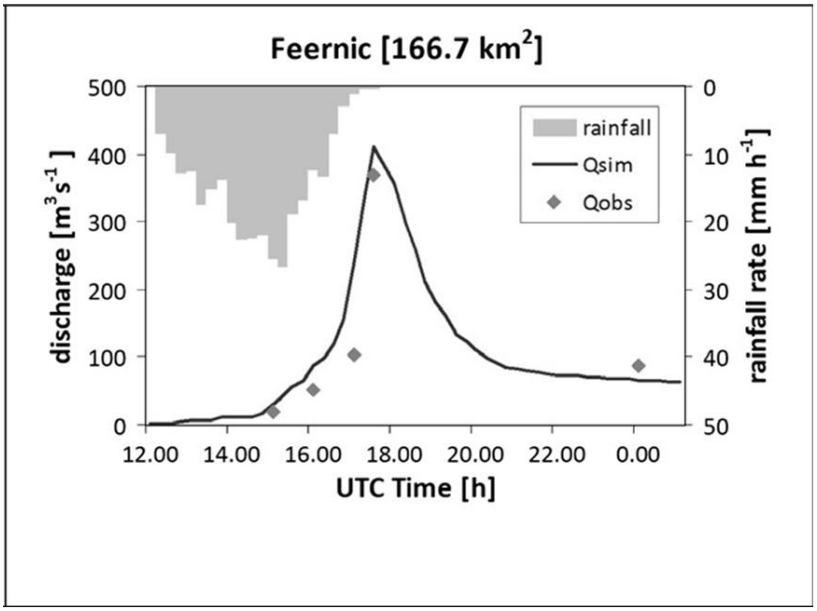

Figure 3.7: Observed and simulated discharge for stream gauges of Feernic at Simonesti [167 km^2]

Based on the observations gathered, the event runoff coefficient is around 0.22, with values much higher (up to 0.6) in the upper portions of the catchment which received the highest rainfall accumulation and intensities. The soil moisture status at the start of the event was moderately wet, as a consequence of a wetter-than-average 30 days period before the flood (with 177 mm of rain compared to 77 mm resulting from the climatological average over the same period).

Clit at Arbore

The Clit river is a tributary of the Solca River in Romania. The Clit catchment closed at Arbore (36 km^2) represents a typical headwater basin of this river system, with elevation ranging from 357 to 928 m a.s.l., and mean slope of 8.4%. Mean annual precipitation is around 620 mm. The 100-year 24-h rainfall is higher than for the Feernic catchment and amounts to 144 mm. The geological properties are rather homogeneous, with almost all the catchment characterized by the semi-permeable rock formation of the mollasse. Forests (about 56% of the basin area) range from conifers to broad leaves. The percentage of arable soils is 25% and the rest of the land is used as pastures and meadows. On June 30th, 2006, the storm event started around 18:00 UTC, lasting for 4 h, although the explosive growth of precipitation occurred in the first 2 h. Extreme rainfall amount was measured in the central portion of the catchment, with values around 130 mm (figure 3.8).

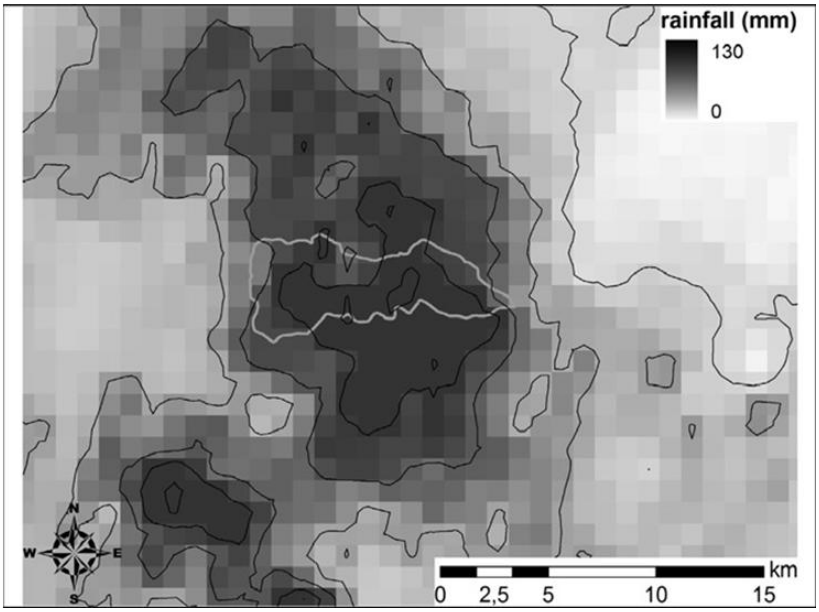

Figure 3.8: rainfall distribution above the Clit catchment for the 30 June 2006 flood.

The catchment average rainfall amount was estimated 80.5 mm. The soil moisture status at the start of the event was moderately wet, as a consequence of a wetter-than-average 30 days period before the flood (with 163 mm of rain compared to 99 mm resulting from the climatological average over the same period). No streamgauge stations are available in the catchment. For this reason, all observations concerning the peak magnitude and timing in the catchment were obtained by means of a post-event survey carried out during 3 weeks after the event. The peak discharge at Arbore was estimated by using a critical-depth method on three different cross sections. Jarrett and England Jr (2002) found that averaging multiple critical-depth estimates (three to six) leads to increase considerably the reliability of peak discharge estimates based on field surveys. This led to an estimate of 175 m^3s^{-1}, corresponding to unit peak discharge of 4.9 $m^3s^{-1}km^{-2}$ (figure 3.9). According to an eyewitness, flooding started around 18:30 with the peak time in the period 19:45‑20:15. Around 22:30 the flooding ended and the discharge was less than the channel conveyance (i.e., 50 m^3s^{-1}) (according to observed water levels). As a consequence of the flood, 11 people died in Arbore and heavy damages to both houses and infrastructures were reported.

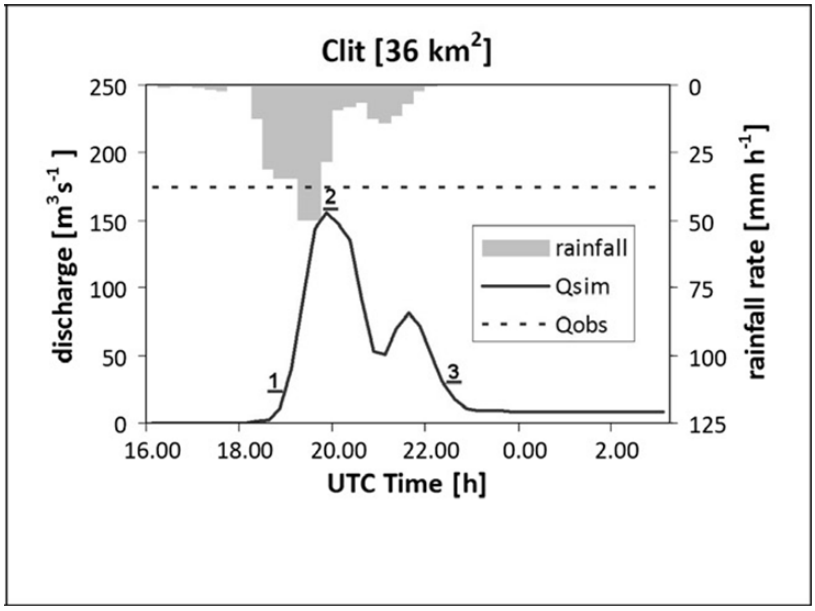

Figure 3.9: Observed and simulated discharge for the Clit at Arbore catchment [36 km^2]

Grinties at Grinties

The Grinties River is a tributary of the Bistricioara River in Romania. The Grinties river catchment closed at Grinties (52 km^2) represents the highest headwater basin examined in this work, with elevation ranging from 545 to 1736, and with mean basin slope of 32%. Mean annual precipitation in this area is around 660‑700 mm, whereas the 100-year 24-h rainfall is intermediate between the case of Feernic and that of Clit, amounting to 108 mm. The geological properties are quite diverse, with 36% of the catchment characterized by the flysch formation and 55% by a metamorphic impermeable geology. Forests (about 81% of the basin area) represent the most important land cover, with the remaining land mainly used as pastures. On August 4, 2007, the storm event started around 14:00 UTC, lasting for 3 h, and with 90% of the precipitation falling within 2 h. The storm rainfall volume was around 66.8 mm, with peaks exceeding 100 mm in the central part of the catchment (figure 3.10).

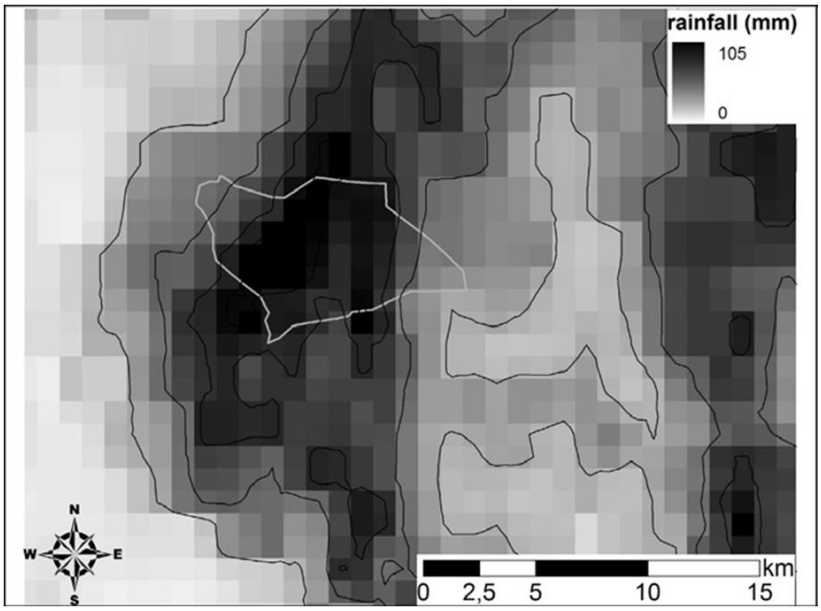

Figure 3.10: rainfall distribution above the Grinties catchment for the 7 August 2004

The soil moisture status at the start of the event was moderately wet (precipitation in the 30 days period before the flood amount to 130 mm, which has to be compared with the climatological amount in the same period, equal to 103). Since no streamgauge stations are available in the catchment, all observations on the event were collected during a survey organised 2 months after the flood. The peak discharge at Grinties (a small town of around 800 inhabitants) was estimated based on the survey of the post-flood river section geometry and by using a critical section method. This led to an estimate of 100 $m^3 s^{-1}$, corresponding to almost 2.0 $m^3 s^{-1} km^{-2}$ (fig. 3.11). Accounts from a number of eyewitnesses were collected and intercompared. The accounts indicates that flooding started in the period between 15:00 and 15:30, reaching the peak between 16:30 and 17:00. Around 17:30 the flooding ended and the discharge was less than 50 $m^3 s^{-1}$ (according to observed water levels). One casualty was reported in relation to the event. Moreover, three bridges were destroyed and 36 buildings were flooded and damaged.

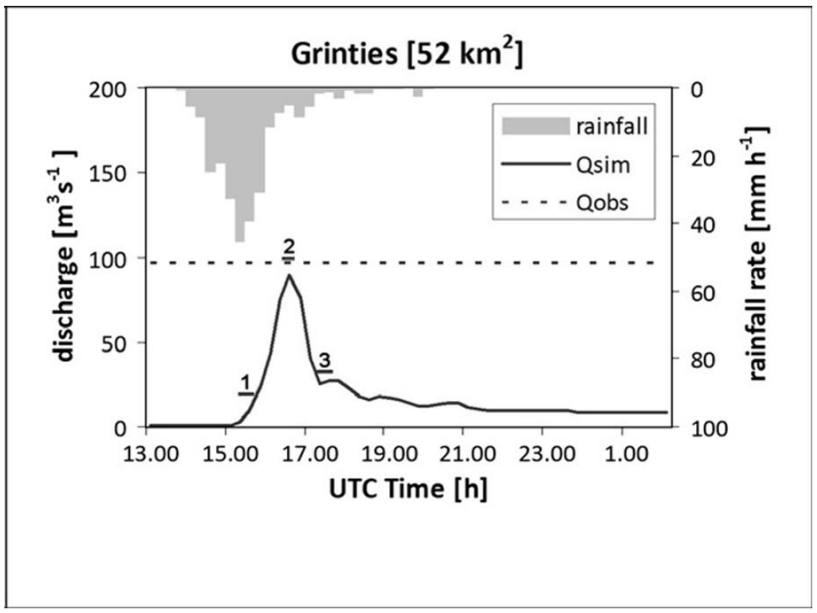

Figure 3.11: Observed and simulated discharge for the catchment of Grinties at Grinties [52 km^2]

Sora at Vester

The Selška Sora river basin is a tributary of the Sava River system, and it is located in the alpine area of North-West Slovenia. The basin is characterized by steep topographic relief (400‑2864 m a.s.l.) and thin soils over hillslopes. Annual rainfall in this region can reach up to 3300 mm, decreasing from West to East due to a rain shadow effect. Forest is the main land use, with grassland and grazing in the floodplains. Miocene clastic rocks prevail and karst features are observed only in relatively small catchments, generally located in the northern portions where some alpine karst plateau are found. The monitoring network is composed of 47 rain gauges (14 measuring hourly discharge) and a C-band radar about 80-100 km from the watershed. Two stream gauges are located within the catchment (figure 3.12), but the Zelezniki steam gauge was damaged during the flood peak.

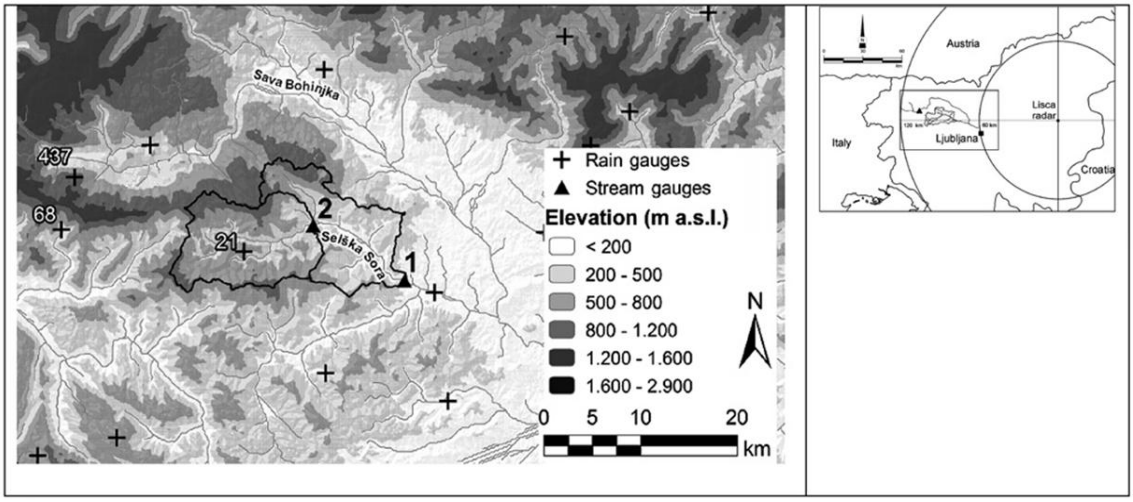

Figure 3.12: distribution of rain gauges and stream gauges for the Sora at Vester catchment. The stream gauges are located at 1) Vester and 2) Zelezniki.

The 18^{th} September 2007 storm was originated by a Mesoscale convective system. Different basins of the region were affected by floods, with six casualties and damages estimated around 0.3 billion Euros (Marchi *et al.* 2009; Rusjan *et al.* 2009). The storm was organized in well defined bands along the West-East direction, with a length of 60-70 km and a width of 8-12 km. Within these bands rainfall cells moved at velocities of 60-70 $km\,h^{-1}$. Neighboring basins had very different hydrologic response because of the strong rainfall gradients generated. Precipitation lasted from 5:00 to 17:00 UTC, with a peak between 9:30 and 10:00 and maximum accumulations over 1h of 72 mm. Local rainfall accumulations over the 12h are exceeding 350 mm (fig. 3.13).

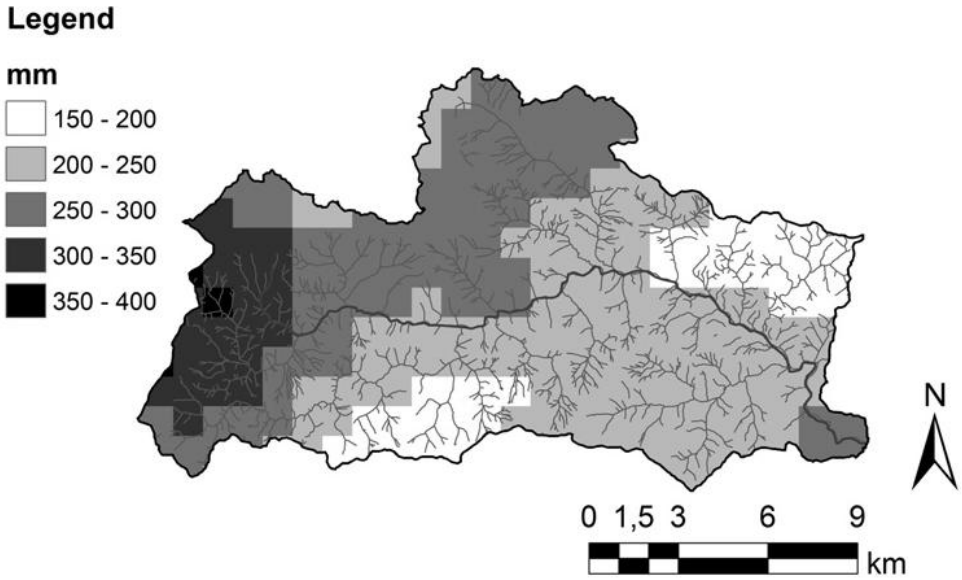

Figure 3.13: rainfall distribution above the Sora at Vester catchment for the 18 September 2007 flood.

The flood hydrograph measured at Vester is sharp and peaky, contrasting with neighboring karst catchments, and the peak discharge was estimated in 351 m^3s^{-1} (fig. 3.14). In basins up to 25

km^2 the unit peak discharges were estimated to be between 5 and 7 $m^2 s^{-1} km^{-2}$. The soil conditions before the storm were dry, with a less than average precipitation in the 30 days before, and probably had an influence in the low runoff coefficients observed (Zanon *et al.* 2010).

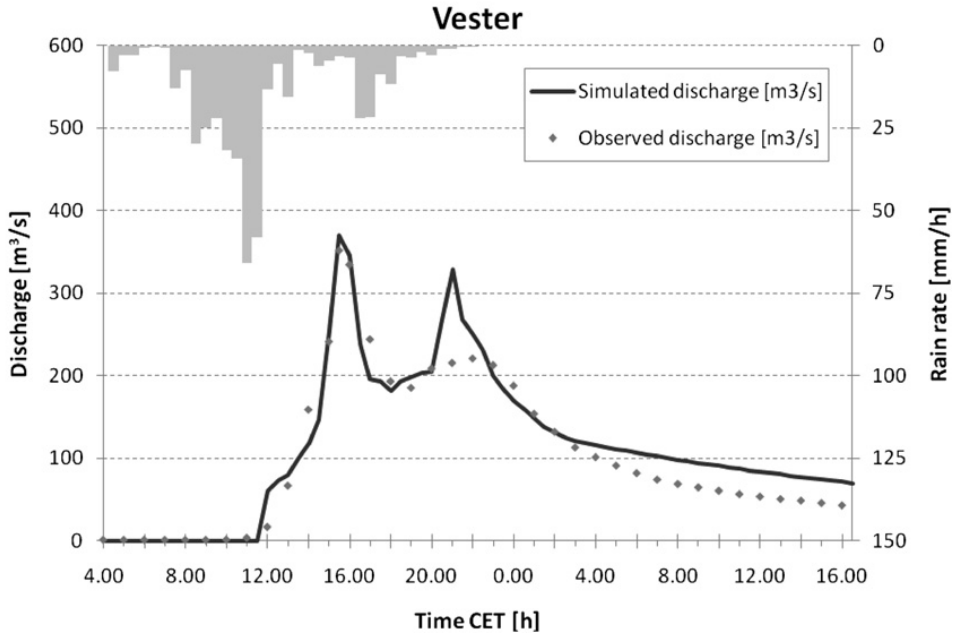

Figure 3.14: Observed and simulated discharge for the catchment of Sora at Vester [212 km^2]

Fella at Moggio

The catchment of Fella at Moggio is located in the Eastern Italian Alps, at the border with Austria and Slovenia. This area is often affected by heavy precipitations that, because of the fractured bedrock and mountainous orography, can translate into flash floods, landslides and debris flows. The Fella at Moggio basin covers 623 km^2, with elevations between 300 and 2000 m a.s.l.. The mean annual precipitation in the pre alpine area, which includes the southern part of our basin, can be up to 3000 mm, while in the inner alpine area the MAP is between 1600 and 1800 mm. The area is mainly composed of limestone and calcareous Flysch, in some portion karsified, and it is tectonically active resulting in faults and overthrusts. The urbanization in the area is low, and the main land use is forest. The monitoring network includes 15 rain gauges and 6 stream gauges (figure 3.15), beside information from the C-band radar located approximately 80 km South.

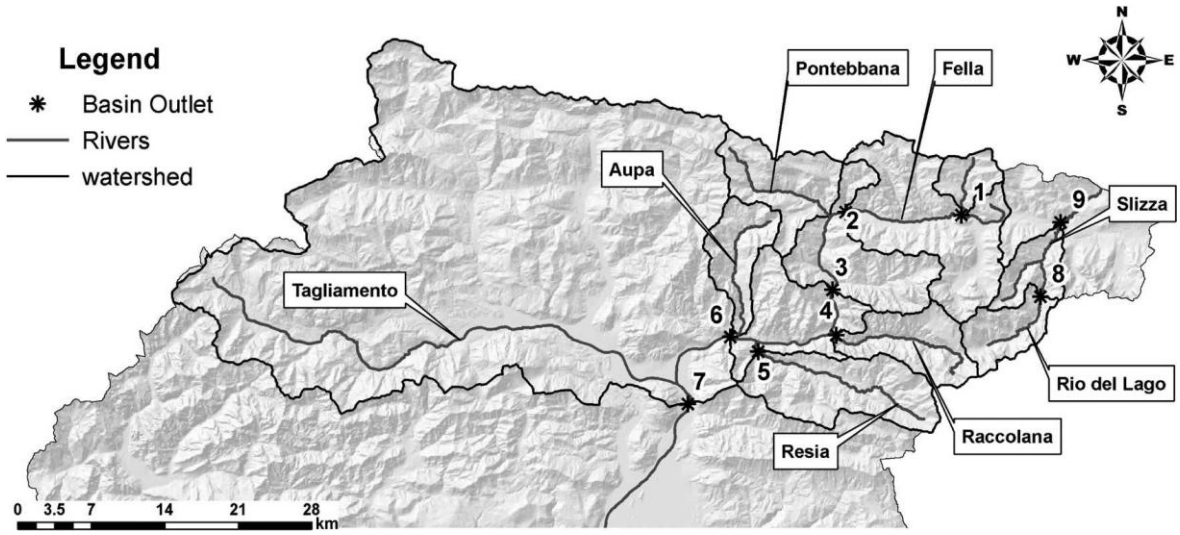

Figure 3.15: Catchment map of the upper Tagliamento River basin, with subcatchments of the Fella River basin: 1) Uqua at Ugovizza; 2) Fella at Pontebba; 3) Fella at Dogna; 4) Raccolana at Raccolana; 5) Resia at Borgo Povici; 6) Fella at Moggio Udinese. Sections 7, 8 and 9 are not included in this study. From Borga *et al.* (2007).

On the 27th August 2003 rainfall started at 9:00 UTC and lasted 12 hours. The mesoscale convective system persisted in the area, generating over 400 mm of rainfall locally (figure 6.00) with high spatial variability. Rainfall intensities in the 15 minutes reached 130 $mm\ h^{-1}$.

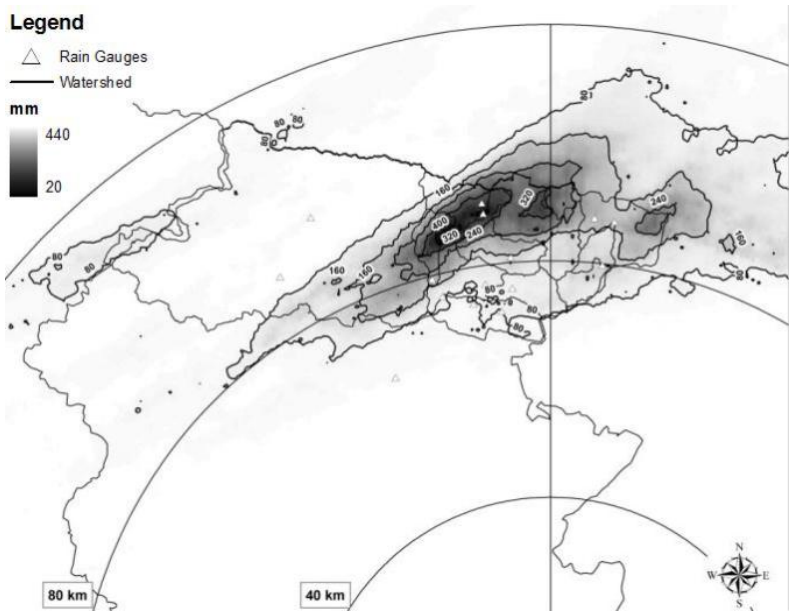

Figure 3.16 Storm total rainfall (mm) in the Friuli Venezia Giulia region for the August 29, 2003 event. The circle represents the distance from the radar.

The antecedent conditions were dry, after a severe summer draught, and this limited the runoff ratios to range between 0.04 and 0.2 (Borga *et al.* 2007). Despite the low runoff coefficients, the specific peak discharges measured during post event surveys exceeded $8\ m^3 s^{-1} km^{-2}$. The hydrographs observed at Pontebba [164.5 km^2] and Moggio Udinese [623 km^2] are reported in

Figure 3.17. The area of Pontebba had the higher precipitations, and it is worth to note a unit peak discharge of 4 $m^3 s^{-1} km^{-2}$ in a catchment of 164.5 km^2.

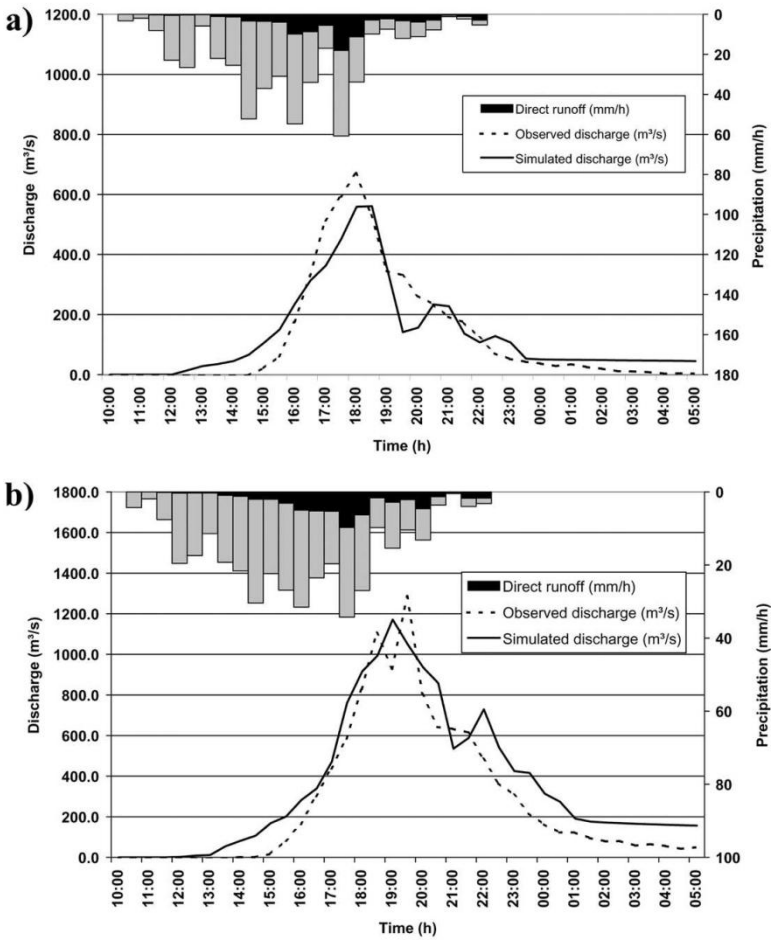

Figure 3.17: observed and simulated discharge for two nested Fella basins closed at (a) Pontebba [164.5 km^2], and (b) Moggio Udinese [623 km^2]. From Borga *et al.* (2007).

3.2. Hydrological model employed

A simple spatially distributed hydrologic model was employed for the simulation of the Flash Flood events and for the validation of the assumptions used in the development of *spatial moments*. In this model the discharge $Q(t)$ [$L^3 T^{-1}$] at the catchment outlet is computed as:

$$Q(t) = Q_g(t) + Q_s(t) \qquad 3.1$$

Where $Q_g(t)$ [$L^3 T^{-1}$] is fraction of discharge at the outlet from subsurface runoff and $Q_s(t)$ [$L^3 T^{-1}$] is the fraction from surface runoff.

Using the Green-Ampt infiltration model with moisture redistribution (Ogden and Saghafian 1997) rainfall in each point of the catchment $P(x, y, t)$ is divided into surface and subsurface runoff

components at point *(x,y)* and time *t*. The Green-Ampt model was chosen as it is a physically based method that provide a simple, but not simplistic (Barry *et al.* 2005), description of the infiltration mechanisms.

A simple drainage system (Da Ros and Borga 1997) is used to propagate surface runoff. From the point *(x,y)* where the runoff is generated the water follows the steepest descending path until the catchment outlet. The surface runoff component of eq. 3.1, $Q_s(t)$, is the sum of surface runoff generated around the catchment at different times $q_s(x,y,t)$ [L^3 T^{-1}] and then conveyed to the catchment outlet. In this propagation a distinction is made between hillslope and channel elements. This division is due to the fact that the velocity of propagation processes in hillslopes and channels differ by orders of magnitude. Each point is defined as hillslope or catchment by using a channelization support area A_s [L^2]. Discharge $Q_s(t)$ [L^3 T^{-1}] at the outlet of the basin is represented by:

$$Q_s(t) = \int_A q_s[x,y,t-\tau(x,y)]dA \qquad 3.2$$

Where $\tau(x,y)$ [T] is the routing time from the location *(x,y)* to the outlet of the basin, defined as:

$$\tau(x,y) = \frac{L_h(x,y)}{v_h} + \frac{L_c(x,y)}{v_c} \qquad 3.3$$

Where $L_h(x,y)$ [L] is the distance from a generic point to the channel network measured though the flow paths and $L_c(x,y)$ [L] is the distance of the subsequent path through the channel network to the basin outlet. The parameters v_h and v_c [L T^{-1}] are two invariant hillslope and channel velocities. Different authors used hydrological models based on infiltration and invariant velocities to simulate Flash Floods (Zhang *et al.* 2001; Giannoni *et al.* 2003; Borga *et al.* 2007; Javier *et al.* 2007; Sangati 2009). This approximation for channel propagation is based on the observation that average flow velocities reach an asymptotic value at high flows (Pilgrim 1976), as it is the case for Flash Floods. The model is thus expected to propagate the flow too fast in the early stage of the storm, generating a steeper rise of the hydrograph compared to observations. The use of an invariant velocity to represent hillslope propagation instead is more conceptual (Botter and Rinaldo 2003). It derives from the great variability of velocities due to local topographic gradients, distribution of partially saturated areas and of preferential flow paths (Dunne 1978; Beven and Wood 1983). The fraction of rainfall that infiltrates goes into a linear conceptual reservoirs, used to model the subsurface fraction of flow at catchment scale (Borga *et al.* 2007). In total the model requires the calibration of six parameters: the channelization support

area, two kinematic propagation parameters and three soil hydraulic parameters used by the Green-Ampt method.

Depending on single events the model used DEM and soil parameter maps with resolutions between 12.5 and 80 meters and timesteps of 15 or 30 minutes. Rainfall estimations were prepared with a spatial resolution of 1 km^2.

In each event the model parameters were estimated over the catchments by a combination of manual and automatic calibration that aimed at minimizing: the Nash Sutcliffe efficiency index for the gauged catchments; the mean square error over the flood peaks estimated though IPEC and to reproduce the timing of the during its development, peak and recession. Details on the calibration of individual events are reported in the relative papers (see table 3.1). Note that the linear routing and the subsurface approach taken by the model are more suitable, and achieved better result, in describing smaller catchment.

Influence of spatial variability on runoff modelling

To isolate the effect of rainfall spatial variability and of storm motion over the simulated hydrographs we simulated and compared these scenarios. In the first scenario, termed *'distributed rainfall*', the input rainfall for the hydrological model consisted in the real radar estimates. These rainfall estimates are the best available for the study and are considered as reference. The second scenario analyzed is the '*uniform rainfall'*. Here rainfall is transformed into a spatially uniform input, preserving the temporal distribution over the catchment. Lastly, we analyzed the '*constant pattern*' scenario, where once again rainfall temporal distribution is maintained, but the pattern of spatial distribution is constant in time and equal to the pattern of cumulated rainfall. The distribution of rainfall cumulated over the whole event in this scenario is identical to the reference distributed case. The difference in hydrograph shape between the first and second scenarios represent the effect that rain spatial distribution has on the flood. The difference between the hydrograph of the first and third scenarios instead describe the effects of neglecting storm motion during the simulation.

4. Spatial moments of catchment rainfall: definition and application to a set of extreme flash floods

As we reported in section 2.1, many hydrological studies have focused on the role of rainfall space-time variability in catchment response, with the aim of developing a rationale for more effective catchment monitoring, modeling and forecasting. From a practical perspective, it is important to know at what space-time scales rainfall has to be monitored, given certain catchment and flood characteristics, and what are the effects of space-time aggregations on model simulations (Berne *et al.* 2004).

An important feature frequently observed in these studies is that catchments act as space-time filters (Skøien and Blöschl 2006) with specific dampening characteristics to the rainfall input. The filtering properties may be strong enough to efficiently smooth out some features of rainfall spatial variability. This means that only some specific characteristics of rainfall spatial organisation will eventually emerge as runoff spatial and temporal variability (Skųien *et al.* 2003). Thus we believe there is a need to introduce measures to quantify the catchment filtering effect which, as a function of rainfall organization, basin scale and the heterogeneities embedded in the basin geomorphic structure, control the possible extent of the influence of rainfall spatial organization on the hydrologic response. As we explained in section 2.3 of this work, the rainfall spatial organization is analyzed with respect to the flow distance, i.e. the distance along the runoff flow path from a given point to the outlet.

The statistics analyzed builds upon the work presented in Woods and Sivapalan (1999) and *Viglione et al. (2010)*. The framework developed in these papers quantifies the contributions of the space-time variability of precipitation, runoff coefficient, hillslope and channel routing to the flood runoff volume and the delay and spread of the resulting hydrograph. The aim there was to analyze rainfall-runoff events (and ways of modeling them) by subdividing the characteristics of the hydrological response into its components. In the present work we reorganize some of these components, by introducing a set of statistics of spatial rainfall organisation measured along the flow distance which are relevant to the analysis of the runoff response. These statistics, termed '*spatial moments of catchment rainfall*', are dimensionless numbers that can be used to establish relationships valid over a wide range of scales. They provide a synthesis of the interaction between rainfall and basin morphometric properties and are useful similarity measures for "comparative hydrology" studies. For instance, in this work we show, both analytically and empirically, how these statistics can be used to quantify the influence of spatial rainfall organization on flood hydrograph characteristics and we compare a number of events in several

catchments. The method based on the *spatial moments of catchment rainfall* provides a theoretical foundation for various measures of rainfall spatial variability based on the flow distance coordinate, which have been reported in the literature in the last decade (Smith *et al.* 2002; Syed *et al.* 2003; Smith *et al.* 2005; Sangati and Borga 2009). Moreover, they extend to the case of runoff propagation under condition of spatial rainfall variability the concept of spatial moments used for analysis of solute transport in porous media (Goltz and Roberts 1987). The development of this similarity, which is not pursued in this paper but is subject of current investigation, aims to order theoretical results that appeared in disparate fields into a coherent theoretical framework for both hydrologic flow and transport, as shown by (Rinaldo *et al.* 2006).

As part of this analysis, we show how the introduction of the spatial moments of catchment rainfall permits derivation of a simple relationship for the quantification of storm velocity at the catchment scale. As we said in the State of the Art, the importance of storm movement on surface runoff has been investigated for nearly four decades. However, to the best of our knowledge, these works are based on 'virtual experiments' using idealized storm profiles and motion as input to watershed models. Results seem to support the conclusion that catchment response is sensitive to storm motion relative to catchment morphology, depending on different processes and scales. With this work we show how it is possible to isolate and quantify the *'catchment scale storm velocity'*, generated by imposing a prescribed space-time storm variability to the catchment morphological properties.

In the following developments, we disregard the differentiation between hillslopes and channel network to the total runoff travel time. While in chapter 5 the methodology will be extended to include a hillslope term, we prefer here to focus on the interaction between the morphological catchment properties and rainfall organisation. The investigations of chapter 5 aim to examine the impact of varying the hillslope residence time on both the spatial moments of catchment rainfall and the catchment scale storm velocity.

The conceptual meaning of the spatial moments is illustrated analyzing five extreme flash floods occurred in various European regions in the period 2002-2007. High resolution, carefully controlled, radar rainfall fields and a spatially distributed hydrologic model are employed to examine the use of these statistics to describe the degree of spatial rainfall organisation which is important for runoff modelling, with a focus on runoff timing. The size of the study catchments ranges between 36 to 982 km^2. Hillslope residence time and spatial variability of runoff ratio, which are disregarded in the derivation of the spatial moments, are included in the distributed hydrological model. Therefore, contrasting model results with information inferred from the

spatial moments provides a necessary evaluation of the impact of the working assumptions on the use of these statistics, at least in the context of extreme floods.

The outline of this chapter is as follows. In Section 4.1 we define the statistics termed *'spatial moments of catchment rainfall'*. In Section 4.2 we show how these rainfall statistics can be related to the flood hydrograph properties. Section 4.5 is devoted to illustrate the derivation of the spatial moments of catchment rainfall for the five flood events. In Section 4.5 we perform numerical experiments in which modelled flood response obtained by using detailed spatial input is contrasted with the corresponding flash flood response obtained by using spatially uniform rainfall. Runoff model sensitivity to spatial organisation of rainfall is examined by exploiting the spatial rainfall statistics. Section 4.6 completes the chapter with discussion and conclusions.

4.1. Definition

Spatial moments of catchment rainfall provide a description of overall spatial rainfall organization at a certain time t, as a function of the rainfall field $r(x,y,t)$ $[L\,T^{-1}]$ value at any position *x,y* inside the watershed and of the distance $d(x,y)[L]$ between the position *x,y* and the catchment outlet measured along the flow path. The *spatial moments of catchment rainfall* are defined after rearranging some of the covariance terms employed in Viglione *et al.* (2010) to represent the mean and the variance of the network travel time, under the hypothesis of constant flow velocity (Appendix A). The n^{th} spatial moment of catchment rainfall p_n $[L^{n+1}T^{-1}]$ is expressed as:

$$p_n(t) = A^{-1} \int_A r(x,y,t) d(x,y)^n dA \qquad 4.1$$

where A $[L^2]$ is the spatial domain of the drainage basin. The zero-th order spatial moment $p_0(t)$ yields the average catchment rainfall rate at time t.

Analogously, the g_n $[L^n]$ moments of the flow distance are given by:

$$g_n = A^{-1} \int_A d(x,y)^n dA \qquad 4.2$$

The zero-th order spatial moment of flow distance yields unity. Non-dimensional (scaled) spatial moments of catchment rainfall can be obtained by taking the ratio between the spatial moments of catchment rainfall and the moments of the flow distance, as follows, for the first two orders :

$$\delta_1(t) = \frac{p_1(t)}{p_0(t) g_1} \qquad 4.3$$

$$\delta_2(t) = \frac{A^{-1}\int_A r(x,y,t)[d(x,y)-\delta_1 g_1]^2 dA}{A^{-1}\int_A r(x,y,t) dA A^{-1}\int_A [d(x,y)-g_1]^2 dA} = \frac{1}{g_2 - g_1^2}\left[\frac{p_2(t)}{p_0(t)} - \left(\frac{p_1(t)}{p_0(t)}\right)^2\right]$$

where for the second order the central moment is reported. The first scaled moment $\delta_1\,[-]$ describes the distance of the centroid of catchment rainfall with respect to the average value of the flow distance (i.e.: the catchment centroid). Values of δ_1 close to 1 reflect a rainfall distribution either concentrated close to the position of the catchment centroid or spatially homogeneous, with values less than one indicating that rainfall is distributed near the basin outlet, and values greater than one indicating that rainfall is distributed towards the catchment headwaters.

The second scaled moment $\delta_2\,[-]$ describes the dispersion of the rainfall-weighted flow distances about their mean value with respect to the dispersion of the flow distances. Values of δ_2 close to 1 reflect a uniform-like rainfall distribution, with values less than 1 indicating that rainfall is characterized by a unimodal distribution along the flow distance. As we will see below, values greater than 1 are generally rare, and indicate cases of multimodal rainfall distributions.

The spatial moments defined in Eq. 4.3 describe the instantaneous spatial rainfall organization at a certain time t. Eq. 4.1 to 4.3 can also be used to describe the spatial rainfall organization corresponding to the cumulated rainfall over a certain time period T_s (e.g., a storm event). These statistics, which are obtained by integrating over time, are termed P_n and Δ_n. These statistics are defined as follows:

$$P_n = A\int_A r_t(x,y) d(x,y)^n dA = \frac{1}{T_s}\int_{T_s} p_n(t) dt \qquad 4.4$$

where $r_t(x,y)$ is the mean value of time integrated rainfall at location *(x,y)*. Δ_1 and Δ_2 are computed based on P_n following Eq. 4.3, as follows

$$\Delta_1 = \frac{P_1}{P_0 g_1} \qquad 4.5$$

$$\Delta_2 = \frac{1}{g_2 - g_1^2}\left[\frac{P_2}{P_0} - \left(\frac{P_1}{P_0}\right)^2\right]$$

Definition of catchment-scale storm velocity

The distance from the rainfall centroid to the catchment outlet is represented by the product $\delta_1 g_1$. Interestingly, the analysis of the evolution in time of this distance enables the calculation of an instantaneous catchment-scale storm velocity along the river network, as follows:

$$V_s(t) = g_1 \frac{d}{dt}\delta_1(t) \qquad 4.6$$

Positive values of the storm velocity V_s $[L\,T^{-1}]$ correspond to upbasin storm movement, whereas downbasin storm movement are related to negative values of V_s. The concept of the catchment-scale storm velocity defined by Eq. 4.6 takes into account the role of relative catchment orientation and morphology with respect to storm motion and kinematics. For instance, for the same storm kinematics, the same elongated basin will be subject to different catchment scale storm velocities by varying its orientation with respect to that of the storm motion. In this work, we will not perform any explicit derivative of δ_1 to obtain the catchment scale storm velocity. Equation 4.6 has been introduced only to formally represent the concept of storm velocity and how this relates to the first scaled moment δ_1. A simple way to derive the mean value of V_s, derived from the methodology introduced by Viglione *et al.* (2010) is reported in the next sections.

4.2. Relationship between the spatial moments of catchment rainfall and the shape of the flood response

Viglione *et al.* (2010) proposed an analytical framework (called V2010 hereafter) to quantify the effects of space-time variability on catchment flood response. V2010 extended the analytical framework developed in Woods and Sivapalan (1999) to characterize flood response in the case where complex space and time variability of both rainfall and runoff generation are considered as well as hillslope and channel network routing.

In the V2010 methodology, the rainfall excess $r_e(x,y,t)[L\,T^{-1}]$ at a point *(x,y)* and at time t generated by precipitation $r(x,y,t)$ is given by

$$r_e(x,y,t) = r(x,y,t)c(x,y,t) \qquad 4.7$$

where $c(x,y,t)$ $[-]$ is the local runoff coefficient, bounded between 0 and 1. V2010 characterizes the flood response with three quantities: (i) the catchment- and storm-averaged value of rainfall

excess, (ii) the mean runoff time (i.e., the time of the center of mass of the runoff hydrograph at a catchment outlet), and (iii) the variance of the runoff time (i.e., the temporal dispersion of the runoff hydrograph). The mean time of catchment runoff is a surrogate for the time to peak. The variance of runoff time is indicative of the magnitude of the peak runoff. For a given event duration and volume of runoff, a sharply peaked hydrograph will have a relatively low variance compared to a more gradually varying hydrograph (for details see Woods 1997).

Since the aim of this study is to establish a relationship between the spatial moments of catchment rainfall and the flood response shape, we modified accordingly the V2010 methodology by assuming that the runoff coefficient is uniform in space and time, and that the hillslope residence time is negligible. Hence, in the following developments the rainfall intensity and accumulation are used in place of the rainfall excess. Owing to this assumption, results obtained by this approach are likely to apply to heavy rainfall events characterized by large rain rates and accumulations. The runoff transport is described by using an advection velocity $v\ [L\ T^{-1}]$ which is considered invariant in space and time. The hypothesis of spatially uniform flow velocity is consistent with the results of previous studies, showing that it is always possible to find a single value of flow celerity v such as the mean travel time across the entire catchment and therefore the catchment response time is unchanged (Robinson *et al.* 1995; Saco and Kumar 2002; D'Odorico and Rigon 2003).

The analytical results are summarized below, by focusing on the elements which are essential to derive the relationship between the spatial moments and the characteristics of the flood response shape, i.e. the mean and the variance of runoff time and the catchment scale storm velocity. Catchment runoff time is treated as a random variable (denoted T_q), which measures the time from the storm beginning until a drop of water exits the catchment. Water that passes a catchment outlet goes through two successive stages in our conceptualization: (i) the generation of runoff at a point (including waiting for the rain to fall), (ii) runoff transport. Each of these stages has an associated ‘‘holding time”, which is conveniently treated as a random variable (Rodriguez-Iturbe and Valdes 1979). Since the water exiting the catchment has passed in sequence through the two stages mentioned above we can write

$$T_q = T_r + T_c \tag{4.8}$$

where T_r and T_c are the holding times for rainfall excess and runoff transport.

4.3. Mean catchment runoff time

Using the mass conservation property (see V2010) we can write the mean of T_q as

$$E(T_q) = E(T_r) + E(T_c) \tag{4.9}$$

The first term $E(T_r)$ represents the time from the start of the event to the centroid of the rainfall time series, and is independent from the rainfall spatial variability. For the conceptualization of $E(T_r)$, which is not of interest here, we refer to V2010. The second term $E(T_c)$ represents the average time to route the rainfall excess from the geographical centroid of the rainfall spatial pattern to the catchment outlet. By using the spatial moments, the term $E(T_c)$ may be expressed as follows:

$$E(T_c) = \frac{\int_{T_S}[\int_A r(x,y,t)d(x,y)dA]dt}{AT_S P_0 v} = \frac{P_1}{P_0 v} = \frac{\Delta_1 g_1}{v} \tag{4.10}$$

where T_s is the duration of the storm event.

Therefore, Eq. 4.9 may be written as follows:

$$E(T_q) = E(T_r) + \frac{\Delta_1 g_1}{v} \tag{4.11}$$

Details concerning the derivation of Eq. **4.11** based on V2010 are reported in the Appendix. It is important to note here that the spatial distribution of the rainfall excess is the same as that of the rainfall pattern, since the runoff coefficient is assumed to be spatially uniform.

It is interesting to note that, from Eq. **4.11**, the first time-integrated scaled moment represents the ratio between the routing time corresponding to the rainfall centre of mass with respect to the catchment response time g_1/v:

$$\Delta_1 = \frac{E(T_c)}{\frac{g_1}{v}} \tag{4.12}$$

Analogously to δ_1, the values of Δ_1 are greater than zero, and are equal to one for the case of spatially uniform precipitation or for a spatially variable precipitation which is concentrated on the catchment centroid. Values of Δ_1 less than one indicate that rainfall is concentrated towards the outlet, and values larger than one indicate that rainfall is concentrated towards the headwater portion of the basin. Based on Eq. **4.11**, the statistic Δ_1 measures the hydrograph

timing shift relative to the position of the rainfall centroid over the catchment. As it will be shown later in the paper, the statistic Δ_1 is related to the normalised mean time difference between the hydrograph obtained by considering the actual rainfall pattern and the hydrograph resulting from a spatially uniform rainfall pattern (all other factors being taken equal). The normalising quantity is given by the response time of the catchment. The effect of a less-than-one value of Δ_1 indicates an anticipation of the mean hydrograph time with respect to the case of spatially uniform precipitation. The opposite holds true for the case of a larger-than-one value of the statistic. As an example, this means that a value of Δ_1 equal to 1.5 indicates that the mean time difference between the two hydrographs corresponds to half the catchment response time, with the hydrograph obtained from the spatially distributed rainfall delayed with respect to the one obtained from uniform rainfall. A value of Δ_1 equal to 0.5 indicates the same normalized mean difference, but with the opposite sign (the hydrograph obtained from the spatially distributed rainfall is anticipated with respect to the one obtained from uniform rainfall).

One should note that the storm velocity has no influence on $E(T_q)$. This is a direct consequence of the hypotheses used to derive the statistics. The catchment response is described as fully kinematic, therefore it is influenced by the averaged spatial organization of the rainfall and not by the variability of the spatial organization within the storm, and the routing is linear.

4.4. Variance of catchment runoff time

The variance of T_q, which represents the dispersion of the hydrograph, is given by

$$var(T_q) = var(T_r) + var(T_c) + 2cov(T_r, T_c) \qquad 4.13$$

We focus here on the terms $var(T_c)$ and $2cov(T_r, T_c)$. For the conceptualization of $var(T_r)$, which is not of interest here, we refer to V2010.

By using the concept of scaled spatial moments, $var(T_c)$ may be written as follows.

$$var(T_c) = \frac{\Delta_2}{v^2}(g_2 - g_1^2) \qquad 4.14$$

Details concerning the derivation of Eq. 4.14 are reported in the Appendix, based on V2010. For the case of $cov(T_r, T_c)$ equal to zero, Δ_2 represents the ratio between the differential variance in runoff timing generated by rainfall spatial distribution, and the variance of the catchment response time. The values of Δ_2 are greater than zero and take the value of one when the rainfall

field is spatially uniform. When the rainfall field is spatially concentrated anywhere in the basin, the values of Δ_2 are less than one. In the less frequent cases when the rainfall field has a bimodal spatial distribution, with concentration both at the headwaters and at the outlet of the catchment, the values of Δ_2 are greater than one. It should be noted that, with the rainfall excess volume remaining unchanged, the effect of decreasing the variance of runoff time is to increase the flood peak. This shows that in general the parameter Δ_1 is expected to have an influence on the runoff timing, whereas the parameter Δ_2 should affect the shape of the hydrograph and then the value of the flood peak.

As discussed in V2010, Eq. (25), the role of catchment scale storm velocity is represented by the term $cov(T_r, T_c)$. By using rainfall weights, defined as

$$w(t) = \frac{p_0(t)}{P_0} \tag{4.15}$$

and based on V2010 (see Appendix for the details of the derivation), the term $cov(T_r, T_c)$ in Eq. 4.13 may be written as follows:

$$cov(T_r, T_c) = g_1 \left\{ \underbrace{\frac{cov_t[T, \delta_1(t)w(t)]}{v}}_{term1} - \underbrace{\frac{cov_t[T, w(t)]}{v}}_{term2} \Delta_1 \right\} \tag{4.16}$$

where $cov_t()$ is the temporal covariance of the space-averaged terms. Here we define the term '*catchment scale storm velocity*' V_s as follows

$$V_s(t) = \underbrace{g_1 \frac{cov_t[T, \delta_1(t)w(t)]}{var[T]}}_{V_s1} - \underbrace{g_1 \frac{cov_t[T, w(t)]}{var[T]}}_{V_s2} \Delta_1 \tag{4.17}$$

where the two velocity terms V_s1 and V_s2 correspond to the groups $term1$ and $term2$ in Eq. 4.16. It is worth recognizing that the groups term1 and term2 represent the slope coefficients of linear space-time regressions. $Term1$ is the slope coefficient of the regression of the product $\delta_1(t)w(t)$ with time; $Term2$ is the slope coefficient of the regression of the weights $w(t)$ with time.

Equation 24 shows that the velocity formulation is given by the difference between two velocity terms. The first term describes the total storm motion, as related to the temporal evolution of the product of the weights of the precipitation $w(t)$ and of the centroid $\delta_1(t)$. The second term

describes the temporal storm variability, as it is summarized by the temporal evolution of the precipitation weights. Some examples may help understand the concept of storm velocity in idealized cases. For the case of temporally uniform mean areal rainfall, $w(t)$ is constant, V_s2 is equal to zero, and the value of V_s depends only on the evolution in time of the position of the rainfall centroid along the flow distance coordinate (V_s1). Conversely, if there is only temporal variation of the mean areal rainfall and $\delta_1(t)$ is constant, the two velocity terms V_s1 and V_s2 will be equal in value and opposite in sign, implying that V_s will be equal to zero. Note that the sign of the velocity is positive (negative) for the case of upstream (downstream) storm motion.

Finally, the term $cov(T_r, T_c)$ may be written as follows:

$$cov(T_r, T_c) = g_1 \left\{ \underbrace{\frac{cov_t[T, \delta_1(t)w(t)]}{v}}_{term1} - \underbrace{\frac{cov_t[T, w(t)]}{v}}_{term2} \Delta_1 \right\} = \frac{V_s}{v} var[T] \qquad 4.18$$

As a result, for downstream moving storm the variance of catchment runoff time tends to reduce and therefore the peak discharge tends to increase, consistently with the findings from several investigations (Niemczynowicz 1984; Ogden *et al.* 1995; De Lima and Singh 2002). The opposite occurs with upstream moving storms, which tend to increase the hydrograph time variance and hence to reduce the peak discharge.

4.5. Application to a set of extreme Flash Floods

Assessment of spatial moments of catchment rainfall is reported for five extreme storms and ensuing floods which have been observed in Europe in the period between 2002 and 2007 (Sect. 3.1). The case studies are the following: Sesia at Quinto (North-western Italy, 982 km^2) occurred on 04/06/2002, Sora at Vester (Slovenia, 212 km^2), occurred on 18/09/2007, Feernic at Simonesti (Romania, 168 km^2), occurred on 23/08/2005, Clit at Arbore (Romania, 36 km^2), occurred on 30/06/2006 and Grinties at Grinties (Romania, 51 km^2), occurred on 04/08/2007.

Analyses of rainfall variability by means of the spatial moments is attempted here to isolate and describe the features of rainfall spatial organization which have significant impact on runoff simulation. As such, spatial moments provide information to quantify hydrological similarities among different storms, and support the transfer of knowledge and exchange of estimation and analysis techniques. The rainfall spatial moments and the catchment-scale storm velocity were computed at each time step (either at 15-min or 30-min time steps) as time series, to examine the variability in time of the statistics. The time series of the first and second scaled moments of

catchment rainfall are reported in figures 4.1 and 4.2, together with the basin-averaged rainfall rate, the fractional coverage of the basin by rainfall rates exceeding 20 mm h^{-1} (this threshold has been selected to indicate a flood-producing rainfall intensity), and the storm velocity. The values of catchment scale storm velocity were computed by applying Eq. 24. The two velocity terms V_{s1} and V_{s2} were computed by assessing the slope of the corresponding linear regressions, by using a moving window with window size equal to the catchment response time.

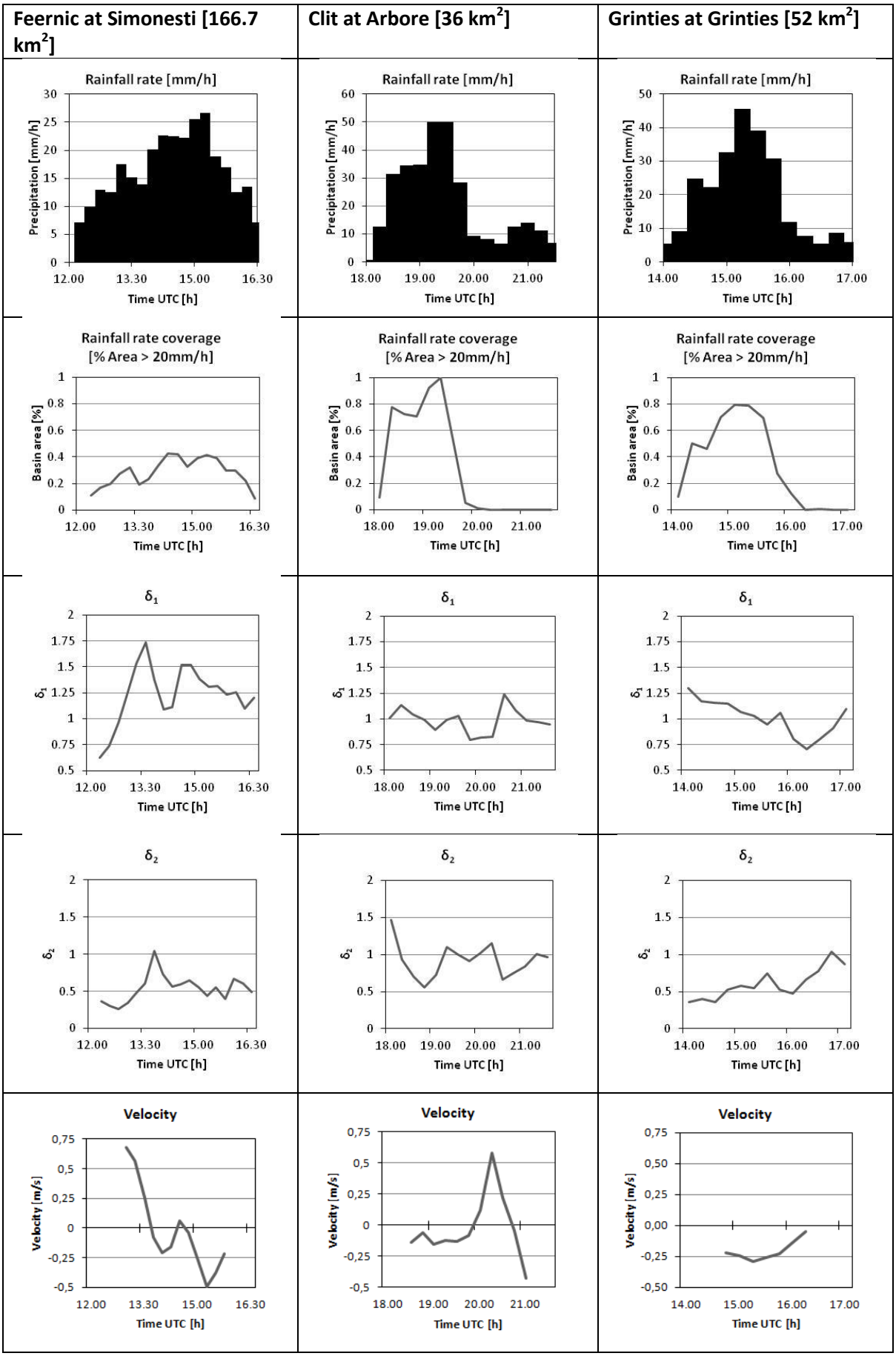

Figure 4.1: Precipitation analyses by using time series of precipitation intensity, coverage (for precipitation intensity > 20 mm h^{-1}), δ_1 (-), δ_2 (-) and storm velocity for Feernic, Clit and Grinties.

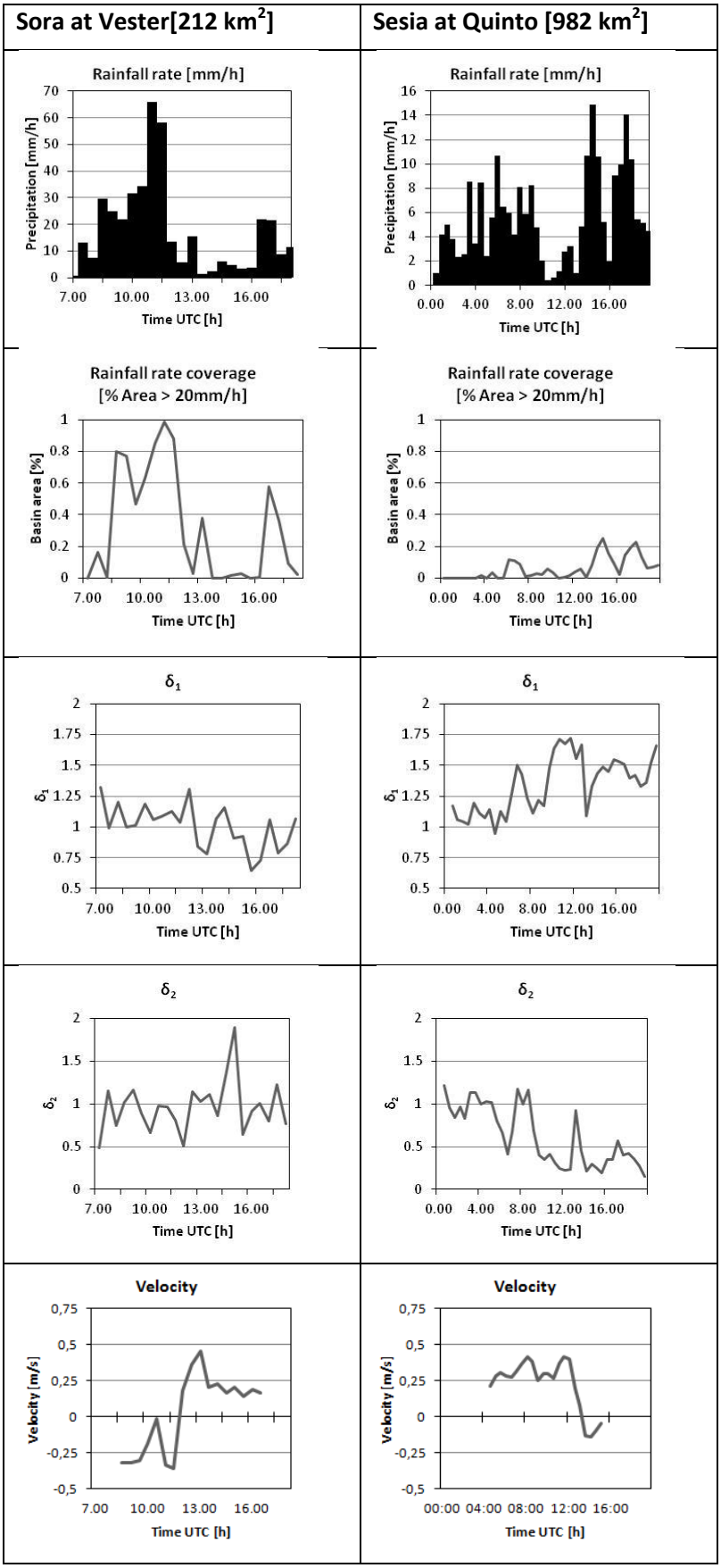

Figure 4.2: Precipitation analyses by using time series of precipitation intensity, coverage (for precipitation intensity > 20 mm h-1), δ1 (-), δ2 (-) and storm velocity for Sora and Sesia.

The time series of the first scaled spatial moment δ_1 exhibit a relatively large variability, particularly in the Feernic case, with the first scaled moments varying from 0.6 to 1.6 in the first 80 minutes (with a clear upbasin storm motion, as reflected in the increasing values of the statistic) and then decreasing in the following three hours, where a downbasin storm motion can be recognized. A strong downbasin storm motion can be recognized even for the Grinties during the period of strong flood-producing rainfall, with values of δ_1 steadily decreasing from 1.2 to 0.7. The case of the Sesia river basin at Quinto, as well as that of Feernic, documents the striking effect of the orography on convection development, with a concentration of the flood producing rainfall on the headwaters and values of δ_1 ranging between 1.4 and 1.6 during the period of flood-producing rainfall. Examination of the values reported for Grinties shows that the spatial moments may take values quite far from one even in small basins. The values of δ_2 generally reflects the trend of δ_1, as expected, with small values of dispersion when δ_1 is both larger or smaller than one, and values of dispersion close to one when δ_1 is also close to unity.

For three cases out of the five (Grinties, Sora and Sesia), the values of the catchment scale storm velocity are significantly different from zero. For the case of Grinties, the value of storm velocity is steadily around -0.2 $m\,s^{-1}$ for the period of strong rain rates, reflecting the important downbasin motion reported for the rainfall center of mass. A similar velocity (-0.3 $m\,s^{-1}$) is found for the event occurred on the Sora. An upbasin storm velocity value ranging between 0.3 and 0.4 $m\,s^{-1}$ is reported for the case of Sesia at Quinto. This value is clearly consistent with the constant upflow of humid air that sustained the formation of convective cells over the steep topography of the basin. In the three cases, the values of the storm velocity are relatively small with respect to the flood flows celerity characterizing flash floods, which was quantified around to 3 $m\,s^{-1}$ by Marchi *et al.* (2010) with reference to several flash floods in Europe. Previous work on the impact of storm velocity on hydrograph shape (Ogden *et al.* 1995) has shown that the effect of storm velocity is important when its magnitude become comparable to that of flood flow celerity. The significant differences between storm velocity and flood flows celerity suggests that even for these cases the values of storm velocity may be not large enough to influence the flood hydrograph shape.

As a further step of the analysis, we examined the relationship between the statistics Δ_1 and Δ_2 (Fig. 4.3). The analysis is carried out by dissecting the five study catchments into a number of nested subcatchments (see Table 3.1), as a means to examine potential catchment scale effects on the relationship between Δ_1 and Δ_2. The subdivision into subcatchments was either based on

earlier hydrological analyses (see Table 3.2) where post-flood observations were used to derive indirect peak discharges (Borga *et al.* 2008) or on availability of internal streamgauges. Details are reported in the papers describing the relevant case studies (Sangati and Borga 2009; Zanon *et al.* 2010; Zoccatelli *et al.* 2010). This subdivision will be used also for the hydrological simulations in Section 4.5. Overall, 27 catchments were used for the computation of Δ_1 and Δ_2. The corresponding catchment size ranges between 5 and 982 km^2, with 9 catchments less than 50 km^2, 10 catchments ranging between 50 and 150 km^2, and 8 catchments larger than 150 km^2.

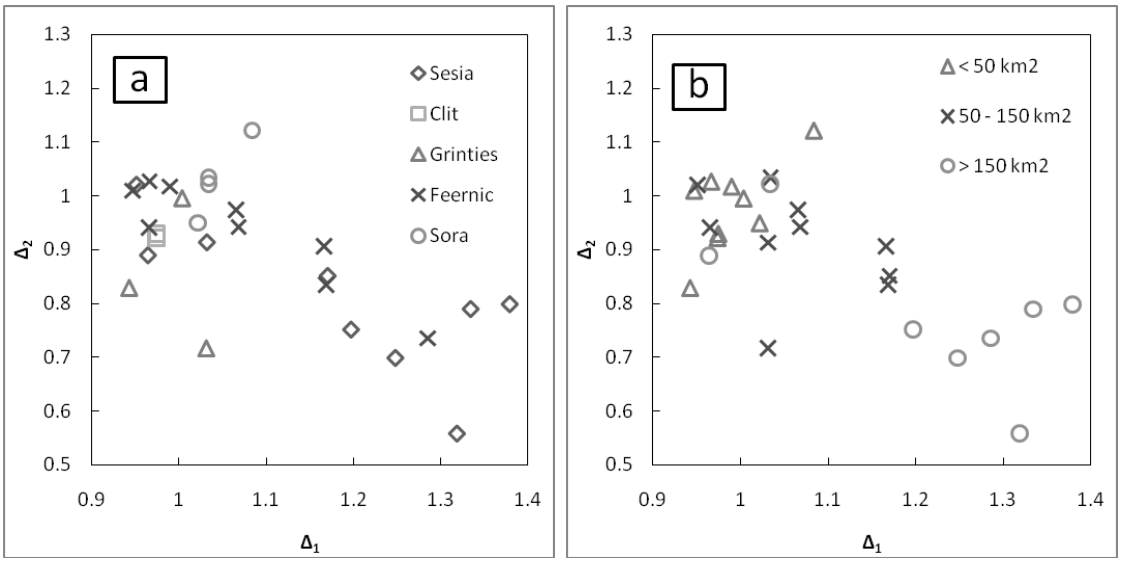

Figure 4.3: Relationship between Δ_1 and Δ_2 : (a) for the study catchments, (b) for specific classes of catchment area.

Inspection of this figure shows that in 16 cases out of 27 the value of Δ_1 falls in a narrow interval around one ($0.95 < \Delta_1 < 1.07$). In 13 cases out of these 16 cases, Δ_2 ranges between 0.9 and 1.02, indicating that generally Δ_2 is close to one when Δ_1 is also close to one. In these cases the first two scaled moments are virtually unchanged with respect to the spatially uniform rainfall case. However, it is interesting to note one case of Grinties, reporting a value of Δ_2 around 0.7 in correspondence to a value of Δ_1 equal to 1.03. This is one of the few cases in which a strong rainfall concentration corresponds spatially to the geomorphologic center of mass of the catchment. When Δ_1 exceeds the upper bound of the interval (1.07), the corresponding value of Δ_2 is lower than 0.9. There is only one case of Δ_2 exceeding 1.1, indicating a case of multimodal spatial distribution of rainfall. More than half of the cases show values of Δ_1 in the range 1.05-1.4, documenting the effect of orography on the spatial rainfall distribution. Indeed, one of the elements that favor the anchoring of convective system is the orography, which play an important role in regulating of atmospheric moisture inflow to the storm and in controlling storm motion

and evolution (Davolio 2006). Consistently with this observation, values of Δ_1 less than 0.95 are not represented in the study floods.

As expected, all but two of the catchments with area less than 50 km^2 are characterized by values of Δ_1 and Δ_2 close to one. For these cases, we expect a limited impact of rainfall spatial organization on flood response. On the other side, six out of the eight cases with catchment area exceeding 150 km^2 are characterized by values of Δ_1 larger than 1.2 and corresponding values of Δ_2 less than 0.8. These values (corresponding to subcatchments of Sesia and Feernic) imply a strong concentration of rainfall towards headwater and a correspondingly low dispersion around the mean values. Accordingly with the analysis reported in this work, these characteristics should translate to a delayed and more peaky hydrograph, with respect to the one obtained by using spatially uniform rainfall.

Relation with hydrograph: the timing error

In this section we quantify the effect of neglecting the rainfall spatial variability on the rainfall-runoff model application. Hydrologic response from the five storm events over the 27 subcatchments analysed in Section 3.1 is examined by using a simple spatially distributed hydrologic model. The distributed model is based on availability of raster information of the landscape topography and of the soil and land use properties. Details on the model are reported in chapter 3.2. The model parameters were estimated over the catchments available for each event by means of a combination of manual and automatic calibration to minimize either the Nash–Sutcliffe efficiency index over the flood hydrographs (for the gauged catchments) or the mean square error over the flood peak and the timing data (rise, peak and recession) (for catchments where runoff data were provided from post-event surveys). Details about the application of the model to the individual events, its calibration and its verification are reported in the relevant papers (Sangati and Borga 2009; Zanon *et al.* 2010; Zoccatelli *et al.* 2010). In general, the model simulations of the flood hydrographs were closer to observations for the smaller basins where the linear routing approach implemented in the model provides a better description of the actual processes.

In this first exploratory work we focus on the timing error (Ehret and Zehe 2011), i.e. the difference in the timing of the centroid of the hydrographs obtained by using either spatially distributed or spatially uniform rainfall, and analyse the relationship between this kind of error and the Δ_1 statistic. As explained in section 3.2, for each subcatchment the flash flood response was simulated by using the actual rainfall spatial variability and then by using spatially uniform

precipitations, hence obtaining two different hydrographs. Moreover, in order to clarify the relative roles of transport paths and of heterogeneity in the runoff generation processes, we performed numerical experiments in which the infiltration and the difference between hillslope and channel travel times are selectively 'turned off', by assuming that the soil is impermeable and the hillslope and channel celerity have the same value.

The statistic Δ_1 is expected to quantify the hydrograph timing error. For storms characterised by Δ_1 larger than one, rainfall is concentrated towards the periphery of the catchment, with the hydrograph delayed relative to the case of a spatially uniform rainfall. The opposite is true for rainfall concentrated towards the outlet (Δ_1 less than one); in these cases the hydrograph should be anticipated relative to the case of spatially uniform rainfall. A statistic, termed "normalised time difference" dT_n , is introduced to quantify the timing error between the two hydrographs. The normalised time difference dT_n is computed by dividing the time difference between the two hydrograph centroids by the response time of the catchment $E(T_c)$, as follows:

$$dT_n = \frac{E\left(T_{q\ Dist}\right) - E\left(T_{q\ Unif}\right)}{T_c} \tag{4.19}$$

where $E(T_{q\ Dist})$ and $E(T_{q\ Unif})$ are the hydrograph centroids corresponding to the hydrographs generated by using spatially distributed rainfall (termed '*reference hydrograph*' hereinafter) and spatially uniform rainfall, respectively. A positive (negative) value of dT_n implies a positive (negative) shift in time of the reference hydrograph with respect to the one produced by using uniform precipitation. It should be noted that Eq. 4.19 may written down by exploiting Eq. 4.11 as follows:

$$dT_n = \frac{E\left(T_{q\ Dist}\right) - E\left(T_{q\ Unif}\right)}{T_c} = \frac{E(T_r) + \frac{\Delta_1 g_1}{v} - E(T_r) - \frac{g_1}{v}}{\frac{g_1}{v}} = \Delta_1 - 1 \tag{4.20}$$

Eq. 4.20 shows that the normalised timing error is related in a simple way to the spatial organisation of the rainfall fields by means of the scaled spatial moment of order one. The comparison between the two hydrographs is exemplified for the cases of Sesia at Quinto (982 km^2) and of Grinties at Grinties (52 km^2) in Fig. 4.4a,b, respectively.

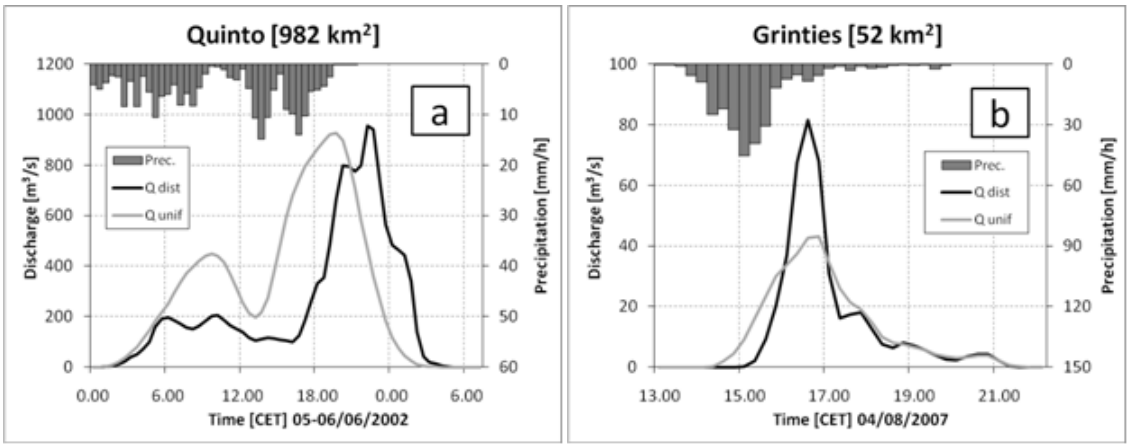

Figure 4.4 a,b: Modelled flood hydrographs obtained by using spatially distributed and uniform precipitation, for the case of a) Sesia at Quinto (982 km^2) and b) Grinties at Grinties (52 km^2).

The storm event which triggered the Sesia flash flood was characterised by a strong concentration of rainfall towards the headwaters (Δ_1 = 1.33, Δ_2 = 0.79) , which implies a longer and more peaked catchment response with respect to that corresponding to the case of spatially uniform precipitation. Correspondingly, the simulated flood peak obtained by using spatially uniform rainfall is too early (dT_n=0.3) and its amplitude is too large with respect to the 'reference' hydrograph. For the case of Grinties, the storm event was heavily concentrated over the catchment centroid (Δ_1 = 1.03, Δ_2 = 0.72), which has no implications in terms of response timing (dT_n=0.05) but translates to a much less peaked catchment response from spatially uniform rainfall with respect to the 'reference'. Both cases show clearly the impact of neglecting the spatial distribution of rainfall in rainfall-runoff modelling even at small and moderate catchment sizes.

Case 1: impervious soil and no hillslopes

To clarify the role of runoff transport processes alone on the sensitivity of runoff model to rainfall spatial organisation, we carried out three different sets of numerical experiments. In the first case, the soil is assumed everywhere completely impervious and the hillslope celerity has the same value as the channel celerity. The rainfall-runoff model in this case is subject to the same assumptions used to derive the spatial moments statistics. Results for the relationship between dT_n and Δ_1 for the various catchments are reported in Fig. 4.5a, whereas Fig. 4.5b displays the same results for various classes of catchment size. The results show a linear relationship between the two variables, as expected. The linear regression is as follows

$$dT_n = 1.0014\,\Delta_1 - 1.0019 \quad r^2 = 1 \qquad 4.21$$

which reproduces very well Eq. 4.20.

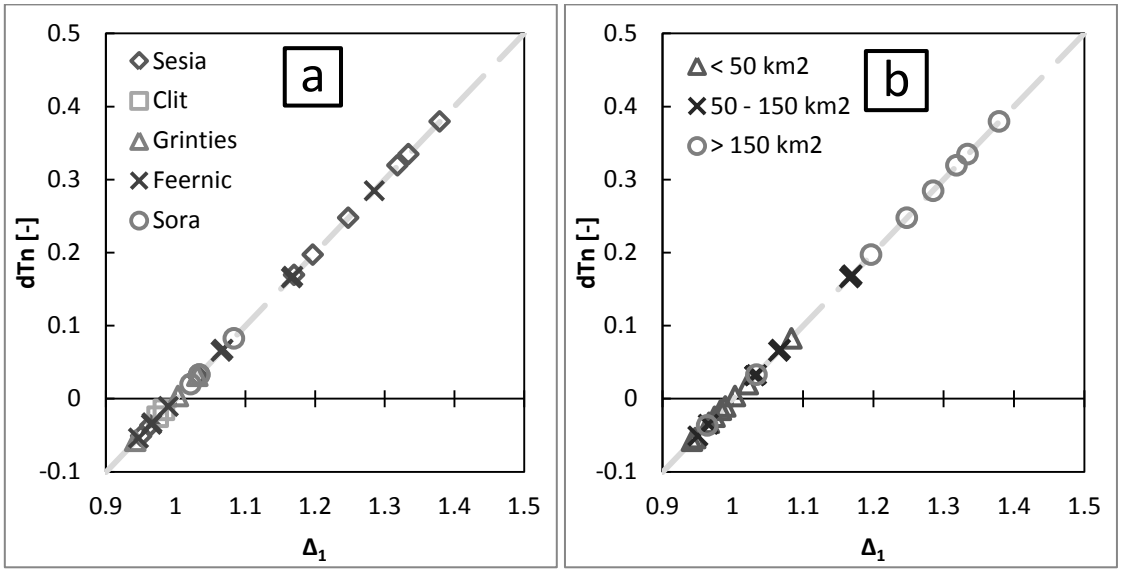

Figure 4.5a,b: Relationship between dT_n and Δ_1 obtained by considering impervious soils and neglecting the hillslope travel time in the hydrological model. The relationship is reported for (a) the study catchments, (b) specific classes of catchment area. The dashed line is the linear regression $dT_n = 1.0014\Delta_1 - 1.0019$ $r^2 = 1$

Case 2: impervious soils with hillslope propagation

In the second case, the soils are again considered impervious, whereas the hillslopes and channels elements are considered separately, and are characterised by the celerities identified by means of the model calibration process. Results for the relationship between dT_n and Δ_1 for the various catchments are reported in Fig. 4.6a,b, showing again a strong linear relationship.

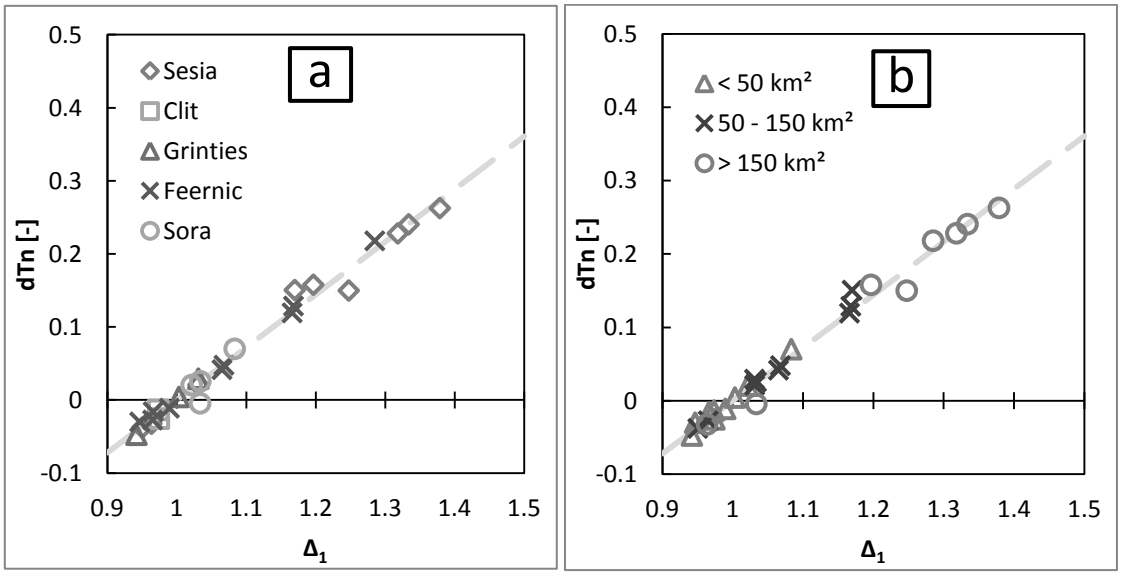

Figure 4.6a,b: Relationship between dTn and Δ_1 obtained by considering impervious soils and the hillslope travel time in the hydrological model. The relationship is reported for (a) the study catchments, (b) specific classes of catchment area.

The linear regression of figure 4.6 is as follows

$$dT_n = 0.72\,\Delta_1 - 0.72 \qquad r^2 = 0.99 \qquad 4.22$$

The introduction of the hillslope travel time leads to a decrease of the slope of the regression line, which decreases from 1.0 to 0.72. This corresponds to a linear decrease of the timing error by 28%, showing that the main effect of introducing the hillslope system is to decrease the influence of the rainfall spatial organization on catchment response. It is likely that increasing the role of the hillslope residence time will further reduce the sensitivity of the hydrological model to rainfall spatial organization. The high determination coefficient of the regression line is a remarkable finding, since the hillslope travel times were calibrated individually to each flood event. This may suggest that the relative contribution of hillslopes and channels to the average residence time is rather similar through the various events. This is not surprising, given the extreme character of all the floods considered in this work.

Case 3: pervious soils with hillslope propagation

In the third case, the model includes the actual distribution of the infiltration parameters and different celerities are used to simulate hillslopes and channels. The relationship between dT_n and Δ_1 is reported in Fig. 4.7a,b, whereas the linear regression is as follows

$$dT_n = 1.98\,\Delta_1 - 2.07 \qquad r^2 = 0.83 \qquad 4.23$$

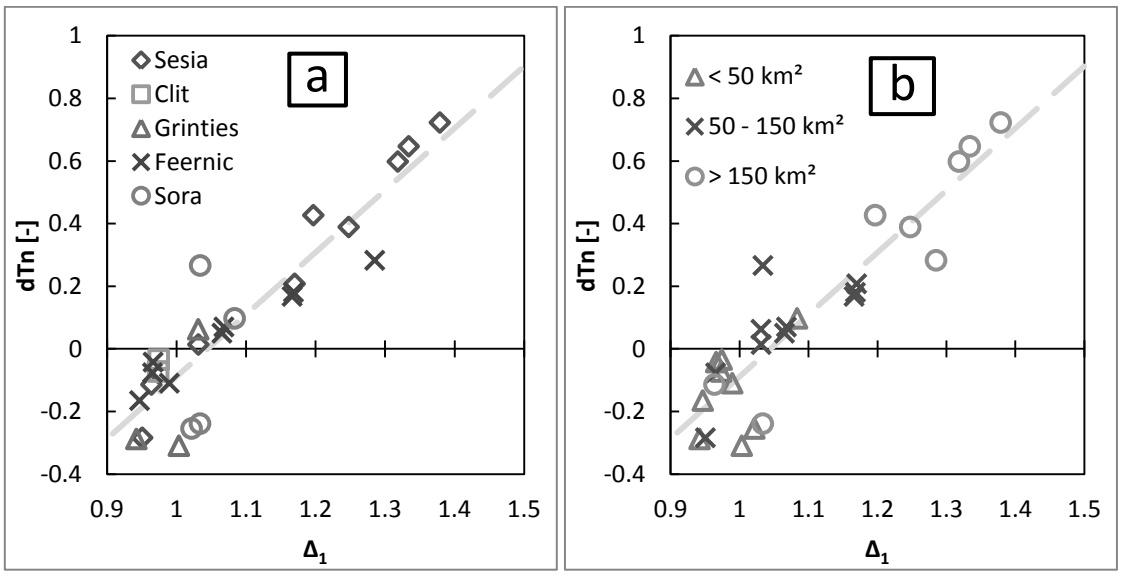

Figure 4.7a,b: Relationship between dTn and Δ_1 obtained by considering infiltration and the hillslope travel time in the hydrological model. The relationship is reported for (a) the study catchments, (b) specific classes of catchment area.

The linear regression is characterized by a lower determination coefficient with respect to the previous cases. This reflects the specific features of each flood event. Results shown in Fig. 4.7 indicates the impact of rainfall spatial organization on flood modeling for small to moderate basin sizes. The timing error introduced by neglecting the rainfall spatial variability ranges between -30% to 72% of the corresponding catchment response time. A feature worth noting in Fig. 4.7a,b is that the slope and the intercept of the linear regression are higher than those corresponding to Eq. 4.20. This effect is the result of the non-linearity characterizing the rainfall to runoff transformation. *Zoccatelli et al. (2010),* in an investigation concerning three extreme flood events, showed that the non-linearity in the rainfall-runoff transformation leads to a magnification of the values of the dT_n statistics with respect to those obtained in the impervious case. Essentially, this means that when rainfall is either focused on the headwaters or on the outlet, the runoff exhibits an even stronger offset towards either the periphery of the catchment or the outlet as a result of the non-linear hydrological processes implied in the runoff generation. This effect leads to a steepening of the linear relationship between dT_n and Δ_1, which increases from 0.72 to 1.98. Overall, the combination of the results displayed in Fig. 4.6a,b and Fig. 4.7a,b shows that the effect of the rainfall-runoff transformation on the relationship between dT_n and Δ_1 are stronger, at least for the considered case studies, than the effect of the hillslope residence time. An important implication of these results is that the method based on the spatial moments provides useful information on the potential impact of the rainfall spatial organisation on the features of the ensuing flood hydrograph, in spite of the assumptions used for its derivation.

4.6. Discussion and conclusions

In this work, we examine a set of spatial rainfall statistics which assess the dependence of the catchment flood response on the space-time interaction between rainfall and the spatial organization of catchment flow pathways. The statistics are derived based on previous work by Woods and Sivapalan (1999) and Viglione *et al.* (2010a,b), and correspond to the statistics reported in Smith *et al.* (2002), Smith *et al.* (2005) and Smith *et al.* (2004). Named '*spatial moments of catchment rainfall*', these statistics describe the spatial rainfall organisation in terms of concentration and dispersion statistics as a function of the distance measured along the flow path coordinate. The introduction of the spatial moments of catchment rainfall permits derivation of the concept of catchment scale storm velocity, which quantifies the up or down-basin rainfall movement as filtered by the catchment morphological properties relative to the storm kinematics. The work shows how the first two spatial moments afford quantification of the impact of rainfall spatial organization on two fundamental properties of the flood hydrograph: timing

(surrogated by the runoff mean time) and amplitude (surrogated by the runoff time variance). The first spatial moment provides a measure of the scaled distance from the geographical centroid of the rainfall spatial pattern to the catchment centroid. The second spatial moment provides a scaled measure of the additional variance in runoff time that is caused by the spatial rainfall organization, relative to the case of spatially uniform rainfall.

The analysis reported here suggests that the proposed rainfall statistics are effective in (i) describing the degree of spatial organisation which is important for runoff modelling and (ii) quantifying the relevance of rainfall spatial variability on flood modeling, with specific reference to the timing error. This is an essential aspect of this work, since our outcome clearly shows that catchment response is sensitive to spatial heterogeneity of rainfall even at small catchment sizes. The timing error introduced by neglecting the rainfall spatial variability ranges between -30% to 72% of the corresponding catchment response time. It should be borne in mind that the floods considered in this work are very intense flash floods characterised by strong rainfall gradients.

We believe that the main strength of the method lies in a better understanding of the linkages between the characteristics of the rainfall spatial patterns with the shape and magnitude of the catchment flood response. This provides an indicator at catchment scale that integrates morphology and rainfall space-time distribution, and that can be used to compare influence of rainfall distribution across basins and scales. This is a fundamental aspect, since it enables evaluating the accuracy with which rainfall space and time distribution need to be observed for a given type of storm event and for a given catchment. For example, this may provide new statistics and criteria both for defining the optimality of raingauge network design in areas where flash floods are expected and for evaluating the accuracy of radar rainfall estimation algorithms and attendant space-time resolution.

The method proved to give reliable results in the context of flash floods. It would be useful to check the rainfall statistics and the methodology behind them for a wider variety of catchments and events, to explore how it can be extended to other cases. The statistics could also be used for assessing and quantifying hydrological similarity across a wide range of rainfall events and catchments, within the broader framework of comparative hydrology. For instance, the method can be used to identify the features of catchment morphology which attenuates (or magnify) the effects of rainfall space-time organization. With the use of the spatial moments, the interaction of rainfall forcing and catchment characteristics can be described not only in terms of mean areal rainfall, but also by considering the features of rainfall spatial concentration and the storm velocity. For example, this may help to reveal the effect of orography not only on the precipitation

accumulation at the catchment scale, but also on the space-time organization of the rainfall patterns.

Further research should also focus on the concept of the catchment scale storm velocity. The introduction of this concept permits assessment of its significance for actual flood cases and analyses of the space and time rainfall sampling schemes which are required for its adequate estimation for various catchment scales and configurations. There is also a need to extend the formulation of the spatial moments of catchment rainfall to incorporate the hillslope transit time as a way to conceptualise the impact of the hillslope system on the catchment's filtering properties.

Finally, the rainfall statistics introduced in this work could be used as an input to a new generation of semi-distributed hydrological models able to use the full range of statistics, and not only the mean areal rainfall, for flood modeling and forecasting. This will permit extending the capabilities of this class of hydrological models to rainfall events characterized by significant rainfall variability.

5. Roles of hillslope processes and river network routing in the hydrologic response to spatially variable rainfall fields

Propagation processes along hillslopes and flow dynamics along the river network combine to shape the hydrologic response of a basin (Naden 1992; Snell and Sivapalan 1994; Robinson *et al.* 1995; Yen and Lee 1997; D'Odorico and Rigon 2003; Giannoni *et al.* 2003; Saco and Kumar 2004; Viglione *et al.* 2010). The relative contribution of hillslope processes and network geomorphology to the hydrologic catchment response has been investigated by several researchers. A general result is that the relative role and mutual interactions of hillslope and channel network transport change substantially with catchment size (Kirkby 1976; Beven and Wood 1993; Robinson *et al.* 1995; Saco and Kumar 2002; Di Lazzaro 2009). Small basins response tends to be dominated by hillslope processes, while flow routing through the river network controls the response of large basins (Botter and Rinaldo 2003).

Less attention has been devoted to examine to what extent relative role of hillslope and river network processes is affected by spatial variability of rainfall fields. Some hypotheses have been put forward to identify the mechanisms through which rainfall spatial variability may affect catchment response, with an emphasis on hydrologic partitioning processes (Shah *et al.* 1996; Winchell *et al.* 1998; Brath and Montanari 2003; Gabellani *et al.* 2007). Several works have focused on the relation between the spatial rainfall organization and the heterogeneities embedded in the basin geomorphic structure, mostly by examining the rainfall variability relative to a distance metric imposed by the drainage network (Zhang *et al.* 2001; Smith *et al.* 2002; Smith *et al.* 2005). Nicótina *et al.* (2008) focused on the effects of transport processes along the hillslopes and the channel network as a key element to clarify the extent of the possible influence of rainfall spatial variability on the hydrologic response. They used a geomorphological model of the runoff response and analyzed the distribution of travel times and found that the hillslope residence time controls the sensitivity of the hydrologic response to rainfall distribution. More specifically, the sensitivity increases with decreasing hillslope residence time. By considering relatively large storm events, they found that rainfall spatial variability does not significantly influence the flood response for basin areas up to about 3500 km^2.

Based on earlier works by Woods and Sivapalan (1999), Zhang *et al.* (2001), Smith *et al.* (2002) and Viglione *et al.* (2010), in chapter 4 we proposed a series of statistics, termed '*spatial moments of catchment rainfall*', which quantify the interaction between rainfall spatial variability and the basin morphometric properties, as described by the flow distance metric. Starting from Viglione *et al.* (2010), we showed how these statistics are able to isolate the effect of rainfall

spatial variability on mean and variance of catchment runoff time. We considered flash flood cases characterized by pronounced rainfall organization and reported large impacts of rainfall spatial variability on hydrologic response for catchments as small as 50 km^2. In the development of the spatial moments of catchment rainfall, it was disregarded the differentiation between hillslopes and channel network contribution to the total runoff travel time, which was explicit in the work of Viglione. However, for most river basins the contribution of hillslopes to the total residence time is relevant to the proper representation of the basin response (Rinaldo *et al.* 1995; D'Odorico and Rigon 2003; Nicótina *et al.* 2008). The correct description of hillslope contribution is even more important in the small to medium catchments (less than 1000 km^2) which are more frequently impacted by flash floods. Dissecting the individual contributions of the hillslope and channel systems to spatial rainfall catchment sensitivity is therefore an important step towards better quantifying the spatial rainfall resolution required to achieve an accurate description of the runoff response.

In this work, we extend the concept of spatial moments of catchment rainfall by incorporating both hillslope and channel contributions to the travel time in the moment formulations. The statistics obtained in this way are used to gain insight into the role of the hillslope residence time, providing a basis for comparing scenarios and identifying dominant controls. Moreover, we derive a simple expression which quantifies the sensitivity of the flood response to rainfall space-time organization as a function of parameters describing the spatial structure of the rainfall event and of the geomorphologic and dynamic parameters characterizing the river routing and the hillslope residence time.

The conceptual meaning of the extended spatial moments is illustrated by analyzing five extreme flash floods occurred in various European regions in the period 2002–2007. These statistics are computed by exploiting high resolution, carefully controlled, radar rainfall fields and a spatially distributed hydrologic model, in order to assess the degree of spatial rainfall organization controlling the simulated runoff, with a focus on runoff timing. The size of the study catchments ranges between 36 to 982 km^2.

5.1. Spatial moments of catchment rainfall: extension to the hillslope processes

Spatial moments of catchment rainfall introduced in chapter 4 provide a description of the spatial rainfall organisation at a certain time *t* as a function of the rainfall field *r(x,y,t)* value at any position *x,y* within a catchment, and of the flow distance *d(x,y)* to the catchment outlet measured along the flow path. Similar statistics have been introduced in previous work by Smith *et al.* (2002) and Smith *et al.* (2005) to describe the rainfall spatial variability from the perspective of a distance metric imposed by the drainage network. In chapter 4 the spatial moments of catchment rainfall have been defined under the assumption of a space and time constant flow velocity. In this section, the spatial moments are extended to include the hillslope processes, after rearranging the covariance terms employed by Viglione *et al.* (2010) to describe the mean and the variance of the catchment runoff time. The celerity of the basin response is modeled here with two different velocities of the surface flow in hillslopes and channels, referred to as v_h and v_c, , respectively. We indicate here with $d_h(x,y)$ the distance from any point in the basin to the channel network following the steepest descent path, while with $d_c(x,y)$ the length of the subsequent drainage path through the streams down to the watershed outlet. Then, the following definitions are provided for the spatial moments of catchment rainfall of order *n* for the channel and hilllslope systems, respectively:

$$p_{n,c}(t) = A^{-1} \int_A r(x,y,t) d_c(x,y)^n dA \qquad 5.1$$
$$p_{n,h}(t) = A^{-1} \int_A r(x,y,t) d_h(x,y)^n dA$$

where A indicates the catchment area. It is easy to verify that the *zero*-th order spatial moment along hillslope and channel flow paths are both equal to the catchment average rainfall at time *t*, $p_0(t)$.

Analogously to chapter 4.1, the terms $P_{n,c}$ and $P_{n,h}$ are employed to indicate the corresponding means of $p_{n,c}$ and $p_{n,h}$ over a time interval T_s, equal to the storm duration:

$$P_{n,c} = A^{-1} \int_A R(x,y) d_c(x,y)^n dA \qquad 5.2$$
$$P_{n,h} = A^{-1} \int_A R(x,y) d_h(x,y)^n dA$$

where *R(x,y)* is the cumulated precipitation over the time interval T_s at point *x,y*.

In a similar way, the moments of the flow distance along the channel and hillslope flowpaths are given by:

$$g_{n,c}(t) = A^{-1} \int_A d_c(x,y)^n dA \qquad 5.3$$
$$g_{n,h}(t) = A^{-1} \int_A d_h(x,y)^n dA$$

The first order moments $g_{1,h}$ and $g_{1,c}$ are the catchment average distance of hillslopes and channels with respect to the catchment outlet, respectively.

Dimensionless spatial moments of catchment rainfall over the hillslope and river system can be obtained by taking the ratio of the spatial moments of catchment rainfall to the moments of the flow distance, as shown below for the first two order:

$$\delta_{1,c}(t) = \frac{p_{1,c}(t)}{p_0(t) g_{1,c}} \qquad 5.4$$
$$\delta_{1,h}(t) = \frac{p_{1,h}(t)}{p_0(t) g_{1,h}}$$
$$\delta_{2,c}(t) = \frac{A^{-1} \int_A r(x,y,t)\left[d_c(x,y) - \delta_{1,c}(t) g_{1,c}\right]^2 dA}{A^{-1} \int_A r(x,y,t) dA \; A^{-1} \int_A \left[d_c(x,y) - g_{1,c}\right]^2 dA} = \frac{1}{g_{2,c} - g_{1,c}^2}\left[\frac{p_{2,c}(t)}{p_0(t)} - \left(\frac{p_{1,c}(t)}{p_0(t)}\right)^2\right]$$
$$\delta_{2,h}(t) = \frac{A^{-1} \int_A r(x,y,t)\left[d_h(x,y) - \delta_{1,h}(t) g_{1,h}\right]^2 dA}{A^{-1} \int_A r(x,y,t) dA \; A^{-1} \int_A \left[d_h(x,y) - g_{1,h}\right]^2 dA} = \frac{1}{g_{2,h} - g_{1,h}^2}\left[\frac{p_{2,h}(t)}{p_0(t)} - \left(\frac{p_{1,h}(t)}{p_0(t)}\right)^2\right]$$

The scaled moment of order one $\delta_{1,c}$ describes the rainfall weighted distance along the river network, with respect to the average value of the flow distance along the river network. A spatially homogeneous rainfall or a rainfall concentrated towards the position of the river network centroid will result in a value of $\delta_{1,c}$ close to 1. Values of $\delta_{1,c}$ less than one indicate that rainfall is distributed near the basin outlet, whereas values greater than one indicate that rainfall is distributed towards the headwaters. The second scaled moment $\delta_{2,c}$ describes the dispersion of the rainfall-weighted flow distances about their mean value with respect to the dispersion of the flow distances along the river network.

The scaled moment $\delta_{1,h}$ and $\delta_{2,h}$ have the same conceptual meaning of the corresponding channel-related moments.

Analogously, the weighted scaled moments $\Delta_{n,h}$ and $\Delta_{n,c}$ are defined with a formalism similar to $\delta_{n,h}$ and $\delta_{n,c}$, but for a mean rainfall intensity over the finite temporal interval equal to T_s:

$$\Delta_{1,c} = \frac{P_{1,c}}{P_0 g_{1,c}} \qquad 5.5$$

$$\Delta_{1,h} = \frac{P_{1,h}}{P_0 g_{1,h}}$$

It can be shown that the overall spatial moment of first order Δ_1, introduced in chapter 4.1 and expressed as a function of the whole flow distance $d(x,y)=d_h(x,y)+ d_c(x,y)$, is a weighted function of the channel and hillslope moments as follows:

$$\Delta_1 = \frac{\Delta_{1,c} g_{1,c} + \Delta_{1,h} g_{1,h}}{g_{1,c} + g_{1,h}} \qquad 5.6$$

5.2. Relationship between the spatial moments of catchment rainfall and the flood hydrograph shape

Viglione et al. (2010) proposed an analytical framework (called *V2010* hereafter) for quantifying the effects of space-time variability on catchment flood response. *V2010* extended the analytical framework developed in Woods and Sivapalan (1999) to characterize flood response in the case where complex space and time variability of both rainfall and runoff generation are considered as well as hillslope and channel network routing.

In the *V2010* methodology, the rainfall excess $r_e(x,y,t)$ at a point (x,y) and at time t generated by precipitation $r(x,y,t)$ is given by

$$r_e(x,y,t) = r(x,y,t)c(x,y,t) \qquad 5.7$$

where $c(x,y,t)$ is the local runoff coefficient, bounded between 0 and 1. *V2010* characterizes the flood response with three quantities: (*i*) the catchment- and storm-averaged value of rainfall excess, (*ii*) the mean runoff time (i.e., the time of the center of mass of the runoff hydrograph at a catchment outlet), and (*iii*) the variance of the runoff time (i.e., the temporal dispersion of the runoff hydrograph, which is not considered in this study).

The mean time of catchment runoff is a surrogate for the time to peak, including the temporal delay due to temporal rainfall distribution and the processes of routing to the outlet. Since the aim of this study is to establish a relationship between the spatial moments of catchment rainfall and the flood response shape, we modified accordingly the *V2010* methodology by assuming that the runoff coefficient is uniform in space and time. Hence, in the following developments the rainfall intensity and accumulation are used in place of the rainfall excess. Owing to this assumption, results obtained by this approach are likely to apply to heavy rainfall events characterized by large rain rates and accumulations.

The runoff transport is described by using two different space-time invariant values of velocity v_h and v_c characterizing the hillslope and the channel system, respectively. The use of invariant channel and hillslope velocities deserves some discussion. Pilgrim (1976) analyzed the relationship of the average velocity with discharge by using tracers, showing that the average flow velocities reach an asymptotic value at high flows. This supports the assumption that models of the hydrologic response employing basin-constant channel celerity explain observed travel time distributions, at least for high flows conditions. The invariant hillslope celerity assumption is more conceptual in nature (Botter and Rinaldo 2003). In fact, great variability in hillslope transport properties is expected, particularly when it is driven by local topographic gradients as subsurface runoff through partially saturated areas and in the presence of preferential flow paths (Dunne 1978; Beven and Wood 1983).

The analytical results are summarized below, by focusing on one of the characteristics essential to derive the relationship between the spatial moments and the characteristics of the flood response shape, i.e. the mean runoff time. Catchment runoff time is treated as a random variable (denoted T_q), which measures the time from the storm beginning until a drop of water exits the catchment. Water that passes a catchment outlet goes through two successive stages in our conceptualisation: (*i*) the generation of runoff at a point (including waiting for the rain to fall), (*ii)* runoff transport. Each of these stages has an associated ‘‘holding time”, which is conveniently treated as a random variable (Rodriguez-Iturbe and Valdes 1979). Since the water exiting the catchment has passed in sequence through the three stages mentioned above we can write

$$T_q = T_r + T_h + T_c \tag{5.8}$$

where T_r, T_h and T_c are the holding times for rainfall excess, hillslope travel and channel travel.

5.2.1. Effect of spatial rainfall variability on the flood hydrograph timing

Using the mass conservation property (see *V2010*) we can write the mean of T_q as:

$$E(T_q) = E(T_r) + E(T_h) + E(T_c) \tag{5.9}$$

The first term $E(T_r)$ represents the time from the start of the event to the centroid of the rainfall time series, and is independent from the rainfall spatial variability. For the conceptualization of $E(T_r)$, which is not of interest here, we refer to *V2010*. The second term $E(T_c)$ represents the average time to route the rainfall excess from the geographical centroid of the rainfall spatial

pattern to the catchment outlet through the channel system. The third term $E(T_h)$ is the corresponding term for the hillslope system.

By using the spatial moments, the term $E(T_c)$ may be expressed as follows:

$$\mathbf{E(T_c)} = \frac{\int_{T_s}\left[\int_A \mathbf{r(x,y,t)d_c(x,y)dA}\right]\mathbf{dt}}{\mathbf{AT_sP_0v_c}} = \frac{\mathbf{P_{1,c}}}{\mathbf{P_0v_c}} = \frac{\mathbf{\Delta_{1,c}g_{1,c}}}{\mathbf{v_c}} \quad 5.10$$

where T_s is the duration of the storm event. Details concerning the derivation of Eq. 5.10 based on V2010 are reported in Zoccatelli et al. (2011). The term $E(T_h)$ is written in a symmetrical way by considering the properties of the hillslope system and the interaction between rainfall spatial organization and the hillslope system.

Therefore, Eq. 5.9 may be written as follows:

$$E(T_q) = E(T_r) + \frac{\Delta_{1,c} g_{1,c}}{v_c} + \frac{\Delta_{1,h} g_{1,h}}{v_h} \quad 5.11$$

It is important to note here that the spatial distribution of the rainfall excess is the same as that of the rainfall pattern, since the runoff coefficient is assumed to be spatially uniform. By using the definition of mean residence time in the river network $\tau_c = g_{1,c}\, v_c^{-1}$ and in the hillslope system $\tau_h = g_{1,h} v_h^{-1}$, Eq 18 can be written as:

$$E(T_q) = E(T_r) + \Delta_{1,c}\tau_c + \Delta_{1,h}\tau_h \quad 5.12$$

A key dimensionless parameter describing the sensitivity of the flood hydrograph timing to the rainfall spatial organization is the following

$$\Theta_1 = \frac{\Delta_{1,c}\tau_c + \Delta_{1,h}\tau_h}{\tau_{tot}} \quad 5.13$$

where $\tau_{tot}=\tau_c + \tau_h$. The parameter Θ_1 represents the ratio between $E(T_h)+E(T_c)$ and the mean runoff propagation time through the hillslope and the channel system.

The values of Θ_1 are greater than zero, and are equal to one for the case of spatially uniform precipitation or for a spatially variable precipitation which is concentrated on the basin locations characterized by average travel times. Values of Θ_1 less (greater) than one indicate that rainfall is concentrated towards the basin's portion characterized by travel times less than (greater than)

the mean travel time. When the hillslope transport processes are negligible with respect to the total runoff travel time, values of Θ_1 less than one indicate that rainfall is concentrated towards the outlet, and values larger than one indicate that rainfall is concentrated towards the headwater portion of the basin. If we compare the hydrograph generated by spatially distributed rainfall (termed '*reference hydrograph*' hereinafter) and spatially uniform rainfall we can isolate the effect of rainfall distribution. We expect that a rainfall distribution with Θ_1 less than one causes an anticipation of the mean hydrograph time in comparison with the case of a uniform rainfall distribution. This means that when rainfall is concentrated towards the outlet, the hydrograph is anticipated relative to the case of spatially uniform rainfall. The opposite is true for rainfall concentrated towards the periphery of the catchment, with the hydrograph delayed relative to the case of a spatially uniform rainfall.

The timing error between the two hydrographs is quantified by a statistic, termed "normalised time difference" dT_n. The normalised time difference dT_n is computed by dividing the time difference between the two hydrograph centroids by the mean response time of the catchment, as follows:

$$dT_n = \frac{E(T_{q\,Dist}) - E(T_{q\,Unif})}{E(T_c) + E(T_h)} \qquad 5.14$$

where $E(T_{q\,Dist})$ and $E(T_{q\,Unif})$ are the centroids of the reference hydrograph and of the hydrograph generated by uniform rainfall, respectively. A positive (negative) value of dT_n implies a positive (negative) shift in time of the reference hydrograph with respect to the one produced by using uniform precipitation. It should be noted that Eq. 5.14 may written down by exploiting Eq. 20 as follows:

$$dT_n = \frac{E(T_{q\,Dist}) - E(T_{q\,Unif})}{E(T_c) + E(T_h)} = \frac{E(T_r) + \frac{\Delta_{1,c} g_{1,c}}{v_c} + \frac{\Delta_{1,h} g_{1,h}}{v_h} - E(T_r) - \frac{g_{1,c}}{v_c} - \frac{g_{1,h}}{v_h}}{\frac{g_{1,c}}{v_c} + \frac{g_{1,h}}{v_h}} = \Theta_1 - 1 \qquad 5.15$$

Eq. 21 shows that the normalised timing error is related in a simple way to the spatial organisation of the rainfall fields by means of the scaled spatial moment of order one for the channel and the hillslope system.

5.2.2. Derivation of a simplified index

A simplified sensitivity index may be developed based on the assumption that rainfall fields do not exhibit a significant spatial correlation with the hillslope flow distance, as it occurs when the

spatial correlation length of the rainfall fields is larger than the hillslope spatial extents. Under this hypothesis, we have:

$$P_{1,h} = A^{-1} \int_A r_t(x,y) d_h(x,y) dA = A^{-1} P_0 \int_A d_h(x,y) dA = P_0 g_{1,h} \quad 5.16$$

Then:

$$\Delta_{1,h} = \frac{P_{1,h}}{P_0 g_{1,h}} = \frac{P_0 g_{1,h}}{P_0 g_{1,h}} = 1 \quad 5.17$$

Under this assumption, it is possible to write Eq. 18 in the following way:

$$\Theta_1^* = \frac{\Delta_{1,c}\tau_c + \Delta_{1,h}}{\tau_{tot}} \quad 5.18$$

Hence, by invoking again the independence between the rainfall distribution and the hillslope flow distances, Eq. 5.18 may be written as follows:

$$\Theta_1^* = \Delta_1 \frac{\tau_c + \frac{g_{1,h}}{v_c}}{\tau_{tot}} + \frac{\tau_h - \frac{g_{1,h}}{v_c}}{\tau_{tot}} \quad 5.19$$

This equation allows to clearly separate and identify the effects of the rainfall spatial organization over the catchment (Δ_1) from those the geomorphologic parameters $g_{1,h}$ and $g_{1,c}$ and of the dynamic parameters τ_c and τ_h. This offers some advantages. For instance, Eq. 22 permits to predict the sensitivity of the timing of the flood response to the spatial rainfall variability by varying the geomorphologic and dynamic parameters of a catchment. This may be used to isolate the circumstances which may attenuate the effect of rainfall spatial organization on the flood timing.

Eq. 22 may be further simplified by considering the generally negligible amount of the term $g_{1,h} \cdot v_c^{-1}$. This permits to obtain the following relationship:

$$\Theta_1^* \sim \Delta_1 \frac{\tau_c}{\tau_{tot}} + \frac{\tau_h}{\tau_{tot}} \quad 5.20$$

Examination of Eq. 5.20 shows that the sensitivity index Θ_1^* is function of two terms: the first term depends on the spatial organization of the rainfall over the catchment, whereas the second term depends on the ratio between the hillslope residence time and the mean catchment response. A dimensionless form of Eq. 5.20 is derived by introducing a dynamic parameter $V^* = \frac{v_h}{v_c}$ ed a morphological parameter $G^* = \frac{g_{1,h}}{g_{1,c}}$, as follows:

$$\frac{\tau_h}{\tau_c} = \frac{g_{1,h}}{g_{1,c}} \frac{v_c}{v_h} = \frac{G^*}{V^*} \qquad 5.21$$

$$\Theta_1^* \sim \Delta_1 \frac{V^*}{V^*+G^*} + \frac{G^*}{V^*+G^*}$$

The difference between Δ_1 and Θ_1^* vanishes under two conditions, i.e. when the values of the channel and hillslope velocities are the same and when the hillslope length vanishes.

5.3. Assessment of the flood timing error sensitivity for five extreme flash floods

We analysed the sensitivity of the flood timing error to the rainfall spatial variability and to the geometric and dynamic characteristics of the hillslope and river system for a number of flood events in Europe for which observational and modeling analyses are available.

The observational data sources used for this study are represented by rainfall and discharge data from five extreme storms and ensuing floods which have been observed in Europe in the period between 2002 and 2007. The main features of the storms and ensuing floods are reported in chapter 3.1. The case studies are the following: Sesia at Quinto (North-western Italy, 982 km^2) occurred on 04/06/2002, Sora at Vester (Slovenia, 212 km^2), occurred on 18/09/2007, Feernic at Simonesti (Romania, 168 km^2), occurred on 23/08/2005, Clit at Arbore (Romania, 36 km^2), occurred on 30/06/2006 and Grinties at Grinties (Romania, 51 km^2), occurred on 04/08/2007. These storms were selected because of the various catchment sizes (ranging from 36 to 982 km^2), storm durations (ranging from 5h30' to 21 hours) and space-time variability which characterize the storm events. The data concerning the events were derived from the flash flood data archive developed in the frame of the EU Project HYDRATE (www.hydrate.tesaf.unipd.it) (Borga *et al.* 2010).

To isolate the role of rainfall distribution for each catchment considered in the analysis we used the methodology explained in chapter 3.2. We compared the reference hydrograph with the hydrograph generated by considering a space-time constant runoff coefficient. With this last assumption, the model should behave exactly as predicted by using the spatial moments. The advantage of this type of analysis is to separate the role of rainfall spatial variability in the runoff generation process from that played in the runoff propagation process (where we consider the rainfall as a proxy for the runoff rate). An example of this analysis is provided in Fig. 5.1 for the 501 km^2-wide catchment of Sesia at Busonengo in the Sesia river system (event of 04/06/2002). The runoff model parameters are reported in Table 5.1, together with the values of the spatial

moments and of the sensitivity index. The simulations carried out by applying a space-time constant runoff coefficient, for spatially uniform and spatially distributed rainfall, are reported in Fig. 5.1a. The comparison between the two hydrograps allows to identify a considerable anticipation of the flood hydrograph obtained by using spatially uniform rainfall with respect to that obtained spatially distributed rainfall. The anticipation is due to the concentration of the event-cumulated rainfall over the catchment headwaters, due to considerable orographic effect on convective precipitation (Sangati 2009). The rainfall concentration is quantified by the overall spatial moment of order one, with a value of 1.38. The sensitivity index Θ_1 has a smaller value, due to effect of the hillslope system, equal to 1.27. The timing error dT_n is equal to 0.27, as indicated by Eq. 21. This is not surprising, since the rainfall-runoff model applied in this way reproduces exactly the assumptions used in the development of the spatial moments.

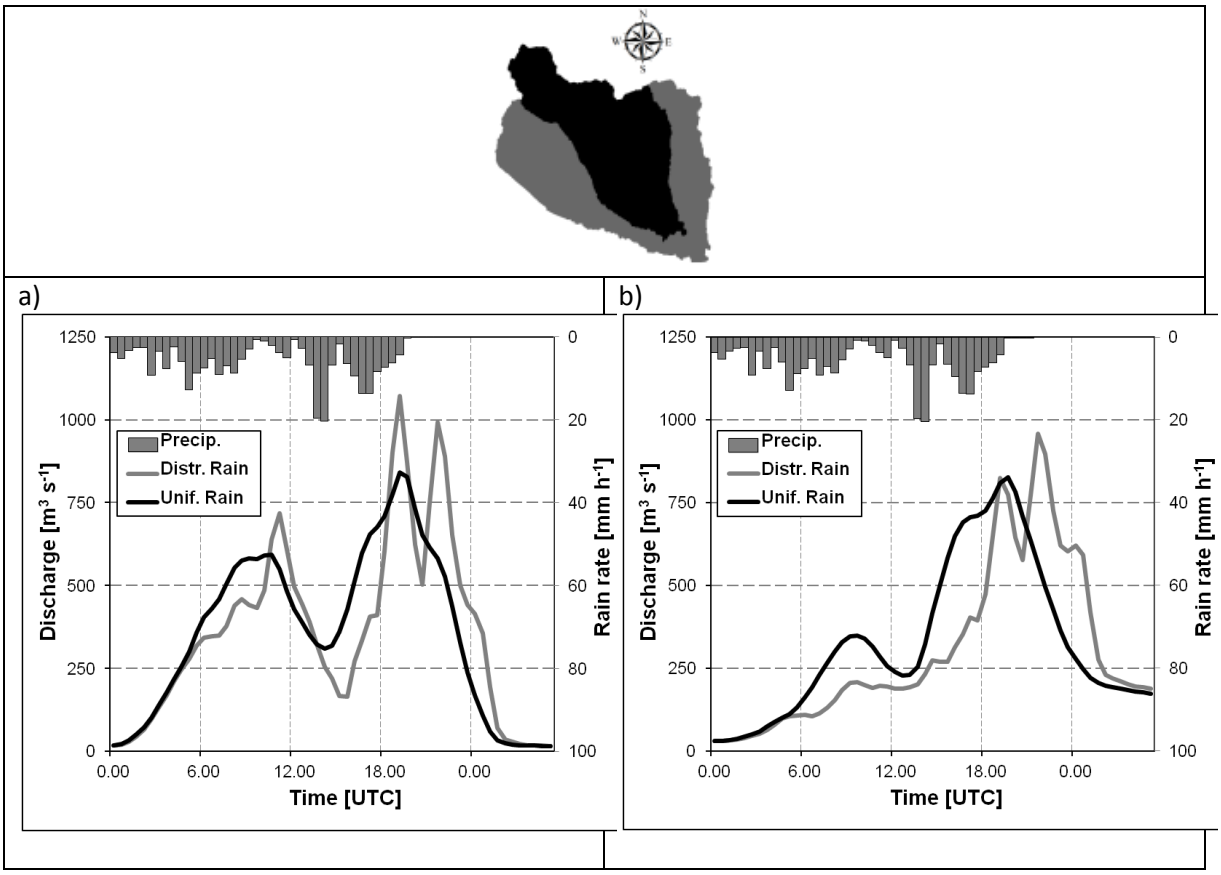

Figure 5.1: Flood hydrographs generated with spatially uniform and distributed rainfall inputs for the basin of Sesia river at Busonengo (501 km^2) (insert). a) Simulations obtained by using a space and time constant runoff coefficient; b) simulations obtained by using the complete distributed rainfall-runoff model. The runoff coefficient used to generate the hydrographs in (a) is the same as that characterizing the simulations displayed in (b).

Table 5.1: Geomorphological parameters, dynamic parameters, spatial moments and sensitivity index for the case of Sesia river at Busonengo (501 km^2)

$g_{1,c}$, $g_{1,h}$	29,8km 0,255km
v_c, v_h, A_s	3.5m/s, 0.1m/s, 2ha

$\boldsymbol{\Delta_{1,c}, \Delta_{1,h}, \Delta_1}$	1.38, 1.06, 1.38
$\boldsymbol{\Theta_1}$	1.26

Fig. 5.1b displays the hydrographs generated by the distributed hydrological model with the variable space-time infiltration by using both spatially distributed and spatially uniform rainfalls. The general behaviour reported in Fig. 5.1b is similar to that shown in Fig. 5.1a, even though a more pronounced anticipation (i.e. timing error) can be identified. Of course, the spatial moments are unchanged with respect to the previous case. However, the timing error dT_n is equal to 0.7, which is more than twice the value obtained by using a space and time constant runoff coefficient. This effect is the result of the non-linearity characterizing the flood runoff generation. Proportionally more runoff is generated with increasing rainfall accumulation, which leads to a magnification of the dT_n statistic with respect to the one obtained under the assumption of a space-time constant runoff coefficient.

The dT_n values obtained for the 27 cases by using a rainfall-runoff model with space-time constant runoff coefficient are reported in Fig. 5.2 together with the corresponding Θ_1 values. As expected, the relationship between dT_n and Θ_1 follows accurately the relationship provided by Eq. 21, since in this case the model application reproduces exactly the assumptions used in the development of the relationship. The values of dT_n range between 0.05 to 0.28, with many more positive values than negative values. This shows that in general, the effect of disregarding the spatial rainfall variability translates to an anticipation of the simulated flood hydrograph with respect to that obtained by considering the rainfall spatial variability in the flood modelling phase. This is due to concentration of rainfall towards the headwater basins, which reflect the orographic enhancement of convection characterising some of the cases analysed here. Also, the figures shows that positive values of dT_n characterise medium-size basins larger than 150 km^2, whereas smaller basins are characterised by very low or negative values of dT_n.

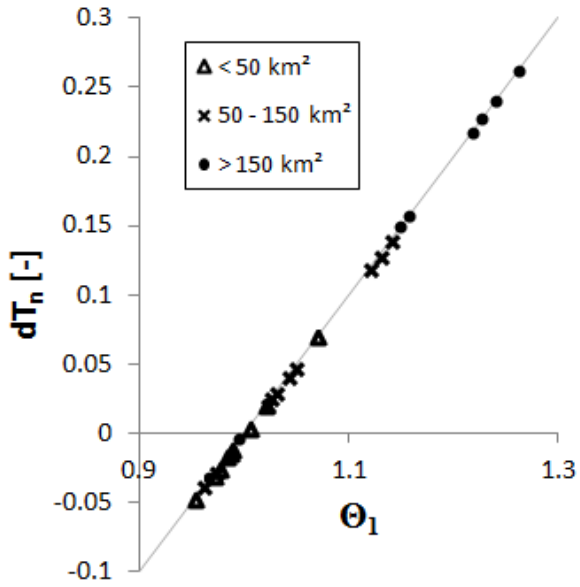

Figure 5.2: Relationship between Θ_1 and dT_n for hydrological simulations with space-time constant runoff coefficient. The continuous line is the line $dT_n = \Theta_1 - 1$, given by Eq. 21.

The values of the morphological parameters g_{1c} and g_{1h} used in the flood simulations are reported in Fig. 5.3a,b. A power equation, with exponent equal to 0.52, fits the relationship between the values of g_{1c} and drainage area. This equation is a version of the classical Hack's law, following Hack (1957) who reported $L \propto A^{0.6}$ for streams in the Shenandoah Valley and adjacent mountains of Virginia. The exponent in this equation is almost in the range 0.53-0.59 reported by Rigon et al. (1996) for the Hack's law in basins ranging from 50 to 2000 km^2. Explanations for the exponent being larger than 0.5 (implying positive allometry) emphasised the role of basin elongation as well as the fractal characteristic of river networks (Rigon et al., 1996). The values of the parameter $g_{1,h}$ are almost constant with respect to varying the drainage area.

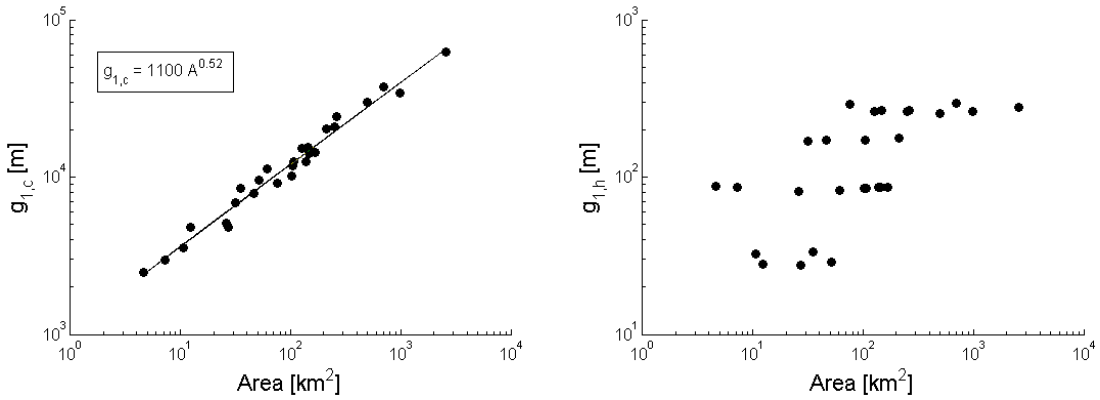

Figure 5.3a,b: Relationship between drainage area and a) $g_{1,c}$ and b) $g_{1,h}$.

Fig. 5.4 reports the results for the 27sub-catchments obtained by removing the assumption of space-time constant runoff coefficient (i.e., by using the whole modeling chain including the infiltration module). The organization of values of dT_n follows the same pattern already reported in Fig. 5.2, with the larger basins characterized by larger positive values of dT_n . However, the range of values of dT_n is much larger than that reported in Fig. 5.2, with values spanning between -0.25 to 0.7. Correspondingly, the regression line $dT_n = 2.71\ \Theta_1 - 2.80$ is much steeper in this figure than in Fig. 5.2.

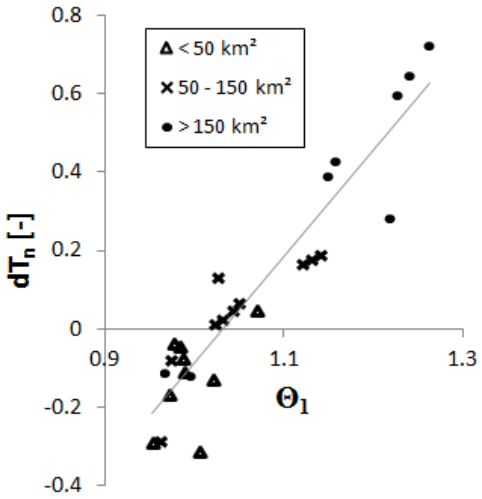

Figure 5.4: Relationship between Θ_1 and dT_n for hydrological simulations obtained by using the complete hydrological model. The continuous line is the regression line dTn=2.71 Θ_1-2.80, which is characterized by r^2=0.83.

As reported in the comment to Fig. 5.1b, this effect is due to the nonlinearity incorporated into the runoff generation modeling, which leads to a magnification of the dT_n statistics with respect to those obtained under the assumption of a space-time constant runoff coefficient. Correspondingly, this shows that the dT_n statistics obtained by means of Eq. 21, i.e. by using the rainfall field as a proxy for the runoff spatial distribution, provides a lower bound for the timing error distribution.

5.3.1. Assessing the hillslope influence on the runoff timing error

The derivation of Eq.5.20 for the sensitivity index relies on the assumption that rainfall fields do not exhibit a significant degree of rainfall organization over the hillslope flow distance. This assumption leads to consider the value $\Delta_{1,h}$ equal to one. This assumption is assessed over the sample of cases considered in this study. Fig.5.5 reports the frequency distribution of the values

of $\Delta_{1,c}$ and of $\Delta_{1,h}$, showing that the values of $\Delta_{1,h}$ are distributed very close to 1. On the contrary, the values of $\Delta_{1,h}$ are distributed over a wider range from 0.95 to 1.4. Fig. 4.0 shows that there is a weak relationship between the values of $\Delta_{1,c}$ and of $\Delta_{1,h}$, with the largest values of $\Delta_{1,h}$ corresponding to the largest values of $\Delta_{1,c}$. This is related with the higher rainfall concentration represented by high $\Delta_{1,c}$, that has a smoothed effect also on $\Delta_{1,h}$.

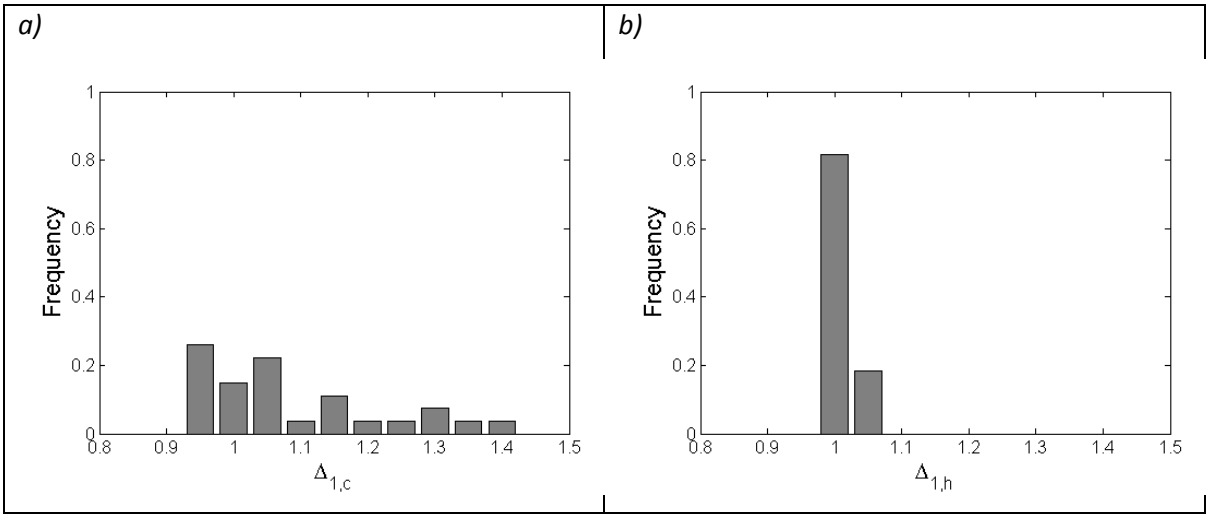

Figure 5.5a,b: Frequency distribution of the values of a) $\Delta_{1,c}$ and (b) $\Delta_{1,h}$.

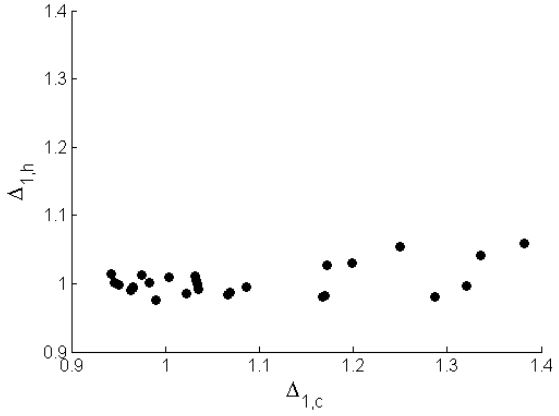

Figure 5.6: Relationship between the values of $\Delta_{1,c}$ and $\Delta_{1,h}$.

The accuracy of the relationship based on Eq. 5.20 has been tested in a series of numerical experiments in which the flood simulations have been repeated by modifying only the hillslope system characteristics and using a space-time constant runoff coefficient (equal to one). The runoff propagation parameters are as follows: the channel velocity v_c and the support area A_s have been kept equal to 3 ms^{-1} and to 0.02 km^2, respectively. Three hillslope velocity v_h scenarios

were considered, corresponding to 0.5 ms^{-1}, 0.1 ms^{-1} and 0.01 ms^{-1}. This corresponds to three scenarios where the hillslope residence time is progressively more important with respect to the catchment runoff response time.

The relationship between dT_n and Θ^*_1 is reported in Fig. 5.7 for the three scenarios.

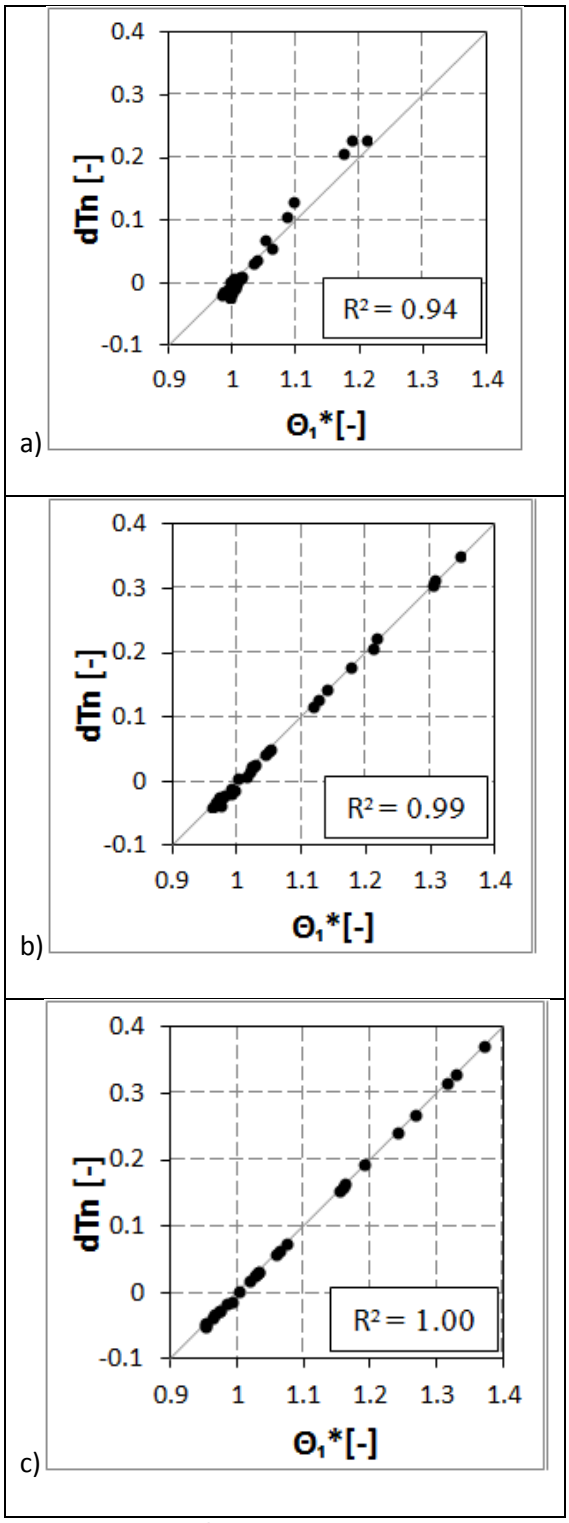

Figure 5.7: Relationship between the timing error dT_n and Θ_1 with increasing hillslope residence time. a) v_h=0.01 ms^{-1}; b) v_h=0. 1 ms^{-1} ; c) v_h=0.5 ms^{-1}.

Two features are noteworthy in figure 5.7. First of all, the figure shows clearly that the simplified sensitivity index Θ^*_1 is able to reproduce effectively the distribution of dT_n for the three cases. Clearly, the quality of the description slightly decreases with increasing the hillslope residence time. However, the correlation between dT_n and Θ^*_1 is very high (equal to 0.94) even in the most

severe scenario characterized by a value of hillslope velocity equal to 0.01 ms^{-1}. This means that Eq. 5.20 provides a robust description of the relative effects of the hillslope and river network routing on the timing error over a wide range of scenarios. Moreover, it is interesting to analyze the distribution of dT_n in the three cases. dT_n ranges between -0.05 to 0.38 for the v_h =0.5 ms^{-1}. It ranges between -0.025 to 0.25 for the v_h =0.01 ms^{-1}. This means that the timing error due to rainfall distribution is generally reduced by 63% when the mean hillslope residence time increases from 200 *s* to 10000 *s*.

5.3.2. A catchment-similarity framework for the assessment of runoff timing error sensitivity

The effect of the hillslope system on the runoff timing error dT_n is captured by the ratio Θ_1^*/Δ_1 based on Eq. 5.21. The relationship between the ratio Θ_1^*/Δ_1 and the parameters V^* and G^* is exemplified in Fig. 5.8a,b for two different values of Δ_1, equal to 1.5 and to 0.5, respectively, based on Eq. 5.21. In these two figures, the red (blue) color means that the hillslope systems has a negligible (considerable) effect on the timing error. The figures shows how, for a given value of $V^* = v_h/v_c$, the effect of the hillslope system increases by increasing the ratio $G^* = g_{1,h}/g_{1,c}$, which means by increasing the support area A_s. The figures can be used to quantify the catchment similarity as far as the timing error is of concern. To exemplify how the figures can be used for this last purpose, we mapped each of the studied sub-catchments, characterized by their geomorphologic and dynamic parameters, over the two spaces. This shows that the sensitivity of the largest basin of the Sesia river system is similar to that of the largest basin of the Grinties river system, in spite of the rather large difference in terms of size.

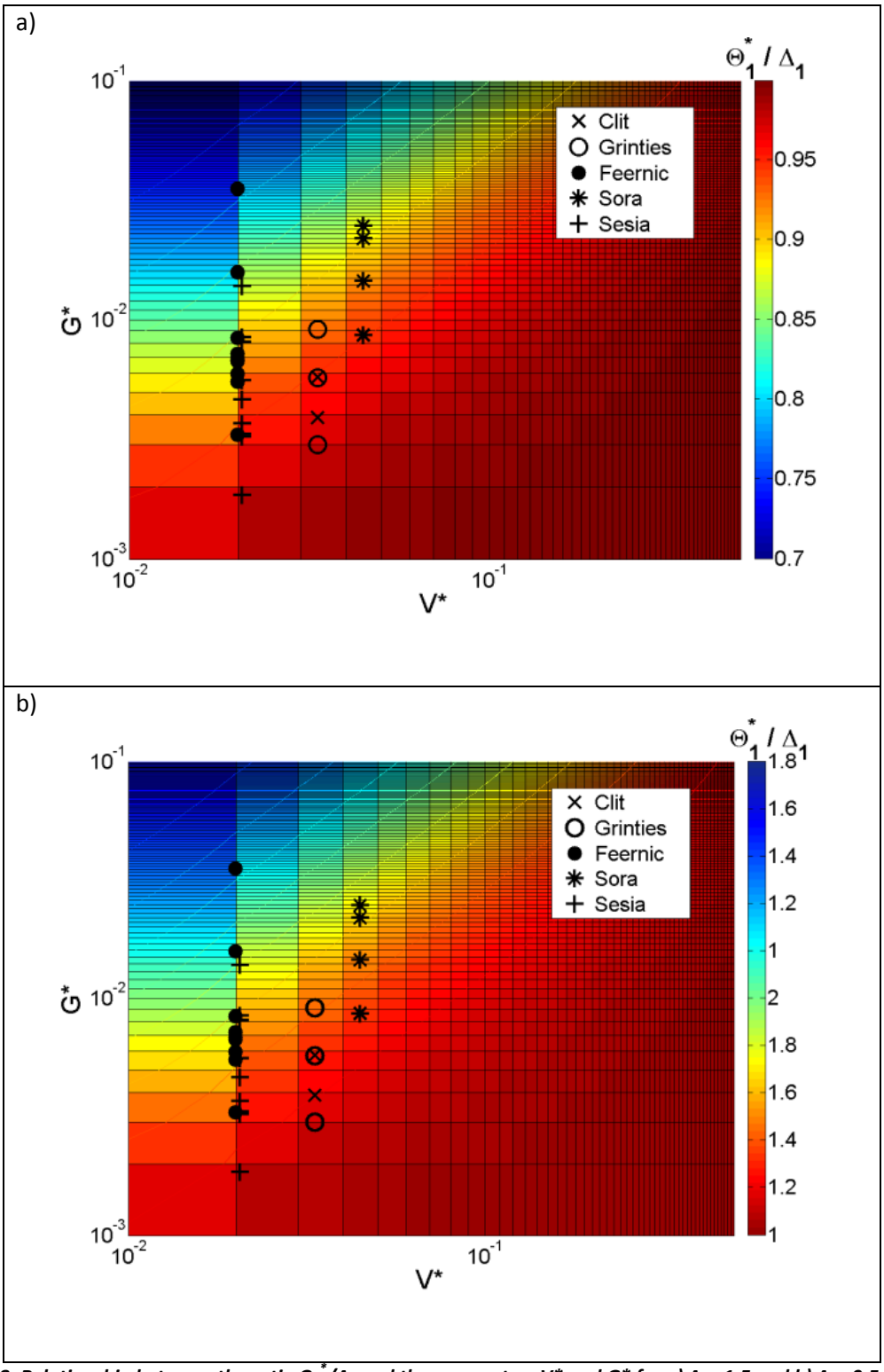

Figure 5.8: Relationship between the ratio Θ_1^*/Δ_1 and the parameters V* and G* for a) Δ_1 =1.5 and b) Δ_1 =0.5.

5.4. Discussion and conclusions

Starting from *spatial moments of catchment rainfall* we integrated the relative role of hillslopes and channel network on timing of the flood hydrograph, accounting for the effect of the spatial

variability of rainfall. This framework can be employed to assess the effects of parameters characterizing the hillslope and channel residence time, allowing the comparison between different scenarios and the identification of dominant controls in the propagation.

The statistics have been developed under the hypothesis of uniform runoff coefficient, this to avoid the uncertainty attached to the prediction of its spatial variability. This assumption restricts the applicability of the method to strong storms, where runoff is produced all across the catchment and surface runoff is dominating hydrograph response. Even in small basins however this assumption proved to be critical. Fig. 5.4 highlights how, despite the high uncertainty, the relation retains some linearity and spatial moments of catchment rainfall are still useful to predict the effect on the hydrograph.

Another hypothesis analyzed is the non-correlation between rainfall and hillslopes, due to their different characteristic lengths. The hypothesis holds for the flash floods analyzed (Fig. 5.5), and the resulting Θ_1^* well describes the normalized time difference dT_n. As we anticipated above, errors may arise in case of strong correlations between hillslope residence time and rainfall distribution. This may happen when the channelization support area is function of rainfall, or because geology creates large scale heterogeneities. However, this hypothesis allows one to draw a direct relation between the sensitivity index Θ_1 and the overall statistic of rainfall organization over the catchment (Δ_1).

The framework presented is useful to assess the role of different rainfall patterns on the timing off the catchment response as function of different hillslope and river network structures. The influence of rainfall variability, as compared with the case of uniform runoff velocity, can be corrected by tuning the geomorphologic and dynamic parameters from the river routing and hillslope. The sensitivity of different basins to the rainfall distribution can be evaluated under different scenarios, and related with other environmental factors such as antecedent soil moisture conditions. The framework can also be useful to understand the optimal resolution required for describing the spatial variability of the rainfall in order to get an accurate prediction of the catchment response time.

6. Quantifying the effect of moving storms on planar flow by using the spatial moments of catchment rainfall: comparison with analytical solutions

This chapter provides an analytical assessment of the spatial moments of catchment rainfall. These statistics provide a synthesis of the interaction between storm properties (including motion) and basin morphometric properties. In the previous chapters on spatial moments of catchment rainfall we investigated the relationship with the statistics introduced by Viglione *et al.* (2010) and analyzed the effect of neglecting the spatial rainfall variability on flood hydrographs simulations. In this work we derive analytically the spatial moments of catchment rainfall for the case of flow from an impervious plane owing to storms travelling downstream. The solutions obtained are used to derive the temporal statistics for the flood hydrograph.

Analytical solutions provide considerable insight into the relation between storm movement and flow dynamics. These solutions are finally compared with those derived by applying the method of characteristics under the assumptions of linear kinematic structure, as in Singh (1998) and Singh (2002). The key aims of this study are to examine how single features of storm and catchment response affect the planar flow wave response, and to find different interactions between features of stationary and moving storm events, with their implications.

The potential conclusions we can draw from this work are:

- The accuracy of the method of the spatial moments of catchment rainfall compared to an analytical solution of the linear kinematic wave;
- The feasibility of writing the first two temporal moments of the flow in a compact and closed way, hence representing the main physical controls on the flow shape (in this work the main physical controls are represented by three main temporal scales);
- The feasibility of writing the catchment scale storm velocity in a compact and closed way.

6.1. Deriving the spatial moments of catchment rainfall for the case of planar flow and downbasin storm

The methodology of the Spatial Moments of Catchment rainfall is applied in this section to the problem of planar flow owing to storms moving down the plane. Consider a plane of length L, width unity ($W=1$) and slope S_0 (Fig. 6.1). A storm travels with velocity V_s down the plane. The

upslope spatial coordinate x is taken parallel to the plane, with the origin at the lowest point. Let the storm last a constant duration *T* at each point of the plan, with constant intensity *r*. Let the celerity of the flow be equal to v. As we will show below, three time scales may be used to describe the shape of the resulting flood hydrographs. The three timescales are as follows: duration of the storm at each point, *T*; the response time scale of the plane, $T_c=L/v$; the travel time of the storm on the plane, $T_s=L/V_s$. Accordingly with the terminology introduced by Seo *et al.* (2012), T_c represent an intrinsic temporal scale, whereas *T* and T_s represent two fundamental extrinsic temporal scales.

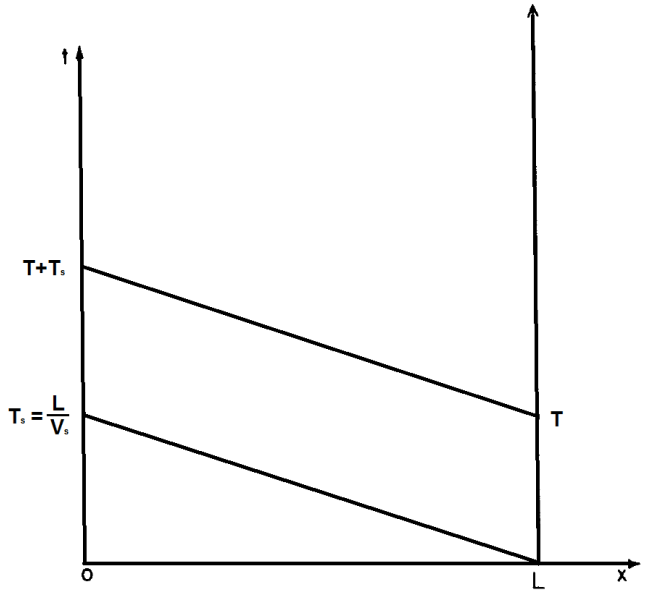

Figure 6.1: Geometry of the planar flow study for a storm moving downstream, where 0 is the outlet.

In the next chapters we are going to analyze two types of downhill storm motion. In the first case *(Figure 6.2a)* the duration of rainfall over each point of the basin is longer than the time the storm takes to travel to the outlet. This generates a time interval where the rain is falling uniformly over the basin, and the storm movement does not change rainfall patterns (grey dashed lines in the figure). Instead, in the second case analyzed rainfall duration is shorter than the travel time of the catchment. This means that rainfall coverage is always partial and that rainfall patterns are always changing within the basin.

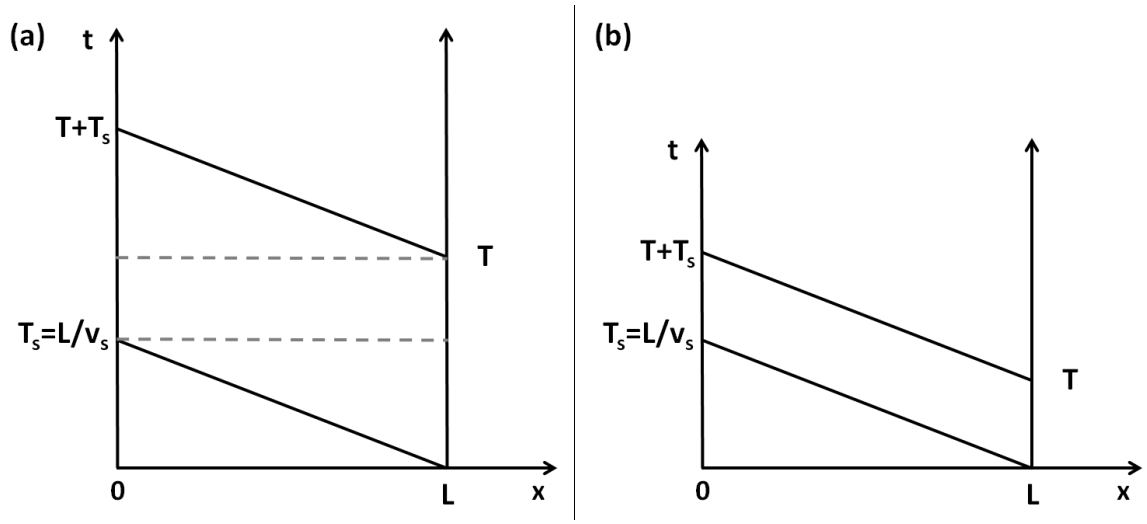

Figure 6.2: case of (a) full rainfall coverage over the basin and (b) partial rainfall coverage. The gray dashed lines indicate the time of full rainfall coverage.

6.2. Case of full basin cover (T>Ts)

Spatial moments are applied to the planar flow in conditions of basin fully cover with rainfall, which is defined by *($T>T_s$) (Figure 6.2).* Computation of $p_0(t)$ (which represents the 0th spatial moment) is as follows:

$$p_0(t) = L^{-1}\int_{L-V_s t}^{L} r\,dx = r\frac{t}{T_s} \qquad 0 \le t \le T_s \tag{6.1}$$

$$p_0(t) = L^{-1}\int_{0}^{L} r\,dx = r \qquad T_s \le t \le T$$

$$p_0(t) = L^{-1}\int_{0}^{L-V_s(t-T)} r\,dx = r\left[1-\frac{(t-T)}{T_s}\right] \qquad T \le t \le T+T_s$$

While the storm is moving down the catchment, mean rainfall rate is equal to intensity r multiplied by the coverage $t\,T_s^{-1}$. When the precipitation completely covers the catchment, mean rainfall rate is equal to r. Finally when rainfall starts to clear in the upper part of the catchment the mean rainfall rate declines with time until $t = T + T_s$. As a consequence, the pluviograph is trapezoidal and the expected value and the variance of the rainfall holding time $E(T_r)$ are given by:

$$E(T_r) = \frac{1}{2}(T + T_s) \tag{6.2}$$

$$Var(T_r) = E\left(T_r^{\,2}\right) - E(T_r)^2 = \frac{1}{12}\left(T_s^2 + T^2\right)$$

The first-order spatial moment of catchment rainfall $p_1(t)$ is given by:

$$p_1(t) = L^{-1}\int_{L-V_s t}^{L} rx\,dx = \frac{1}{2}rL\left[1-\left(1-\frac{t}{T_s}\right)^2\right] \qquad 0 \le t \le T_s \tag{6.3}$$

$$p_1(t) = L^{-1}\int_{0}^{L} rx\,dx = \frac{1}{2}rL \qquad T_s \le t \le T$$

$$p_1(t) = L^{-1}\int_{0}^{L-V_s(t-T)} rx\,dx = \frac{1}{2}rL\left[1-\frac{t-T}{T_s}\right]^2 \qquad T \le t \le T+T_s$$

Hence, the non-dimensional form of the first-order spatial moment is as follows:

$$\delta_1(t) = 2-\frac{t}{T_s} \qquad 0 \le t \le T_s \tag{6.4}$$

$$\delta_1(t) = 1 \qquad T_s \le t \le T$$

$$\delta_1(t) = 1-\frac{t-T}{T_s} \qquad T \le t \le T+T_s$$

As expected, the rainfall position index $\delta_1(t)$ describes a value larger than 1, thus concentrated in the upper section of the basin, until T_s. Later rainfall becomes uniform, positioning the centre of mass in the centre of the basin. In the end we have $\delta_1 < 1$, representing rainfall moving near the outlet.

The second-order spatial moment of catchment rainfall p_2 is given by:

$$p_2(t) = L^{-1}\int_{L-V_s t}^{L} rx^2\,dx = \frac{1}{3}rL^2\left[1-\left(1-\frac{t}{T_s}\right)^3\right] \qquad 0 \le t \le T_s \tag{6.5}$$

$$p_2(t) = L^{-1}\int_{0}^{L} rx^2\,dx = \frac{1}{3}rL^2 \qquad T_s \le t \le T$$

$$p_2(t) = L^{-1}\int_{0}^{L-V_s(t-T)} rx^2\,dx = \frac{1}{3}rL^2\left[1-\frac{(t-T)}{T_s}\right]^3 \qquad T \le t \le T+T_s$$

This statistic describes more concentration of rainfall (lower δ_2 values) at the rising and falling limb of the hydrographs. The time-integrated values of the spatial moments are given as follows:

$$P_0 = r\frac{T}{T+T_s} \tag{6.6}$$

$$P_1 = \frac{1}{2}rL\ \frac{T}{T+T_s}$$

$$P_2 = \frac{1}{3}rL^2\frac{T}{T+T_s}$$

We can use the time-integrated values of the spatial moments to define the non dimensional indexes of position and distribution Δ_1 and Δ_2:

$$\frac{P_2}{P_0} = \frac{L^2}{3} \qquad 6.7$$
$$\frac{P_1}{P_0} = \frac{L}{2}$$

$$\left[\frac{P_2}{P_0} - \left(\frac{P_1}{P_0}\right)^2\right] = \frac{L^2}{12} \qquad 6.8$$

$$g_1 = \frac{L}{2} \qquad 6.9$$
$$g_2 = \frac{L^2}{3}$$

$$\Delta_1 = 1 \qquad 6.10$$
$$\Delta_2 = 1$$

Because for each point in the catchment rainfall lasted the a time *T* with a constant intensity *r*, the result of eq. 6.10 was expected. The position and distribution of the event cumulated rainfall is equal to the ones of completely uniform rainfall and thus has no effect on the hydrograph. However the movement of storm through the plane is expected to influence the flow at the outlet. To see the effect we can compute the catchment-sale storm velocity using the formula derived in chapter 4.2:

$$V = g_1 \frac{\mathrm{cov}_t\left[T, \delta_1(t) w(t)\right]}{\mathrm{var}[T]} - g_1 \frac{\mathrm{cov}_t\left[T, w(t)\right]}{\mathrm{var}[T]} \Delta_1 \qquad 6.11$$

$$w(t) = \frac{T_s + T}{T}\frac{t}{T_s} \qquad 0 \le t \le T_s$$
$$w(t) = \frac{T_s + T}{T} \qquad T_s \le t \le T$$
$$w(t) = \frac{T_s + T}{T}\left[1 + \frac{T - t}{T_s}\right] \qquad T \le t \le T + T_s$$

6.12

$$w(t)\delta_1(t) = \frac{T_s + T}{T} 2\frac{t}{T_s}\left(1 - \frac{1}{2}\frac{t}{T_s}\right) \qquad 0 \le t \le T_s$$
$$w(t)\delta_1(t) = \frac{T_s + T}{T} \qquad T_s \le t \le T$$
$$w(t)\delta_1(t) = \frac{T_s + T}{T}\left[1 + \frac{T - t}{T_s}\right]^2 \qquad T \le t \le T + T_s$$

6.13

$$\mathrm{cov}_t\left[T, \delta_1(t)w(t)\right] = -\frac{1}{6}T_s$$
$$\mathrm{cov}_t\left[T, w(t)\right] = 0$$

6.14

$$V\,\mathrm{var}[T] = g_1\,\mathrm{cov}_t\left[T, \delta_1(t)w(t)\right] - g_1\,\mathrm{cov}_t\left[T, w(t)\right]\Delta_1 = -\frac{1}{12}LT_s$$

6.15

Because $V\,var[T] = cov[T_r, T_c]v$ where v is the velocity of flow propagation down the catchment, eq. 6.15 isolated the effect of storm motion on the hydrograph. To isolate the catchment scale storm velocity we can write:

$$\mathrm{var}[T] = \frac{1}{12}\left(T + T_s\right)^2$$

6.16

$$V = -V_s \frac{1}{\left(1 + \frac{T}{T_s}\right)^2}$$

6.17

Since the *catchment scale storm velocity* represent the effect of the motion on the hydrograph, the relation found connects the motion of the storm front v_s with its effect on the hydrograph V

for planar flow in the conditions of full coverage and downbasin motion. This relation depends on the ratio between the duration of rainfall T and the duration of the travel across the basin T_s.

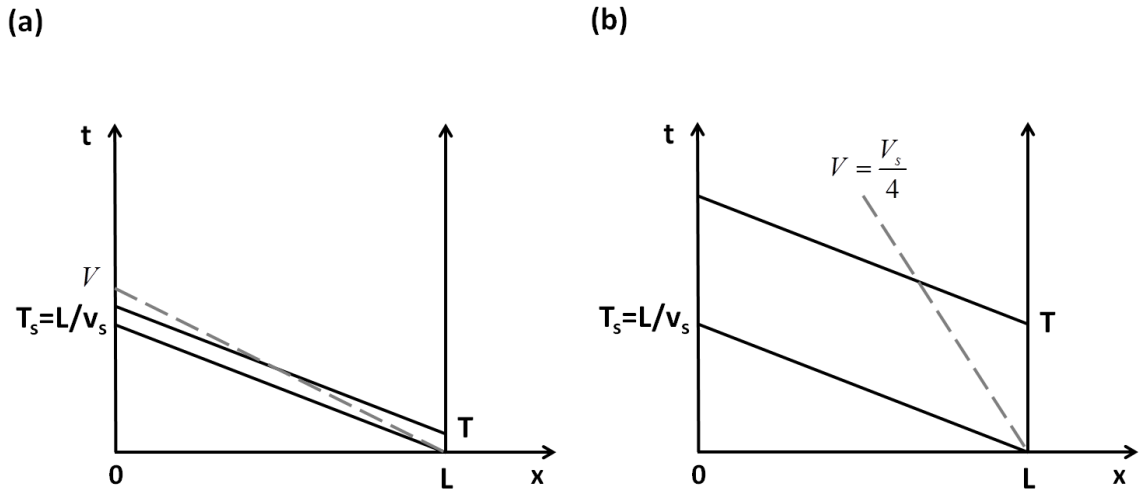

Figure 6.3: Representation of the catchment scale storm velocity (dashed grey line) for the case of (a) short rainfall duration; (b) $T = T_s$.

From equation 6.17 we know that when the duration of rainfall is low, the value of catchment scale storm velocity V tends to the velocity of the storm front V_S (*Figure 6.3*a). Instead, at the transition between full and partial coverage of rainfall over the basin ($T = T_S$), the value of V is equal to $1/4V_S$. This velocity allows to travel half of the basin length $L/2$ during the total storm time $(T + T_s)$. Catchment scale storm velocity is negative, since we are analyzing a storm moving downhill, and will be lower for longer storms (higher *T*). At this point, we have all the elements to compute the total variance of the hydrograph Var(T_q), as follows:

$$\mathrm{var}[T_q] = Var[T_r] + \frac{\Delta_2}{v^2}\left(g_2 - g_1^{\,2}\right) + 2\frac{V}{v}Var[T] \qquad 6.18$$

which gives:

$$\mathrm{var}[T_q] = \frac{1}{12}\left(T_s^{\,2} + T^2\right) + \frac{1}{12}T_c^{\,2} - \frac{1}{6}T_cT_s = \frac{1}{12}T_s^{\,2} + \frac{1}{12}T^2 + \frac{1}{12}T_c^{\,2} - \frac{1}{6}T_cT_s \qquad 6.19$$

The hydrograph dispersion for the case analyzed is function of the time of travel of the storm front across the catchment T_S, of the duration of the storm T and of the time of corrivation T_c. On the other hand the mean runoff time can be expressed as:

$$E(T_q) = \frac{1}{2}(T_s + T_c + T) \qquad 6.20$$

It is easy to show that Eq. 6.19 is corresponding exactly with the variance computed based on the solution of the flow equations provided with the simple method of characteristics, which is given below:

$$\begin{aligned} Q(t) &= 0 && 0 \le t \le \frac{L}{V_s} \\ Q(t) &= \frac{rv}{V_s - v}(tV_s - L) && \frac{L}{V_s} < t \le \frac{L}{v} \\ Q(t) &= rL && \frac{L}{v} \le t \le T + \frac{L}{V_s} \\ Q(t) &= rvV_s \frac{T + \frac{L}{v} - t}{V_s - v} && T + \frac{L}{V_s} \le t \le T + \frac{L}{v} \end{aligned} \qquad 6.21$$

$$E(T_q) = \frac{1}{2}\left(T + \frac{L}{V_s}\right) + \frac{1}{2}\frac{L}{v} \qquad 6.22$$

$$E(T_q^2) = \frac{1}{6V_S^2 v^2}\left(2V_S^2 v^2 T^2 + 3v^2 T V_S L + 2L^2 v^2 + 3vTLV_S^2 + 2vL^2 V_S + 2L^2 V_S^2\right) \qquad 6.23$$

$$\mathrm{var}(T_q) = \frac{1}{12}\left(\frac{L^2}{V_S^2} + T^2\right) + \frac{1}{12}\frac{L^2}{v^2} - \frac{1}{6}\frac{L^2}{V_S v} \qquad 6.24$$

Eq. 6.24 is equivalent to Eq. 6.19 above.

6.3. Case of partial basin coverage (T<Ts)

In the second case we want to analyze the partial rainfall coverage of the basin *($T<T_s$)* as described in *Figure 6.2a*. A storm moving down the plane, similarly to what observed in the last chapter, but with storm extent smaller than the basin. This means that when the front of the storm reaches the outlet at the headwater rainfall has already stopped, and the catchment is never going to be fully covered by the storm. The pluviograph for the catchment will have a triangular shape,

instead of the trapezoidal of the previous case, with a peak lower than *r*. Computation of $p_0(t)$ (which represents the 0th spatial moment) is as follows:

$$p_0(t) = L^{-1}\int_{L-V_s t}^{L} r dx = r\frac{t}{T_s} \qquad 0 \le t \le T$$
$$p_0(t) = L^{-1}\int_{L-V_s t}^{L-V_s(t-T)} r dx = r\frac{T}{T_s} \qquad T \le t \le T_s \qquad 6.25$$
$$p_0(t) = L^{-1}\int_{0}^{L-V_s(t-T)} r dx = r\left[1-\frac{(t-T)}{T_s}\right] \qquad T_s \le t \le T+T_s$$

The statistics of T_r doesn't change:

$$E(T_r) = \frac{1}{2}(T+T_s) \qquad 6.26$$
$$Var(T_r) = E\left(T_r^{\,2}\right) - E(T_r)^2 = \frac{1}{12}\left(T_s^2 + T^2\right)$$

The first-order spatial moment of catchment rainfall $p_1(t)$ is given by:

$$p_1(t) = L^{-1}\int_{L-V_s t}^{L} r x dx = \frac{1}{2} rL\left[1-\left(1-\frac{t}{T_s}\right)^2\right] \qquad 0 \le t \le T$$
$$p_1(t) = L^{-1}\int_{L-V_s t}^{L-V_s(t-T)} r x dx = rL\frac{T}{T_s}\left[1-\frac{t}{T_s}+\frac{1}{2}\frac{T}{T_s}\right] \qquad T \le t \le T_s \qquad 6.27$$
$$p_1(t) = L^{-1}\int_{0}^{L-V_s(t-T)} r x dx = \frac{1}{2} rL\left[1-\frac{t-T}{T_s}\right]^2 \qquad T_s \le t \le T+T_s$$

Hence, the non-dimensional form of the first-order spatial moment is as follows:

$$\delta_1(t) = 2-\frac{t}{T_s} \qquad 0 \le t \le T$$
$$\delta_1(t) = 2\left(1-\frac{t}{T_s}+\frac{1}{2}\frac{T}{T_s}\right) T \le t \le T_s \qquad 6.28$$
$$\delta_1(t) = 1-\frac{t-T}{T_s} \qquad T_s \le t \le T+T_s$$

The second-order spatial moment of catchment rainfall p_2 is given by:

$$p_2(t) = L^{-1}\int_{L-V_s t}^{L} rx^2 dx = \frac{1}{3}rL^2\left[1-\left(1-\frac{t}{T_s}\right)^3\right] \qquad 0 \le t \le T \qquad 6.29$$

$$p_2(t) = L^{-1}\int_{L-V_s t}^{L-V_s(t-T)} rx^2 dx = \frac{1}{3}rL^2\left[\left(1-\frac{t-T}{T_s}\right)^3 - \left(1-\frac{t}{T_s}\right)^3\right] \qquad T \le t \le T_s$$

$$p_2(t) = L^{-1}\int_{0}^{L-V_s(t-T)} rx^2 dx = \frac{1}{3}rL^2\left[1-\frac{(t-T)}{T_s}\right]^3 \qquad T_s \le t \le T+T_s$$

The time-integrated values of the spatial moments are given as follows:

$$P_0 = r\frac{T}{T+T_s} \qquad 6.30$$

$$P_1 = \frac{1}{2}rL\ \frac{T}{T+T_s}$$

$$P_2 = \frac{1}{3}rL^2\frac{T}{T+T_s}$$

Hence:

$$\frac{P_2}{P_0} = \frac{L^2}{3} \qquad 6.31$$

$$\frac{P_1}{P_0} = \frac{L}{2}$$

$$\left[\frac{P_2}{P_0} - \left(\frac{P_1}{P_0}\right)^2\right] = \frac{L^2}{12} \qquad 6.32$$

$$g_1 = \frac{L}{2} \qquad 6.33$$

$$g_2 = \frac{L^2}{3}$$

$$\Delta_1 = 1 \qquad 6.34$$

$$\Delta_2 = 1$$

Also in this case the cumulated value of rainfall over each point of the basin is constant, and thus the non dimensional indicators of rainfall position and dispersion have values as in uniform rainfall distribution. However in sec. 6.2 we saw that catchment scale storm velocity *V* has an impact on the hydrograph. The computation follows the precedure of the previous case:

$$V = g_1 \frac{\mathrm{cov}_t\left[T, \delta_1(t) w(t)\right]}{\mathrm{var}[T]} - g_1 \frac{\mathrm{cov}_t\left[T, w(t)\right]}{\mathrm{var}[T]} \Delta_1 \qquad 6.35$$

$$w(t) = \frac{T_s + T}{T} \frac{t}{T_s} \qquad 0 \le t \le T \qquad 6.36$$

$$w(t) = \frac{T_s + T}{T_s} \qquad T \le t \le T_s$$

$$w(t) = \frac{T_s + T}{T} \left[1 + \frac{T - t}{T_s}\right] \qquad T_s \le t \le T + T_s$$

$$w(t)\delta_1(t) = \frac{T_s + T}{T} 2 \frac{t}{T_s} \left(1 - \frac{1}{2} \frac{t}{T_s}\right) \qquad 0 \le t \le T \qquad 6.37$$

$$w(t)\delta_1(t) = \frac{T_s + T}{T_s} 2 \left(1 - \frac{t}{T_s} + \frac{1}{2} \frac{T}{T_s}\right) \qquad T \le t \le T_s$$

$$w(t)\delta_1(t) = \frac{T_s + T}{T} \left[1 + \frac{T - t}{T_s}\right]^2 \qquad T_s \le t \le T + T_s$$

$$\mathrm{cov}_t\left[T, \delta_1(t) w(t)\right] = -\frac{1}{6} T_s \qquad 6.38$$

$$\mathrm{cov}_t\left[T, w(t)\right] = 0$$

$$V\,\mathrm{var}[T] = g_1\,\mathrm{cov}_t\left[T, \delta_1(t) w(t)\right] - g_1\,\mathrm{cov}_t\left[T, w(t)\right]\Delta_1 = -\frac{L}{12} T_s \qquad 6.39$$

Since

$$\mathrm{var}[T] = \frac{1}{12}\left(T + T_s\right)^2 \qquad 6.40$$

$$V = -V_s \frac{1}{\left(1 + \frac{T}{T_s}\right)^2} \qquad 6.41$$

At this point, we have all the elements to compute Var(T_q), as follows

$$\mathrm{var}[T_q] = Var[T_r] + \frac{\Delta_2}{v^2}\left(g_2 - g_1^{\,2}\right) + 2\frac{V}{v}Var[T] \qquad 6.42$$

which gives:

$$\mathrm{var}[T_q] = \frac{1}{12}\left(T_s^{\,2} + T^2\right) + \frac{1}{12}T_c^{\,2} - \frac{1}{6}T_cT_s = \frac{1}{12}T_s^{\,2} + \frac{1}{12}T^2 + \frac{1}{12}T_c^{\,2} - \frac{1}{6}T_cT_s \qquad 6.43$$

On the other hand:

$$E(T_q) = \frac{1}{2}(T_s + T_c + T) \qquad 6.44$$

The results of eq. 6.43 and 6.44 are the same of eq. 6.19 and 6.20 in the previous section. This means that relation of mean runoff time and variance of the hydrograph does not change between rainfall duration *T* longer or shorter than the travel time of the storm on the plane T_s.

6.4. Discussion and conclusions

This work investigates the flow response of an hypothetical impervious plane under a simplified moving rainstorm. Rainfall is represented schematically, assuming constant storm movement and rainfall intensity. Also the propagation velocity of the flow moving down the plane is assumed to be constant. In spite of all simplifying assumptions, this analytical study aims to clarify how rainstorm movement is influencing the variability of peak response. This analysis have shown that:

- The solution based on the method of the spatial moments of catchment rainfall provides an exact solution to the temporal moments of the resulting wave;
- The catchment scale storm velocity, which describes how the temporal spread of the wave form is linearly related to rainfall movement, decreases with increasing the ratio T/T_s. This shows that the effect of storm velocity reduces in a non-linear way with increasing the point duration of the storm and with decreasing the storm velocity;

- The two temporal moments (expectation and variance) may be written in a closed form which depends on the three fundamental temporal scales introduced in this work.

This three conclusions shed light on the fundamental implications that moving storms may have on flood shapes with respect to those of stationary storms.

7. Quantifying catchment-scale storm motion and its effects on flood response

In this section we want to analyze the concept of *'catchment scale storm velocity'*, as derived in section 4, which quantifies the rate of storm motion up and down the basin accounting for the interaction between the rainfall space-time storm variability and the structure of the drainage network. Quantification and catchment scale dependency is examined with reference to an extreme flash flood that occurred in North-eastern Italy on 2003 (Borga *et al.* 2007). Moreover, we introduce a methodology to test the impact of neglecting the storm velocity in flood modeling. To investigate potential model dependency on results, two spatially distributed rainfall-runoff models, of varying complexity in terms of process description and parameter space, are used together with fine scale rainfall observations to examine the impact of storm motion and velocity on hydrograph simulation at various spatial scales.

Contents of the sections are as follows. Section 7.1 provides a description of the study area, data and the flash flood event under examination. The analytical derivations regarding the definition of catchment-scale storm velocity along with the presentation of the quantification results are presented in Section 7.2. Section 7.3 involves the hydrologic modeling evaluations used to assess the impact of storm velocity on flood response.

7.1. Study area and data

The basin considered in this study is the Fella basin, a major left-hand tributary of the Tagliamento River located within the Friuli-Venezia Giulia region, northeastern Italy (Fig. 6.0). Fella river basin at the confluence with the Tagliamento has a drainage area of approximately 700 km^2 and a very complex terrain with elevations that range from approximately 300 m a.s.l. close to the outlet to more than 2000 m a.s.l. near the mountain tops. The land cover is dominated by broad-leaf and conifer forests and the area receives on average 1920 mm of precipitation annualy (Borga *et al.* 2007). For the purpose of this work, we considered 21 sub-basins of the Fella river system (Fig. *7.2*), with area ranging between 8 and 623 km^2.

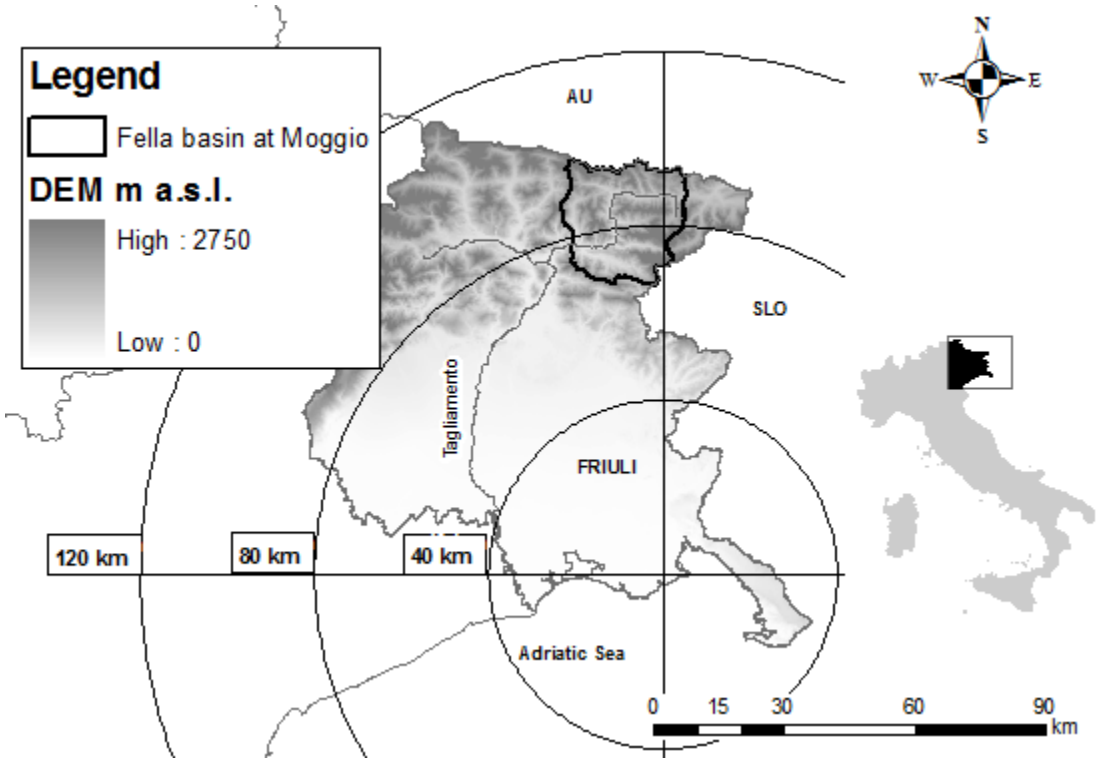

Figure 7.1: Digital elevation map of Friuli region showing the location of the OSMER radar and the outline boundaries of Fella basin at Moggio.

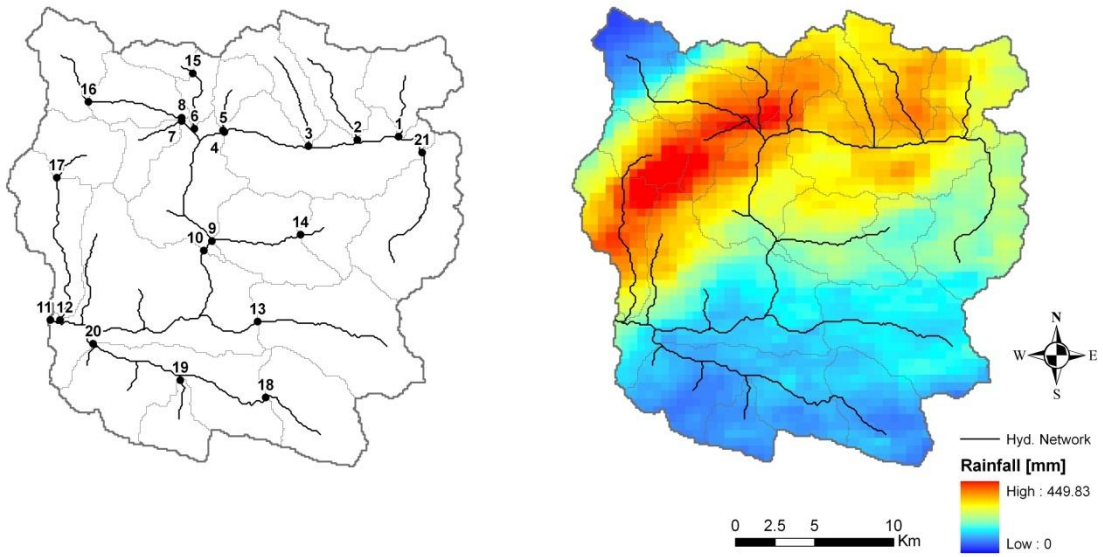

Figure 7.2: Left: Map of Fella basin at Moggio (Basin 11) showing the outlet locations of the subbasins examined in this study. Right: Total rainfall accumulation map over the study areas for the 2003 storm event examined.

The flash flood event examined in this study was one of the most devastating floods in northeastern Italy since the start of systematic observations in the (Sangati and Borga 2009) and resulted in losses of lives and damages close to one billion euro (Tropeano *et al.* 2004) in the area of the upper Tagliamento river. The flood inducing storm started at 09:00 UTC (Coordinated Universal Time) during August 29, 2003 and lasted for approximately 12 hrs. The mesoscale convective system responsible for the flooding exhibited a characteristic persistence of the convective bands over the northern part of the basin that resulted in very large rainfall accumulations and high spatial variability (Fig. *7.2*). In some parts of the basin the 15min rainfall intensities exceeded 130 $mm\ h^{-1}$, while the total rainfall accumulation over the 12 hour duration exceeded 400 mm. The combined effect of dry initial conditions, due to a prolonged summer drought, and the high spatial variability of rainfall caused a highly heterogeneous runoff response with runoff ratios ranging from 0.04 to 0.2 in different parts of the basin (Borga *et al.* 2007). Despite the overall low values of runoff ratio, specific peak discharge exceeded 8 m^3s^{-1} km^{-2} in some parts of the basin indicating the severity of flash flooding in those areas. The flood response was flashy, with a lag time (computed as the difference between the time of the centroid of the generating rainfall sequence and the time of the discharge peak) ranging from 1 hour for 20 km^2 size catchments to 3 hours and half for the largest basin (623 km^2) (Marchi *et al.* 2010).

A complete analysis of the event was carried out, with runoff data from stream gauges and a post event campaign as described in chapter 3.1. Rainfall data were derived from the reflectivity scans of a Doppler, dual-polarized C-band radar (OSMER radar station) located at Fossalon di Grado, approximately 80 km south of the basin (figure 6.0). The methods used for the corrections are the same of the others Flash Flood events analyzed and we refer to chapter 3.1 for the description. Radar-rainfall estimates were compared with observations from 15 gauges available within the area (11 of which inside the Fella river system). Radar-gauge statistical comparisons of hourly rainfall accumulations showed a generally good agreement with squared-correlation equal to 0.73 and limited (10%) radar rainfall overestimation (Borga *et al.* 2007). A striking characteristic of the event was its organization in four well-defined banded structures, characterised by lifetime of 2 to 3 hours. Convective cells, characterised by lifetimes of around 30 min, moved along the convective bands. Storm motion characteristics were analyzed based on the temporal sequence of radar images by using two methodologies: i) centroid tracking of the storm cells; and ii) cross-correlation technique over a storm-wide region in two successive radar images. The two techniques capture the storm at different spatial scales and therefore provide different estimates of storm motion characteristics. The motion of the convective cells through the region was tracked by using the procedure developed by (Bacchi *et al.* 1996). The tracks are reported in Fig. 7.3 for three different periods of the most intense phase of the storm (1200–1800 UTC). The

motion vector reported for each cell is obtained from cell locations computed for each volume scan. The velocity magnitude of these storm elements computed by the tracking technique was around 6 ms^{-1} with peaks of 10 ms^{-1}. The direction of the storm elements motion was generally from South-West to North-East, and was almost parallel to the main drainage line for several subbasins of the Fella, with a clear upbasin direction. The cross-correlation method (Browning and Collier 1989; Wilson *et al.* 1998) was applied over a 40 km by 40 km region centered over the Fella River basin covering the whole storm system. This method provided values of storm velocity which were considerably less intense than those obtained by the tracking technique, with peaks around 3 ms^{1}, and direction of motion which was almost normal to the vectors obtained by the tracking technique. These results are not unexpected, as several studies investigated the contrasting characteristics of fast moving convective cells and slow moving convective systems within the same storm (Doswell *et al.* 1996; Collier 2007; Aylward and Dyer 2010). This flash flood event provides therefore a template for examining how the emerging characteristics of the storm motion transmit to the flood response at various spatial scales.

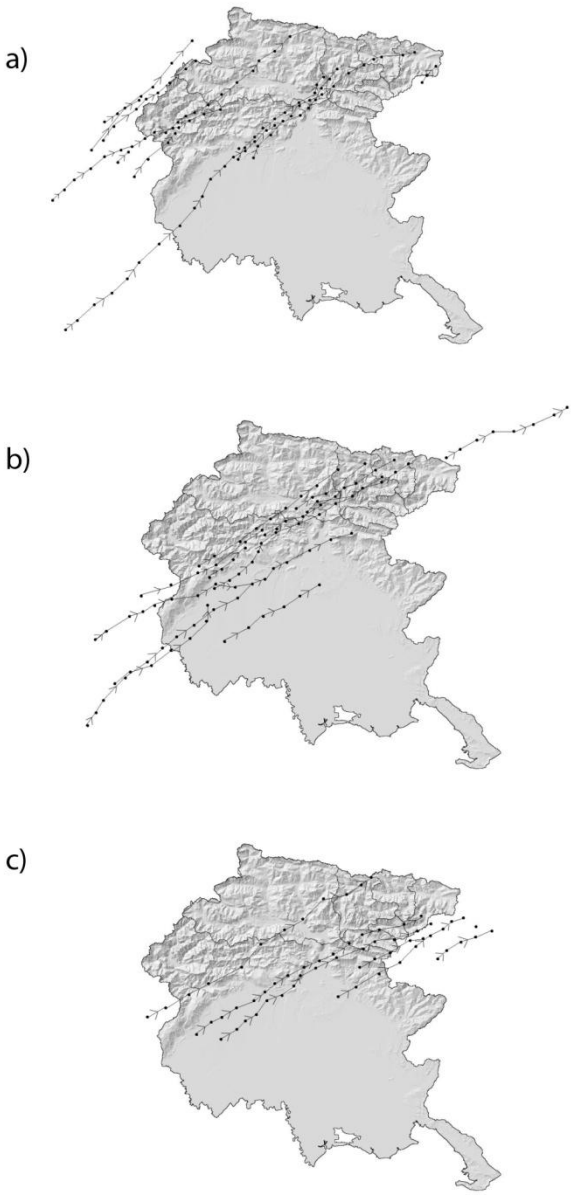

Figure 7.3: Figure showing tracks of rainfall cells for the 29 August 2003 storm: (a) 12:00-14:00 UTC, (b) 14:00-16:00 UTC, and (c) 16:00-18:00 UTC. (Borga *et al.* 2007)

7.2. Catchment scale storm velocity

The term "catchment scale storm velocity" is based on the concept of "spatial moments of catchment rainfall" presented by in chapter 4. These statistics, based on previous work by (Viglione *et al.* 2010) and corresponding in part to the catchment rainfall statistics reported in Smith *et al.* (2002) and Smith *et al.* (2005), provide a metric for rainfall's spatial organization in relation to a fundamental descriptor of the structure of the drainage network, i.e. the flow distance. From chapter 4.2 we extract the equation of catchment scale storm velocity as:

$$V_s(t) = \underbrace{g_1 \frac{cov_t[T,\delta_1(t)w(t)]}{var[T]}}_{V_s1} - \underbrace{g_1 \frac{cov_t[T,w(t)]}{var[T]}}_{V_s2} \Delta_1 \qquad 7.1$$

The term *Var[T]* denotes the variance of the uniform variable time *T* over the duration considered for the computation of the velocity V_s. For a time duration equal to T_s, *Var[T]* is computed as (1/12) T_s^2 .

Equation 24 shows that the storm velocity is defined as the difference between the slope terms of two linear regressions with time (Zoccatelli *et al.* 2011). The first slope term is estimated based on the space-time regression between weighted scaled first moments and time, and the second term is based on the regression between weights and time. Conceptually, this means that storm motion may produce changes both in the rainfall centroid coordinate and in the mean areal rainfall values. Both are taken into account in the estimation of the catchment scale storm velocity. For the case of temporally uniform mean areal rainfall, *w(t)* is constant and the value of V_s depends only on the evolution in time of the position of the rainfall centroid along the flow distance coordinate. In the opposite case, if there is only temporal variation of the mean areal rainfall and no motion ($\delta_1(t)$ is constant), the two slope terms will be equal in value and opposite in sign, which means that the V_s will be equal to zero. Note that the sign of the velocity is positive (negative) for the case of upstream (downstream) storm motion.

The concept of catchment scale storm velocity provides an assessment of the impact of storm motion on flood shape, considering a specific spatial scale (the catchment size) and temporal scale. In chapter 6 we investigated how the temporal scale of analysis influences the catchment scale storm velocity by considering the simple problem of planar flow owing to storms moving up and down the plane. This is an interesting case since the solution obtained through the rainfall spatial moments can be compared with the analytical solution obtained through the method of characteristics. We found that the catchment scale storm velocity depends on the storm travel velocity and the ratio between storm duration and the travel time (which is the time taken by the storm to move through the plane). More specifically, the ratio between catchment scale storm velocity and storm travel time decreases with increasing the ratio between storm duration and travel time. An interesting outcome of these findings is that, when considering a specific storm of a certain duration and the ensuing flood event, the impact of storm motion should decrease with decreasing the storm travel time, i.e. with decreasing the catchment scale. An examination of scale dependency of catchment scale storm velocity is reported below.

Quantification of catchment scale storm velocity and scale dependence

Fig. 7.4 reports the time series of the basin-averaged rainfall, basin coverage with rain > 20 mm hr^{-1}, coefficient of variation (standard deviation divided by the mean) of rainfall rate (for positive bins) and the spatial moments δ_1 and δ_2. Time series are shown for three basins of varying size: Basin 9 (46 km^2), Basin 10 (329 km^2) and Basin 11 (623 km^2, corresponding to the largest basin examined in this study). Results in Fig. 7.4 highlight the high variability of the storm properties with time. Flood-producing rainfall for Basin 9 and Basin 10 was concentrated over a period of 7 hours and half, lasting from 10:30 to 18:00 UTC. Four peak values of basin averaged rainfall can be recognized for Basins 9 and 10, at 11:00, 13:00, 14:30 and 16:00. Correspondingly, the peaks of fractional coverage of heavy rainfall (greater than 20 $mm\ h^{-1}$) are up to 90% for the Basin 9 and up to 75% for Basin 11. The coefficient of variation ranges steadily between 0.7 and 1.8 over the periods of intense rainfall; these values correspond to those reported for other extreme flash flood-inducing storms observed in northern Italy (Sangati *et al.* 2009).

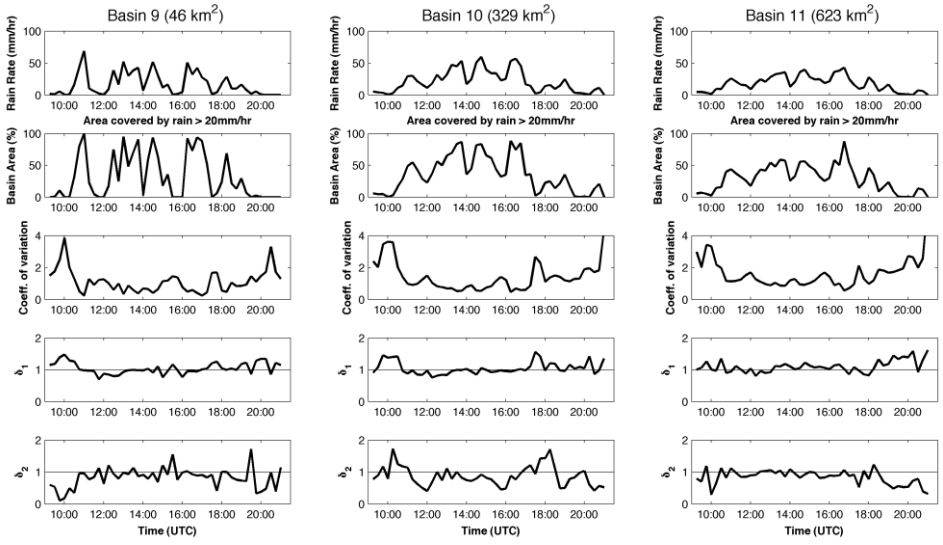

Figure 7.4: Time series (15 min) showing (from top to bottom) the basin-averaged rainfall, the fraction of basin area covered by rain > 20mm h^{-1}, coefficient of variation of non-zero rainrates, δ_1 and δ_2. Each column corresponds to a different basin.

Despite the large rainfall variability, the fluctuations of δ_1 remained close to 1 for most of the time, particularly during the period of high rain intensity, suggesting that the rainfall centroid was close to the catchment centroid. The slight fluctuation of δ_1 around 1 means that rainfall centroid was oscillating (up/down) catchment centroid thus resulting in fluctuation in the direction of catchment scale storm velocity (upbasin/downbasin). The temporal variation of rainfall dispersion (δ_2) was more distinct with the majority of the values below 1 suggesting spatial concentration

over the catchment centroid. Few instances, characterised by low rain rate, show values exceeding 1 (suggesting multimodal distribution).

To examine the characteristics of storm velocity distributions, the analysis was extended to the 21 basins indicated in Fig. 7.2. We used two time windows to compute the storm velocity: i) 1 hour (the corresponding storm velocity is indicated with V), and ii) the mean catchment response time (the corresponding storm velocity is indicated with V_s) with values that ranged from 0.75 to 3 hours and half for the scales examined. Note that the mean response time for each basin was derived based on the application of the propagation module of the KLEM model (see section 3.2 below for details). While we consider V_s as the hydrologically relevant velocity, V corresponds to the storm motion kinematics as filtered by catchment morphological properties. We believe that both velocity values are important and each one delivers complementary information, thus we present our subsequent analysis based on both. The temporal distributions of absolute velocity values *V* and V_s for all basins are presented in Fig. 8.0a,b, respectively, as box-plots ordered in increasing basin area. We chose to plot absolute values since at this stage we are interested only on the magnitude and not the direction of velocity. Results from Fig. 8.0 show that values for *V* range between 0-5.5 $m\ s^{-1}$ with several values exceeding 1 $m\ s^{-1}$; moreover, the mean absolute values of V increase with increasing basin size. On the other hand, values for V_s are below 1 $m\ s^{-1}$ for almost all cases and no relationship with basin size is apparent. This suggests that while the rainfall motion effect may be significant over an hourly time window (high *V* value), this does not hold for generally longer times (most of the 21 basins are associated with a response time larger than 1 hour) associated with calculation of V_s.

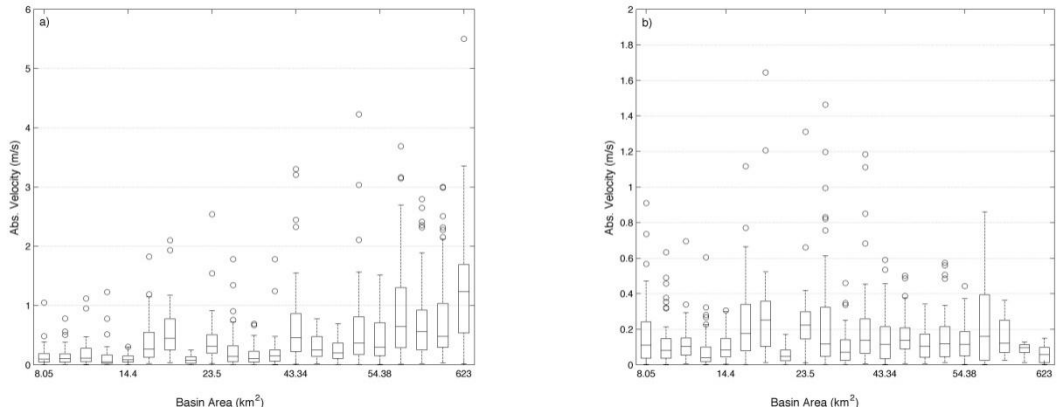

Figure 7.5: Boxplots showing the distribution of absolute velocity for each subbasin vs basin area. The values in first panel (Fig. 7.5a) are based on using a fixed regression window of 1hr. In Fig. 7.5b, the velocity values are calculated by using a variable regression window based on mean response time for each basin. Note that open circles correspond to values that exceed 1.5 times the interquartile range of the distribution at each case.

To investigate the features of scale dependency of catchment-scale storm velocity, we analyzed the mean absolute values of velocity V and V_s for all 21 basins examined (Fig. 7.6a,b, respectively). As shown in Fig. 7.6a the magnitude of velocity V exhibits a strong linear dependence (correlation coeff. > 0.8) with the logarithm of basin area, suggesting the existence of a logarithmic relationship between velocity and basin scale. This indicates that storm velocity increases nonlinearly with basin scale, as expected based on results reported in chapter 6. On the other hand, results for velocity V_s (Fig. 7.6b) show no scale dependence. More specifically, low values of velocity are found for very small catchments and for large basins. The distribution of V_s shows a peak around 0.3 m s^{-1} in the range 15-100 km^2. Hence, the distributions reported in Fig 7.6a and 7.6b differ essentially for the case of relatively large basins. This is likely to be due to the high temporal variability of velocity V. When a temporal window larger than 1 hr is used for the computation of the catchment scale velocity V_s, as it is the case for medium size and large basins characterised by a longer response time, this results in a smoothing of the velocity magnitudes with a strong reduction of their values. Overall, results from this analysis indicate that the velocity values relevant to hydrologic response times are low, suggesting that catchment rainfall storm velocity was not significant during the 2003 flash flood event. Consequently it is not expected that it played an important role in shaping the flood hydrograph.

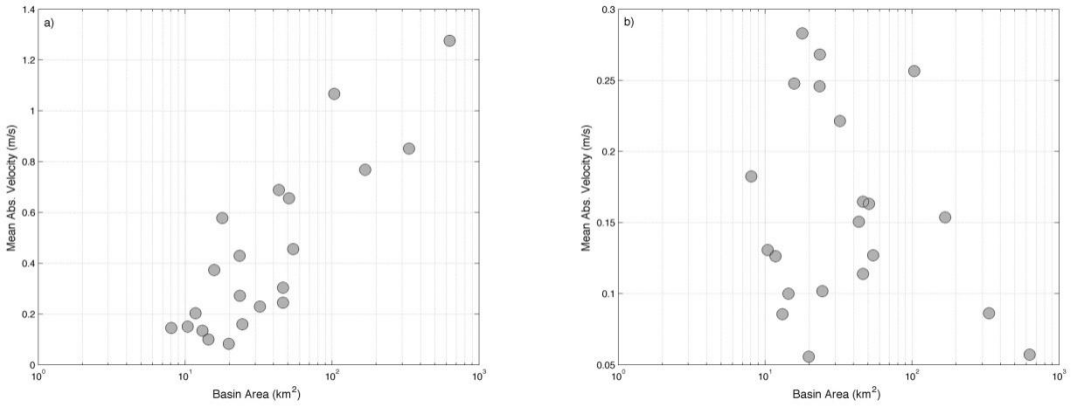

Figure 7.6:. Mean absolute storm velocity versus basin area. Fig.7.6a shows the average V velocity values calculated based on a fixed hourly regression window and Fig. 7.6b the averaged V_s values based on a variable time window equal to basin's mean response time.

7.3. Hydrological simulations

In this section we introduce a methodology, based on hydrologic simulations, to test the impact of neglecting the storm motion and velocity on flood hydrograph. To investigate potential model dependency on results, two spatially distributed hydrologic models, of varying complexity in terms of process description and parameter space, are used together with fine scale rainfall

observations. This is expected to highlight potential model dependencies on the results and thus provide a range of results (in case of differences) or a more robust conclusion (in case of agreement).

Hydrologic models

Two different hydrologic models were used in this study. The first is the TIN (triangulated irregular network)-based Real-time Integrated Basin Simulator (tRIBS) model (Ivanov *et al.* 2004; Ivanov *et al.* 2004; Vivoni *et al.* 2007). tRIBS is a distributed physics-based model that explicitly accounts for the spatial variability of land surface descriptors (terrain, soil, vegetation), soil moisture and atmospheric forcing. Infiltration is simulated in a sloped heterogeneous and anisotropic soil based on a kinematic approximation for unsaturated flow (Cabral *et al.* 1992; Garrote and Bras 1995). An adaptive multiple resolution approach based on TINs (Vivoni *et al.* 2004), is used to represent the complexity of the simulation domain. Runoff is generated at each computational element of the domain via a variety of mechanisms (infiltration excess, saturation excess, interflow, groundwater exfiltration) depending on the soil saturation state. A detailed description regarding the setup, calibration and validation of the model for the Fella basin is provided in (Nikolopoulos *et al.* 2011).

The second model used is the Kinematic Local Excess Model (KLEM) described in section 3.2. Model parameterization was based on previous work by Borga *et al.* (2007) that used a very similar model for the Fella basin, calibrated and validated for the same storm event examined in this study. The model calibration used observed runoff data at the Fella outlet supported by further peak flood observations made for internal subbasins (Borga *et al.* 2007). In particular, the values of the flow velocities ranged between 2.5 m s^{-1} and 5 m s^{-1} (channel velocity) and 0.03 m s^{-1} and 0.2 m s^{-1} (hillslope velocity), whereas the channelization support area ranged between 0.01 and 0.01 km^2. Post-flood surveys confirmed the accuracy of the calibrated high values of channel velocity (Borga *et al.* 2007).

Catchment scale storm velocity effect on flood response

To investigate the effect of storm velocity on flood response, we carried out a series of hydrologic simulations for which we used rainfall scenarios with different levels of rainfall space-time variability. More specifically, the hydrologic response resulting from the original rainfall field (control simulation) was contrasted with the results obtained from a) spatially uniform and b)

constant spatial rainfall pattern case. In all cases the basin-averaged rainfall remained constant (i.e. constant rainfall volume applied at each time) while the spatial rainfall pattern was a) completely removed (in the uniform case) or b) kept constant and equal to the total rainfall accumulation pattern (constant pattern case). The later was achieved by scaling the total rainfall pattern with an appropriate factor so that the basin-averaged rainfall remained equal to the original rain. Note that because the overall spatial rainfall organization is preserved in constant pattern case, the values of Δ_1 and Δ_2 are the same with the original rainfall case.

The rationale for developing the three rainfall scenarios is as follows. In our methodology, based on spatial moments, we assume that the shape of the flood hydrograph is controlled by: i) the catchment drainage structure, ii) the temporal pattern of basin-average rainfall rates (hyetograph); iii) the two descriptors of overall rainfall organization at catchment scale Δ_1 and Δ_2, and iv) the catchment scale storm velocity. The control simulation is the result of the combination of factors i) to iv), the constant pattern simulation is controlled by factors i) to iii), whereas the uniform-rainfall simulation is controlled by factors i) and ii). Comparison of control simulation with constant pattern simulation permits isolation of the effect of catchment scale storm velocity on flood hydrograph, whereas the comparison of control simulation with uniform-rainfall simulation afford isolation of the combined effect of Δ_1 , Δ_2, and catchment scale storm velocity on flood hydrograph.

Simulations were carried out for the 21 basins indicated in Fig. 7.2. Comparisons between uniform and control flood hydrographs and between constant pattern and control flood hydrographs were summarized by using the Nash-Sutcliffe (NS) index. The NS index was selected because is non dimensional and permits a quick assessment of the quality of the simulations. The NS indexes are reported in Fig. 7.7 for the two comparisons, for all basins examined and for the two hydrological models. NS scores are ranked in ascending order for both uniform versus control, and constant pattern versus control cases. Thus note that the figure presents the distribution of values for each case without providing a one-to-one correspondence between cases or between models. Results for constant pattern case show that, with the only exception of basin 9 (for tRIBS results), for all other basins NS values are greater than 0.9 for both models. This clearly indicates that the essential elements of spatial rainfall variability which play a role in hydrograph shape are captured by rainfall patterns which preserve the spatial moments Δ_1 and Δ_2, but neglect storm motion. These results show that storm motion and velocity plays a negligible role in controlling the flood response at the various spatial scales examined here. The agreement between the two hydrological models shows that this is a particularly robust outcome of this work.

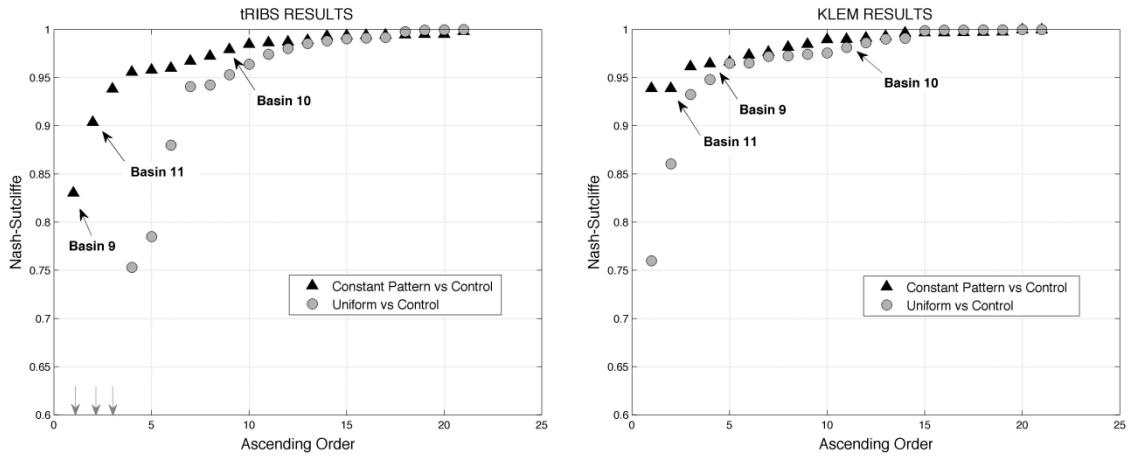

Figure 7.7: Nash-Sutcliffe scores calculated between the control hydrographs and the hydrographs corresponding to a) constant pattern (triangles) and b) uniform (circles) rainfall. Results are ranked in ascending order. The three selected basins are identified with respect to the constant pattern results. Also the arrows points downwards in the first plot (left) indicate that there are three points at these locations below the threshold of 0.5 N-S score.

Comparison between the results for the two hydrologic models revealed discrepancies for the uniform rainfall case. Specifically tRIBS simulations exhibit relatively lower NS values than KLEM suggesting higher sensitivity when a spatially uniform forcing is applied. This finding confirms earlier results obtained when considering models of varying complexity and their sensitivity to input errors (Michaud and Sorooshian 1994; Moore 1999; Andreassian *et al.* 2001; Segond *et al.* 2007). Comparison of the tRIBS simulations for uniform and original rainfall indicates that the soil buffers a significant amount of rainfall before runoff is generated. This suggests that saturation-excess is the dominant mechanism and subsequently runoff generation is essentially a threshold process, controlled by the infiltration module. Negligible runoff is generated when the rainfall is less than the threshold required to saturate the soil column and trigger surface runoff. This clearly enhances the sensitivity to the averaging process which is carried out when the model is forced with spatially-uniform rainfall. In the case of KLEM, both surface runoff generated by the infiltration excess mechanism and the subsurface stormflow mechanism were important contributors to the flood volume. Owing to this reason, computation of runoff depends both on rainfall volume and rainfall intensity, which makes less dramatic the sensitivity to the use of spatially uniform rainfall.

To provide an example of the differences in sensitivity between the two models, Fig. 7.8 shows the simulated hydrographs for the three selected basins: basin 9 (46 km^2), basin 10 (329 km^2) and Basin 11 (623 km^2) for tRIBS (Fig. 7.8a,c,e) and KLEM (Fig. 7.8b,d,f) respectively. The figure reports the three simulations based on the three rainfall scenarios considered in the comparisons. Simulated response based on original rainfall fields (control) differs for the two models, with relative discrepancies that increase with decreasing catchment size. Comparison of results

reported in Fig. 7.8 show that the relative difference between tRIBS and KLEM simulated flood peaks is around 19% for the two larger basins, and increases to 50% for the smallest basin. It should be noted that discharge values were available for calibration only for the Fella outlet section, the two internal basins representing ungauged catchments. These results point to the large uncertainty in representing the internal hydrological functioning for extreme flash floods, particularly when extremely dry initial conditions are coupled with extreme rain rates and depths. For the case of the constant rainfall pattern scenario, both models show that the discrepancy relative to the control simulation is insignificant. However, for the uniform case the response from the two models is different with tRIBS showing significantly higher sensitivity than KLEM especially for the larger basin scales, as reported above. The simulated hydrographs with tRIBS shows a significant decrease in the flood response for the larger basins while the corresponding KLEM simulations are affected at less degree by the uniform rainfall forcing. Apparently KLEM exhibits a less nonlinear response than tRIBS, which is attributed to the inherent differences of the dominant runoff generation mechanisms in the two models, as previously explained. These findings point out a) the importance of investigating model dependencies and b) the fact that two different models that do not always agree showed consistent results for the case of constant pattern. The latter indicates that the storm velocity did not play an important role in shaping the flood hydrograph during this event. It was mainly the spatial distribution of rainfall volume over the basin, and not its motion, that controlled the flood response.

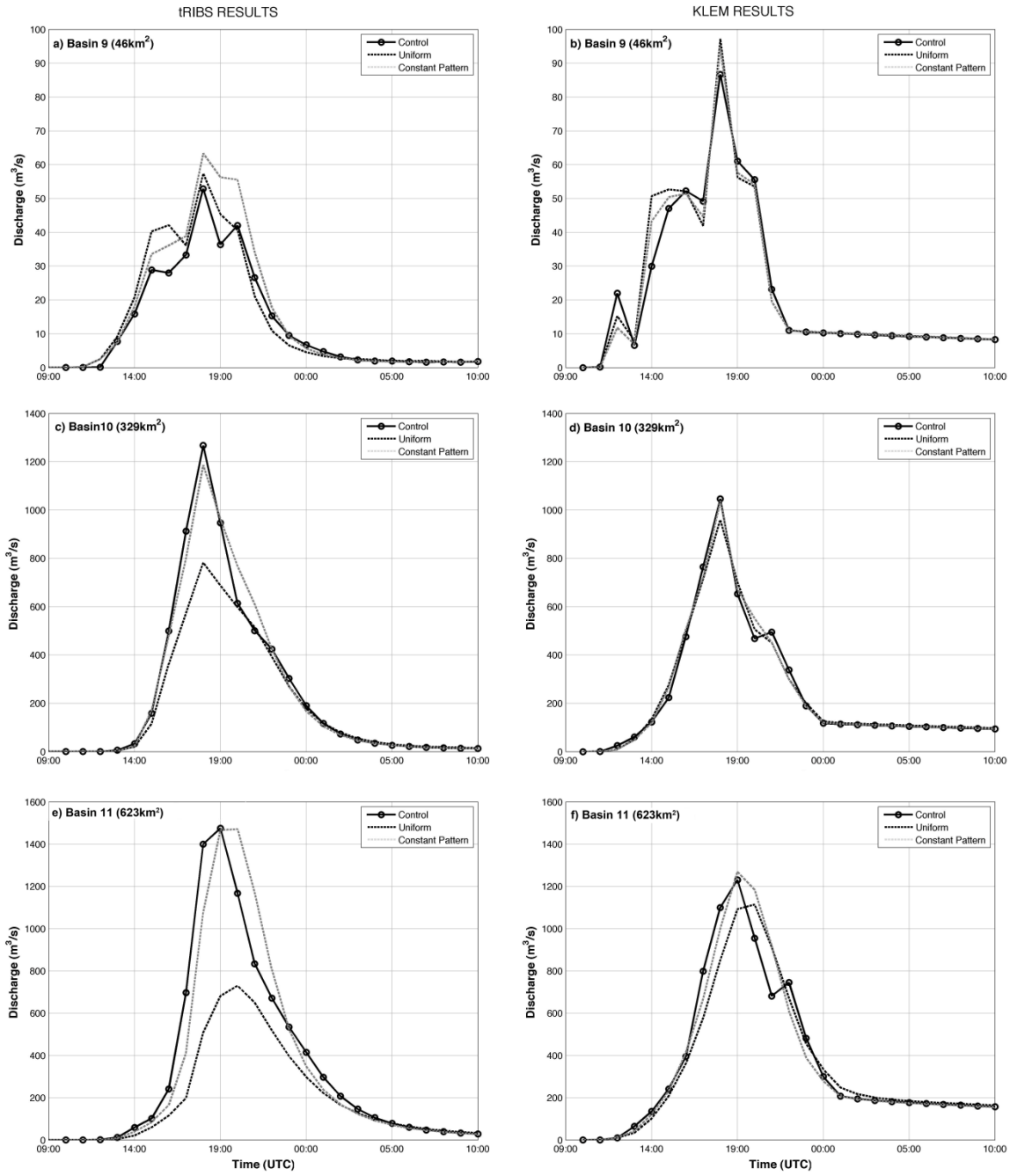

Figure 7.8: Simulated hydrographs based on tRIBS (left) and KLEM (right) model for three selected basins. Results are shown for the cases of original rainfall forcing (control), uniform rainfall (uniform) and constant rainfall pattern (constant pattern) scenarios.

7.4. Discussion and conclusions

Starting from spatial moments of catchment rainfall we introduced a methodology to quantify storm velocity at the catchment scale and to assess its effect on flood response modeling. The methodology is based on the observation that catchment shape, direction and morphology impose a filtering to the effect of storm motion over the catchment, in spite of the inherent

kinematics of the storm elements.

Catchment-scale storm velocity was quantified for a major flash flood-triggering storm based on analyses carried out on 21 sub-basins with areas ranging between 8 and 623 km^2. Derivation of velocity was based on two different approaches that involved the calculation of storm velocity over a a) fixed 1hr time window (V) and b) variable time window equal to basin mean response time (V_s). These two different approaches were chosen in order to present velocity values calculated consistently for all basins (case of$V$) but also to demonstrate the magnitude of the velocity over characteristic time scales which is relevant to the hydrologic response of each basin (case of V_s). The obtained results showed that values of V reach up to 5.5 $m\,s^{-1}$ and are much higher than values of V_s, that only exceptionally exceed 1 $m\,s^{-1}$. Apart from the differences in magnitude there is another distinct difference related to the scale dependence of velocities V and V_s. It was shown that there is a strong nonlinear dependence between catchment scale and velocity V according to which, velocity increases linearly with the logarithm of area. A possible explanation for this dependence is the relationship between the ratio of catchment scale storm velocity to storm travel velocity and the ratio of storm duration to travel time, as found in chapter 6. According to this dependence, when considering a specific storm of a certain duration and the ensuing flood event, the impact of storm motion should decrease with decreasing the storm travel time, i.e. with decreasing the catchment scale. This dependence was masked in the case of V_s because the application of a variable regression window smoothed effectively the velocity pattern (see text in Figure 7.6. Moreover, the values of V_s were remarkably low with respect to the velocity of the travelling convective cells. It is speculated that this is due to the effect of two different controls emerging at various scales. At basin scales less than 20 km^2, the ratio between storm duration and cell travel time is small hence reducing the magnitude of V_s. At basin scales larger than 20 km^2, the temporal variability of the hourly catchment scales storm velocity values is too high, which also limits the magnitude of V_s. This statement is in contrast with the literature presented in section 2.2, where it is argued that small basins are more sensitive to storm movement.

A methodological approach was introduced that allows to isolate and to investigate the effect of catchment scale storm velocity on flood hydrograph. Hydrologic simulations carried out for constant rainfall pattern permit the isolation of the effect of velocity on flood response when compared with the original rainfall hydrographs. Results from the hydrologic simulations with tRIBS and KLEM showed that the simulations based on original and constant pattern rainfall fields were in good agreement. However, comparison for the uniform case scenario showed significant differences (mainly for the larger scale basins) suggesting a higher sensitivity of tRIBS to the

relative distribution of rainfall volume over the basin. Nevertheless, the main conclusion of this analysis, consistent for both models, is that the constant pattern hydrographs were almost identical (NS scores > 0.9) with the original rainfall hydrographs. This implies that the movement of rainfall over the basins had no effect in shaping the flood response. This may suggest that for this storm and flood event it was the slow moving convective systems, rather than the fast moving convective cells, that controlled the space-time distribution of rainfall and the flood response. The effect of storm velocity on flood response was examined in this study for a single flash flood-induced storm, thus findings cannot be used to derive generalized conclusions. However, the methodology developed in this study may be used to advance the understanding of the effect of storm motion on flood response by considering multiple flood and flash flood events. Basin scale was hypothesized and proven to have a strong effect on the magnitude of storm velocity, but there are also other factors such as basin shape (e.g. elongation) and orientation (relative to storm movement) that can potentially depict a strong relationship with velocity. These aspects require further research to gain a holistic understanding on the effect of storm motion on hydrologic response during flash floods.

8. Conclusions

In this work we presented a set of statistics, named '*spatial moments of catchment rainfall*', that describe the interactions between rainfall spatial distribution, catchment morphology and flood response. The effect of rainfall distribution over the hydrograph, termed rainfall spatial organization, is described in terms of concentration and dispersion statistics along the flow path coordinate. The work shows how the first two spatial moments afford quantification of the impact of rainfall spatial organization on two fundamental properties of the flood hydrograph: timing (surrogated by the runoff mean time) and amplitude (surrogated by the runoff time variance). The first spatial moment provides a measure of the scaled distance from the geographical centroid of the rainfall spatial pattern to the catchment centroid. The second spatial moment provides a scaled measure of the additional variance in runoff time that is caused by the spatial rainfall organization, relative to the case of spatially uniform rainfall. Starting from *spatial moments of catchment rainfall* we integrated the relative role of hillslopes and channel network on timing of the flood hydrograph, accounting for the effect of the spatial variability of rainfall. A sensitivity index $\Theta_1$was created with a meaning similar to the first non-dimensional spatial moment Δ_1, and it was made explicit the effect that parameters of channel and hillslope propagation have. The introduction of spatial moments of catchment rainfall permits derivation of a catchment scale storm velocity, which quantifies the up or down-basin rainfall movement as filtered by the catchment morphological properties relative to the storm kinematics and its effect on flood response modeling.

The main results of the study are:

- The statistics presented are effective in describing the spatial organization of rainfall and its effect on the timing error. Hillslope play an important role in this relation, but its inclusion improves only slightly the descriptive power of the statistics.
- For the extreme floods analyzed, neglecting rainfall spatial variability induces a timing error between -30% and 72% of the catchment response time, with large errors even in small catchments (< 50 km^2).
- The hypothesis of non-correlation between rainfall and hillslopes seems to hold for the cases analyzed, allowing to directly assess the effect of different hillslope conditions on the hydrograph timing.

- Catchment scale storm velocity was quantified for a major flash flood-triggering storm on 21 sub-basins with areas between 8 and 623 km^2. The application shows that while the velocity calculated over a 1h time window increases with scale, its effect on the response of basins is lower and similar across basin sizes.
- A methodology was introduced to isolate and to investigate the effect of catchment scale storm velocity on the flood hydrograph starting from hydrologic simulations. This methodology showed that in the case analyzed, despite the large velocities of single convective cells over the basin, rainfall movement had no effect in shaping flood response.

Spatial moments represent a descriptive tool able to capture the interaction of rainfall forcing and catchment characteristics beyond common indicators such as mean areal rainfall, including the features of rainfall spatial concentration and movement. This may be used to reveal the effect of orography not only on the precipitation accumulation at the catchment scale, but also on the space-time organization of the rainfall patterns. However we believe that the main strength of *spatial moments of catchment rainfall* lies in a better understanding of the linkages between the characteristics of the rainfall spatial patterns with the shape and magnitude of the catchment flood response. The indicators introduced at catchment scale can be used to compare influence of rainfall distribution across basins and scales. This is a fundamental aspect, since it enables evaluating the accuracy with which rainfall space and time distribution need to be observed for a given type of storm event and for a given catchment. For example, this may provide new statistics and criteria both for defining the optimality of raingauge network design in areas where flash floods are expected and for evaluating the accuracy of radar rainfall estimation algorithms and attendant space-time resolution. Another example of application can be the calibration of a lumped model, where knowing the influence of rainfall spatial distribution allows to avoid epistemic errors. An eventual influence of rainfall spatial distribution may even be disinformative for the calibration, creating errors that may even not be reduced by longer records {Beven, 2011 #321;Beven, 2011 #322}. The statistics could also be used for assessing and quantifying hydrological similarity across a wide range of rainfall events and catchments, within the broader framework of comparative hydrology. For instance, the method can be used to identify the features of catchment morphology which attenuates (or magnify) the effects of rainfall space-time organization. Since the influence of rainfall distribution is higher in extreme storms, it may also be an important factor to consider in the statistical distribution of extreme

events. In this case the statistics proposed can help to perform a synthesis across events, and isolate storms with similar conditions. The extension of the framework to hillslope propagation can be employed to assess the effects of parameters characterizing the hillslope and channel residence time, allowing the comparison between different scenarios and the identification of dominant controls in the propagation. This means for example that we can evaluate the effect that a particular rainfall pattern has on the timing of catchment response as a function of different hillslope and river network structures. This allows also to evaluate the sensitivity of different basins under different scenarios, and related with other environmental factors such as antecedent soil moisture conditions. Again, the framework can also be useful to understand the optimal rainfall resolution required in order to get an accurate prediction of the catchment response time under different hillslope conditions.

Beside the analysis done on flash floods, it would be useful for future research to evaluate the effectiveness of the methodology for a wider variety of catchments and events. The rainfall statistics introduced in this paper could also be used as an input to a new generation of semi-distributed hydrological models able to use the full range of statistics, and not only the mean areal rainfall, for flood modeling and forecasting. This will permit extending the capabilities of this class of hydrological models to rainfall events characterized by significant rainfall variability. Regarding the work on hillslope, future research may assess the hypothesis of non-correlation between rainfall and hillslopes in case the channelization support area (and thus hillslope lengths) are related with the amount of rainfall, or in case of large scale heterogeneities related, for example, with basin geology. Finally, the methodology presented on the effect of storm velocity may be useful in advancing our understanding on the effects of storm motion on flood response. Beside the analysis on basin scale, which was proven to be related with storm velocity, other factors may deserve attention such as basin shape (e.g. elongation) and orientation (relative to storm movement) and can potentially depict a strong relationship with velocity. These aspects require further research to gain a holistic understanding on the effect of storm motion on hydrologic response during flash floods.

9. References

Ajami, N. K., H. Gupta, T. Wagener and S. Sorooshian (2004). "Calibration of a semi-distributed hydrologic model for streamflow estimation along a river system." Journal of Hydrology **298**(1): 112-135.

Andreassian, V., C. Perrin, et al. (2001). "Impact of imperfect rainfall knowledge on the efficiency and the parameters of watershed models." Journal of Hydrology **250**(1-4): 206-223.

Arnaud, P., C. Bouvier, L. Cisneros and R. Dominguez (2002). "Influence of rainfall spatial variability on flood prediction." Journal of Hydrology **260**(1-4): 216-230.

Aylward, R. P. and J. L. Dyer (2010). "Synoptic Environments Associated with the Training of Convective Cells." Weather and Forecasting **25**(2): 446-464.

Bacchi, B., R. Ranzi and M. Borga (1996). "Statistical characterization of spatial patterns of rainfall cells in extratropical cyclones." Journal of geophysical research **101**(D21): 26277-26226,26286.

Barry, D., J. Y. Parlange, et al. (2005). "Green–Ampt approximations." Advances in Water Resources **28**(10): 1003-1009.

Berndtsson, R. and J. Niemczynowicz (1988). "Spatial and temporal scales in rainfall analysis—Some aspects and future perspectives." Journal of Hydrology **100**(1): 293-313.

Berne, A., G. Delrieu, J. D. Creutin and C. Obled (2004). "Temporal and spatial resolution of rainfall measurements required for urban hydrology." Journal of Hydrology **299**(3-4): 166-179.

Berne, A. and W. Krajewski (2012). "Radar for Hydrology: Unfulfilled Promise or Unrecognized Potential?" Advances in Water Resources.

Beven, K. (1979). "On the generalized kinematic routing method." Water Resources Research **15**(5): 1238-1242.

Beven, K. (2006). "A manifesto for the equifinality thesis." Journal of Hydrology **320**(1): 18-36.

Beven, K., P. Smith and A. Wood (2011). "On the colour and spin of epistemic error (and what we might do about it)." Hydrology and Earth System Sciences **15**: 3123-3133.

Beven, K. and I. Westerberg (2011). "On red herrings and real herrings: disinformation and information in hydrological inference." Hydrological processes **25**(10): 1676-1680.

Beven, K. and E. Wood (1993). "Flow routing and the hydrological response of channel networks." Channel network hydrology **99**.

Beven, K. and E. F. Wood (1983). "Catchment geomorphology and the dynamics of runoff contributing areas." Journal of Hydrology **65**(1): 139-158.

Beven, K. J. and G. M. Hornberger (1982). "ASSESSING THE EFFECT OF SPATIAL PATTERN OF PRECIPITATION IN MODELING STREAM FLOW HYDROGRAPHS1." JAWRA Journal of the American Water Resources Association **18**(5): 823-829.

Bloschl, G. (2006). "Hydrologic synthesis: Across processes, places, and scales." Water Resources Research **42**(3).

Blöschl, G., R. B. Grayson and M. Sivapalan (1995). "On the representative elementary area (REA) concept and its utility for distributed rainfall-runoff modelling." Hydrological processes **9**(3-4): 313-330.

Bloschl, G. and M. Sivapalan (1995). "Scale Issues in Hydrological Modeling - a Review." Hydrological processes **9**(3-4): 251-290.

Borga, M., E. N. Anagnostou, G. Bloschl and J. D. Creutin (2010). "Flash floods Observations and analysis of hydro-meteorological controls." Journal of Hydrology **394**(1-2): 1-3.

Borga, M., E. N. Anagnostou, G. Bloschl and J. D. Creutin (2011). "Flash flood forecasting, warning and risk management: the HYDRATE project." Environmental Science & Policy **14**(7): 834-844.

Borga, M., P. Boscolo, F. Zanon and M. Sangati (2007). "Hydrometeorological analysis of the 29 August 2003 flash flood in the Eastern Italian Alps." Journal of Hydrometeorology **8**(5): 1049-1067.

Borga, M., E. Gaume, J. D. Creutin and L. Marchi (2008). "Surveying flash floods: gauging the ungauged extremes." Hydrological processes **22**(18): 3883-3885.

Botter, G. and A. Rinaldo (2003). "Scale effect on geomorphologic and kinematic dispersion." Water Resources Research **39**(10): 1286.

Bouilloud, L., G. Delrieu, et al. (2009). "Radar rainfall estimation for the post-event analysis of a Slovenian flash-flood case: application of the Mountain Reference Technique at C-band frequency." Hydrology and Earth System Sciences **13**(7): 1349-1360.

Bouilloud, L., G. Delrieu, B. Boudevillain and P. E. Kirstetter (2010). "Radar rainfall estimation in the context of post-event analysis of flash-flood events." Journal of Hydrology **394**(1): 17-27.

Brath, A. and A. Montanari (2003). "Sensitivity of the peak flows to the spatial variability of the soil infiltration capacity for different climatic scenarios." Physics and Chemistry of the Earth **28**(6-7): 247-254.

Browning, K. and C. G. Collier (1989). "Nowcasting of precipitation systems." Reviews of Geophysics **27**(3): 345-370.

Cabral, M. C., L. Garrote, R. L. Bras and D. Entekhabi (1992). "A kinematic model of infiltration and runoff generation in layered and sloped soils." Advances in Water Resources **15**(5): 311-324.

Castillo, V. M., A. Gomez-Plaza and M. Martinez-Mena (2003). "The role of antecedent soil water content in the runoff response of semiarid catchments: a simulation approach." Journal of Hydrology **284**(1-4): 114-130.

Collier, C. (2007). "Flash flood forecasting: What are the limits of predictability?" Quarterly Journal of the royal meteorological society **133**(622): 3-23.
Costa, J. E. and R. D. Jarrett (2008). An evaluation of selected extraordinary floods in the United States reported by the US Geological Survey and implications for future advancement of flood science.
D'Odorico, P. and R. Rigon (2003). "Hillslope and channel contributions to the hydrologic response." Water Resources Research **39**(5).
Da Ros, D. and M. Borga (1997). "Use of digital elevation model data for the derivation of the geomorphological instantaneous unit hydrograph." Hydrological processes **11**(1): 13-33.
Davolio, S. B., A.; Malguzzi, P. (2006). "Orographic influence on deep convention: case study and sensitivity experiments." Meteorologische Zeitschrift **15**: 215-223.
Dawdy, D. and J. Bergmann (1969). "Effect of rainfall variability on streamflow simulation." Water Resources Research **5**(5): 958-966.
De Lima, J. and V. Singh (2002). "The influence of the pattern of moving rainstorms on overland flow." Advances in Water Resources **25**(7): 817-828.
Di Lazzaro, M. (2009). "Regional analysis of storm hydrographs in the rescaled width function framework." Journal of Hydrology **373**(3): 352-365.
Dodov, B. and E. Foufoula-Georgiou (2005). "Incorporating the spatio-temporal distribution of rainfall and basin geomorphology into nonlinear analyses of streamflow dynamics." Advances in Water Resources **28**(7): 711-728.
Doswell, C. A., H. E. Brooks and R. A. Maddox (1996). "Flash flood forecasting: An ingredients-based methodology." Weather and Forecasting **11**(4): 560-581.
Dunne, T. (1978). "Field studies of hillslope flow processes." Hillslope hydrology **227**: 293.
Ehret, U. and E. Zehe (2011). "Series distance–an intuitive metric to quantify hydrograph similarity in terms of occurrence, amplitude and timing of hydrological events." Hydrology and Earth System Sciences.
Faurès, J. M., D. Goodrich, D. A. Woolhiser and S. Sorooshian (1995). "Impact of small-scale spatial rainfall variability on runoff modeling." Journal of Hydrology **173**(1): 309-326.
Gabellani, S., G. Boni, et al. (2007). "Propagation of uncertainty from rainfall to runoff: A case study with a stochastic rainfall generator." Advances in Water Resources **30**(10): 2061-2071.
Garrote, L. and R. L. Bras (1995). "A distributed model for real-time flood forecasting using digital elevation models." Journal of Hydrology **167**(1): 279-306.
Gaume, E. (2006). "Post flash-flood investigation–methodological note." Floodsite European Research Project, report D **23**.
Gaume, E. and M. Borga (2008). "Post-flood field investigations in upland catchments after major flash floods: proposal of a methodology and illustrations." Journal of flood risk management **1**(4): 175-189.
Gaume, E., M. Livet, M. Desbordes and J. P. Villeneuve (2004). "Hydrological analysis of the river Aude, France, flash flood on 12 and 13 November 1999." Journal of Hydrology **286**(1-4): 135-154.
Giannoni, F., J. A. Smith, Y. Zhang and G. Roth (2003). "Hydrologic modeling of extreme floods using radar rainfall estimates." Advances in Water Resources **26**(2): 195-203.
Goltz, M. N. and P. V. Roberts (1987). "Using the method of moments to analyze three-dimensional diffusion-limited solute transport from temporal and spatial perspectives." Water Resources Research **23**(8): 1575-1585.
Ivanov, V. Y., E. R. Vivoni, R. L. Bras and D. Entekhabi (2004). "Catchment hydrologic response with a fully distributed triangulated irregular network model." Water Resources Research **40**(11): W11102.
Ivanov, V. Y., E. R. Vivoni, R. L. Bras and D. Entekhabi (2004). "Preserving high-resolution surface and rainfall data in operational-scale basin hydrology: a fully-distributed physically-based approach." Journal of Hydrology **298**(1): 80-111.
Jarrett, R. D. and J. F. England Jr (2002). "Reliability of paleostage indicators for paleoflood studies." Ancient Floods, Modern Hazards: Principles and Applications of Paleoflood Hydrology **5**: 91-109.
Javier, J. R. N., J. A. Smith, et al. (2007). "Flash flood forecasting for small urban watersheds in the Baltimore metropolitan region." Weather and Forecasting **22**(6): 1331-1344.
Kirkby, M. (1976). "Tests of the random network model, and its application to basin hydrology." Earth Surface Processes **1**(3): 197-212.
Koren, V., B. Finnerty, et al. (1999). "Scale dependencies of hydrologic models to spatial variability of precipitation." Journal of Hydrology **217**(3): 285-302.
Krajewski, W. F., V. Lakshmi, K. P. Georgakakos and S. C. Jain (1991). "A Monte-Carlo Study of Rainfall Sampling Effect on a Distributed Catchment Model." Water Resources Research **27**(1): 119-128.
Krajewski, W. F. and J. A. Smith (2002). "Radar hydrology: rainfall estimation." Advances in Water Resources **25**(8-12): 1387-1394.
Le Lay, M. and G. M. Saulnier (2007). "Exploring the signature of climate and landscape spatial variabilities in flash flood events: Case of the 8–9 September 2002 Cévennes-Vivarais catastrophic event." Geophysical research letters **34**(13): L13401.
Lee, K. T. and J. K. Huang (2007). "Effect of moving storms on attainment of equilibrium discharge." Hydrological processes **21**(24): 3357-3366.
Lopes, V. L. (1996). "On the effect of uncertainty in spatial distribution of rainfall on catchment modelling." Catena **28**(1-2): 107-119.

Maksimov, V. (1964). "Computing runoff produced by a heavy rainstorm with a moving center." Soviet Hydrology **5**: 510-513.
Marchi, L., M. Borga, E. Preciso and E. Gaume (2010). "Characterisation of selected extreme flash floods in Europe and implications for flood risk management." Journal of Hydrology **394**(1-2): 118-133.
Marchi, L., M. Borga, et al. (2009). "Comprehensive post event survey of a flash flood in Western Slovenia: observation strategy and lessons learned." Hydrological processes **23**(26): 3761-3770.
Marcus, N. (1968). A laboratory and analytical study of surface runoff under moving rainstorms, University of Illinois at Urbana-Champaign.
McDonnell, J. J. and R. Woods (2004). "On the need for catchment classification." Journal of Hydrology **299**(1-2): 2-3.
Merz, R. and G. Bloschl (2003). "A process typology of regional floods." Water Resources Research **39**(12): 1340.
Merz, R. and G. Bloschl (2009). "A regional analysis of event runoff coefficients with respect to climate and catchment characteristics in Austria." Water Resources Research **45**(1): W01405.
Michaelides, K. and J. Wainwright (2002). "Modelling the effects of hillslope–channel coupling on catchment hydrological response." Earth Surface Processes and Landforms **27**(13): 1441-1457.
Michaud, J. and S. Sorooshian (1994). "Comparison of Simple Versus Complex Distributed Runoff Models on a Midsized Semiarid Watershed." Water Resources Research **30**(3): 593-605.
Michaud, J. D. and S. Sorooshian (1994). "Effect of Rainfall-Sampling Errors on Simulations of Desert Flash Floods." Water Resources Research **30**(10): 2765-2775.
Moore, R. (1999). "Real-time flood forecasting systems: Perspectives and prospects." Floods and landslides: Integrated risk assessment: 147-189.
Naden, P. S. (1992). "Spatial Variability in Flood Estimation for Large Catchments - the Exploitation of Channel Network Structure." Hydrological Sciences Journal-Journal Des Sciences Hydrologiques **37**(1): 53-71.
Ngirane-Katashaya, G. and H. Wheater (1985). "Hydrograph sensitivity to storm kinematics." Water Resources Research **21**(3): 337-345.
Nicótina, L., E. Alessi Celegon, A. Rinaldo and M. Marani (2008). "On the impact of rainfall patterns on the hydrologic response." Water Resources Research **44**(12): W12401.
Niemczynowicz, J. (1984). "Investigation of the Influence of Rainfall Movement on Runoff Hydrograph. Part I-Simulation on Conceptual Catchment." Nordic hydrology **15**(2).
Niemczynowicz, J. (1999). "Urban hydrology and water management–present and future challenges." Urban water **1**(1): 1-14.
Nikolopoulos, E. I., E. N. Anagnostou, et al. (2011). "Sensitivity of a mountain basin flash flood to initial wetness condition and rainfall variability." Journal of Hydrology **402**(3): 165-178.
Norbiato, D., M. Borga, et al. (2009). "Controls on event runoff coefficients in the eastern Italian Alps." Journal of Hydrology **375**(3-4): 312-325.
Obled, C., J. Wendling and K. Beven (1994). "The Sensitivity of Hydrological Models to Spatial Rainfall Patterns - an Evaluation Using Observed Data." Journal of Hydrology **159**(1-4): 305-333.
Ogden, F., H. Sharif, et al. (2000). "Hydrologic analysis of the Fort Collins, Colorado, flash flood of 1997." Journal of Hydrology **228**(1): 82-100.
Ogden, F. L. and P. Y. Julien (1993). "Runoff Sensitivity to Temporal and Spatial Rainfall Variability at Runoff Plane and Small Basin Scales." Water Resources Research **29**(8): 2589-2597.
Ogden, F. L., J. R. Richardson and P. Y. Julien (1995). "Similarity in Catchment Response .2. Moving Rainstorms." Water Resources Research **31**(6): 1543-1547.
Ogden, F. L. and B. Saghafian (1997). "Green and Ampt infiltration with redistribution." Journal of Irrigation and Drainage Engineering-Asce **123**(5): 386-393.
Orlanski, I. (1975). "A rational subdivision of scales for atmospheric processes." Bull. Amer. Meteor. Soc **56**(5): 527-530.
Pathiraja, S., S. Westra and A. Sharma (2012). "Why continuous simulation? The role of antecedent moisture in design flood estimation." Water Resources Research **48**(6): W06534.
Pellarin, T., G. Delrieu, et al. (2002). "Hydrologic visibility of weather radar systems operating in mountainous regions: Case study for the Ardèche catchment (France)." Journal of Hydrometeorology **3**(5): 539-555.
Pilgrim, D. H. (1976). "Travel times and nonlinearity of flood runoff from tracer measurements on a small watershed." Water Resources Research **12**(3): 487-496.
Rinaldo, A., G. Botter, et al. (2006). "Transport at basin scales: 1. Theoretical framework." Hydrology and Earth System Sciences Discussions **10**(1): 19-29.
Rinaldo, A., A. Marani and R. Rigon (1991). "Geomorphological Dispersion." Water Resources Research **27**(4): 513-525.
Rinaldo, A., G. K. Vogel, R. Rigon and I. Rodriguez-Iturbe (1995). "Can one gauge the shape of a basin?" Water Resources Research **31**(4): 1119-1127.
Roberts, M. C. and P. C. Klingeman (1970). "The influence of landform and precipitation parameters on flood hydrographs." Journal of Hydrology **11**(4): 393-411.
Robinson, J. S. and M. Sivapalan (1997). "An investigation into the physical causes of scaling and heterogeneity of regional flood frequency." Water Resources Research **33**(5): 1045-1059.

Robinson, J. S. and M. Sivapalan (1997). "Temporal scales and hydrological regimes: Implications for flood frequency scaling." Water Resources Research **33**(12): 2981-2999.
Robinson, J. S., M. Sivapalan and J. D. Snell (1995). "On the relative roles of hillslope processes, channel routing, and network geomorphology in the hydrologic response of natural catchments." Water Resources Research **31**(12): 3089-3101.
Rodriguez-Iturbe, I. and J. B. Valdes (1979). "The geomorphologic structure of hydrologic response." Wat. Resour. Res **15**(6): 1409-1420.
Rusjan, S., M. Kobold and M. Mikoš (2009). "Characteristics of the extreme rainfall event and consequent flash floods in W Slovenia in September 2007." Natural Hazards and Earth System Sciences **9**(3): 947-956.
Saco, P. M. and P. Kumar (2002). "Kinematic dispersion in stream networks - 1. Coupling hydraulic and network geometry." Water Resources Research **38**(11): 1244.
Saco, P. M. and P. Kumar (2004). "Kinematic dispersion effects of hillslope velocities." Water Resources Research **40**(1): W01301.
Sangati, M. (2009). "Flash flood analysis and modelling in mountain regions." PhD thesis available at: http://paduaresearch.cab.unipd.it/1686/.
Sangati, M. and M. Borga (2009). "Influence of rainfall spatial resolution on flash flood modelling." Nat. Hazards Earth Syst. Sci **9**: 575-584.
Sangati, M., M. Borga, D. Rabuffetti and R. Bechini (2009). "Influence of rainfall and soil properties spatial aggregation on extreme flash flood response modelling: an evaluation based on the Sesia river basin, North Western Italy." Advances in Water Resources **32**(7): 1090-1106.
Savenije, H. (2009). "HESS Opinions" The art of hydrology"." Hydrology and Earth System Sciences **13**(2): 157.
Schuurmans, J. M. and M. F. P. Bierkens (2007). "Effect of spatial distribution of daily rainfall on interior catchment response of a distributed hydrological model." Hydrology and Earth System Sciences **11**(2): 677-693.
Segond, M. L., H. S. Wheater and C. Onof (2007). "The significance of spatial rainfall representation for flood runoff estimation: A numerical evaluation based on the Lee catchment, UK." Journal of Hydrology **347**(1-2): 116-131.
Seo, Y., A. R. Schmidt and M. Sivapalan (2012). "Effect of storm movement on flood peaks: Analysis framework based on characteristic timescales." Water Resources Research **48**(5): W05532.
Shah, S., P. O'Connell and J. Hosking (1996). "Modelling the effects of spatial variability in rainfall on catchment response. 1. Formulation and calibration of a stochastic rainfall field model." Journal of Hydrology **175**(1): 67-88.
Singh, V. (2002). "Effect of the duration and direction of storm movement on infiltrating planar flow with full areal coverage." Hydrological processes **16**(7): 1479-1511.
Singh, V. P. (1998). "Effect of the direction of storm movement on planar flow." Hydrological processes **12**(1): 147-170.
Sivapalan, M., K. Beven and E. F. Wood (1987). "On Hydrologic Similarity." Water Resources Research **23**(12): 2266-2278.
Sivapalan, M., K. Takeuchi, et al. (2003). "IAHS Decade on Predictions in Ungauged Basins (PUB), 2003–2012: Shaping an exciting future for the hydrological sciences." Hydrological Sciences Journal **48**(6): 857-880.
Skøien, J. and G. Blöschl (2006). "Catchments as space-time filters? a joint spatio-temporal geostatistical analysis of runoff and precipitation." Hydrology and Earth System Sciences Discussions **3**(3): 941-985.
Skųien, J., G. Bloschl and A. Western (2003). "Characteristic space scales and timescales in hydrology." Water Resour. Res **39**(10): 1304.
Smith, J. A., M. L. Baeck, et al. (2005). "Field studies of the storm event hydrologic response in an urbanizing watershed." Water Resources Research **41**(10): W10413.
Smith, J. A., M. L. Baeck, J. E. Morrison and P. Sturdevant-Rees (2000). "Catastrophic rainfall and flooding in Texas." Journal of Hydrometeorology **1**(1): 5-25.
Smith, J. A., M. L. Baeck, et al. (2002). "The regional hydrology of extreme floods in an urbanizing drainage basin." Journal of Hydrometeorology **3**(3): 267-282.
Smith, M. B., V. I. Koren, et al. (2004). "Runoff response to spatial variability in precipitation: an analysis of observed data." Journal of Hydrology **298**(1-4): 267-286.
Smith, M. B., D. J. Seo, et al. (2004). "The distributed model intercomparison project (DMIP): motivation and experiment design." Journal of Hydrology **298**(1-4): 4-26.
Snell, J. D. and M. Sivapalan (1994). "On Geomorphological Dispersion in Natural Catchments and the Geomorphological Unit-Hydrograph." Water Resources Research **30**(7): 2311-2323.
Sturdevant-Rees, P., J. A. Smith, J. Morrison and M. L. Baeck (2001). "Tropical storms and the flood hydrology of the central Appalachians." Water Resources Research **37**(8): 2143-2168.
Surkan, A. (1974). "Simulation of storm velocity effects on flow from distributed channel networks." Water Resources Research **10**(6): 1149-1160.
Syed, K. H., D. C. Goodrich, D. E. Myers and S. Sorooshian (2003). "Spatial characteristics of thunderstorm rainfall fields and their relation to runoff." Journal of Hydrology **271**(1-4): 1-21.
Thorsteinsson, P. B. (2010). "On the classification and estimation of costs in information technology."
Tropeano, D., L. Turconi and S. Sanna (2004). "Debris flow triggered by the 29 August 2003 cloudburst in Val Canale, eastern Italian Alps." Proceedings International Symposium INTERPRAEVENT 2004, Riva del Garda, Italy: 121-132.

Viglione, A., G. B. Chirico, et al. (2010). "Quantifying space-time dynamics of flood event types." Journal of Hydrology **394**(1-2): 213-229.
Viglione, A., G. B. Chirico, R. Woods and G. Blöschl (2010). "Generalised synthesis of space–time variability in flood response: An analytical framework." Journal of Hydrology **394**(1): 198-212.
Vivoni, E., D. Entekhabi, R. Bras and V. Ivanov (2007). "Controls on runoff generation and scale-dependence in a distributed hydrologic model." Hydrology and Earth System Sciences Discussions Discussions **4**(3): 983-1029.
Vivoni, E. R., V. Y. Ivanov, R. L. Bras and D. Entekhabi (2004). "Generation of triangulated irregular networks based on hydrological similarity." Journal of Hydrologic Engineering **9**(4): 288-302.
Western, A. W., G. Blöschl and R. B. Grayson (2001). "Toward capturing hydrologically significant connectivity in spatial patterns." Water Resources Research **37**(1): 83-97.
Wilson, J. W., N. A. Crook, et al. (1998). "Nowcasting thunderstorms: A status report." Bulletin of the American Meteorological Society **79**(10): 2079-2099.
Winchell, M., H. V. Gupta and S. Sorooshian (1998). "On the simulation of infiltration- and saturation-excess runoff using radar-based rainfall estimates: Effects of algorithm uncertainty and pixel aggregation." Water Resources Research **34**(10): 2655-2670.
Wood, E. F., M. Sivapalan, K. Beven and L. Band (1988). "Effects of Spatial Variability and Scale with Implications to Hydrologic Modeling." Journal of Hydrology **102**(1-4): 29-47.
Wooding, R. A. (1965). "A hydraulic model for the catchment-stream problem: I. Kinematic-wave theory." Journal of Hydrology **3**(3): 254-267.
Woods, R. and M. Sivapalan (1999). "A synthesis of space-time variability in storm response: Rainfall, runoff generation, and routing." Water Resources Research **35**(8): 2469-2485.
Woods, R. A. (1997). A search for fundamental scales in runoff generation: combined field and modelling approach, University of Western Australia, Nedlans.
Yen, B. and K. T. Lee (1997). "Unit Hydrograph Derivation for Ungauged Watersheds by Stream-Order Laws." Journal of Hydrologic Engineering **2**(1): 1-9.
Zanon, F., M. Borga, et al. (2010). "Hydrological analysis of a flash flood across a climatic and geologic gradient The September 18, 2007 event in Western Slovenia." Journal of Hydrology **394**(1-2): 182-197.
Zhang, Y., J. A. Smith and M. L. Baeck (2001). "The hydrology and hydrometeorology of extreme floods in the Great Plains of Eastern Nebraska." Advances in Water Resources **24**(9-10): 1037-1049.
Zoccatelli, D., M. Borga, et al. (2011). "Spatial moments of catchment rainfall: rainfall spatial organisation, basin morphology, and flood response." Hydrology and Earth System Sciences **15**(12): 3767-3783.
Zoccatelli, D., M. Borga, et al. (2010). "Which rainfall spatial information for flash flood response modelling? A numerical investigation based on data from the Carpathian range, Romania." Journal of Hydrology **394**(1-2): 148-161.

APPENDIX A

We are here deriving equations 4.10 and 4.14. of this work using eq. 19, 23 and 25 of Viglione *et al.* (2010).

Derivation of Equation 4.10

Equation 19 in V2010 (called eq. V19 hereinafter) describes the routing time from the center of mass of rainfall excess to the catchment outlet. We can write V19 using the notation and the assumptions presented in this work as:

$$E(T_c) = \frac{g_1}{v} + \frac{cov_{x,y}[d(x,y),r_t(x,y)]}{vP_0} \quad \text{(A1)}$$

Where $cov_{x,y}$ identifies the spatial covariance above the catchment, and can be written as:

$$E(T_c) = \frac{g_1}{v} + \frac{\int_A d(x,y) r_t(x,y) dA}{vP_0} - \frac{g_1}{v} = \frac{P_1}{P_0 v} = \frac{\Delta_1 g_1}{v} \quad \text{(A2)}$$

Derivation of Equation 4.14

Equation 23 in V2010 (called eq. V23 hereinafter) describes the variance of routing times from the the center of mass of rainfall excess to the catchment outlet. We can write V23 using the notation and the assumptions presented in this work as:

$$var(T_c) = \frac{g_2 - g_1^2}{v^2} + \frac{cov_{x,y}[d(x,y)^2, r_t(x,y)]}{v^2 P_0} - \frac{cov_{x,y}[d(x,y), r_t(x,y)]}{vP_0}\left[\frac{2g_1}{v} + \right. \quad \text{(A3)}$$

$$covx,ydx,y,rtx,yvP0$$

From A3 we can derive eq. 4.14 as follows:

$$var(T_c) = \frac{g_2 - g_1^2}{v^2} + \frac{\int_A d(x,y)^2 r_t(x,y) dA}{Av^2 P_0} - \frac{g_2}{v} - \left(\frac{P_1}{P_0 v} - \frac{g_1}{v}\right)\left(\frac{P_1}{P_0 v} + \frac{g_1}{v}\right) = \quad \text{(A4)}$$

$$\left(\frac{P_2}{P_0} - \frac{P_1^2}{P_0^2}\right)\frac{1}{v^2} = \frac{\Delta_2}{v^2}(g_2 - g_1^2)$$

Derivation of Equation 4.16

Equation 25 in V2010 (called eq. V25 hereinafter) describes the covariance between the spatial distribution of routing times and the temporal distribution of rainfall over the basin. We can write V25 using the notation and the assumptions presented in this work as:

$$cov(T_r, T_c) = \frac{cov_t\left[T, cov_{x,y}[d(x,y), r_t(x,y)]\right]}{vP_0} - \frac{cov_t[T, p_0(t)]}{P_0}\frac{cov_{x,y}[d(x,y), r_t(x,y)]}{vP_0} \quad \text{(A5)}$$

Where cov_t is the temporal covariance. From A5 we can derive eq. 4.16 as follows:

$$cov(T_r, T_c) = g_1 \frac{cov_t[T, \delta_1(t)w(t)]}{v} - g_1 \frac{cov_t[T, w(t)]}{v} - \frac{cov_t[T, w(t)]}{v} \frac{cov_{x,y}[D, P(x,y)]}{P_0} \quad \text{(A6)}$$

$$= g_1 \frac{cov_t[T, \delta_1(t)w(t)]}{v} - \frac{cov_t[T, w(t)]}{v} (g_1 + \Delta_1 g_1 - g_1)$$

$$= g_1 \left\{ \frac{cov_t[T, \delta_1(t)w(t)]}{v} - \frac{cov_t[T, w(t)]}{v} \Delta_1 \right\}$$

APPENDIX B

We report here the calculation of the mean and variance for a trapezoidal distribution as presented in Thorsteinsson (2010).

A trapezoidal distribution A is defined on the interval $[a_1, a_2]$. It has a flat segment on the interval $[b_1, b_2]$. Trapezoidal distribution can be denoted by:

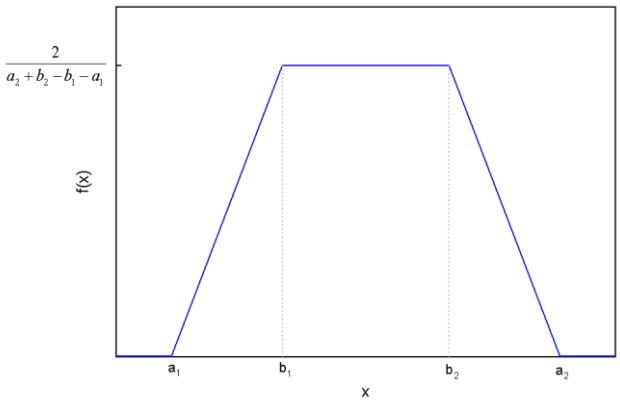

Fig. B1: Trapezoidal probability density function

$$A = (a_1, b_1, b_2, a_2) \tag{B1}$$

The trapezoidal probability density function takes the value $2/(a_2 - a_1 + b_2 - b_1)$ on the interval $[b_1, b_2]$, which is the flat segment.

The formula for the trapezoidal probability density function is:

$$f(x|a_1, b_1, b_2, a_2) = \begin{cases} \frac{2}{b_2+a_2-a_1-b_1}\frac{1}{b_1-a_1}(x-a_1), & a_1 \le x < b_1 \\ \frac{2}{b_2+a_2-a_1-b_1}, & b_1 \le x < b_2 \\ \frac{2}{b_2+a_2-a_1-b_1}\frac{1}{a_2-b_2}(a_2-x), & b_2 \le x \le a_2 \\ 0, & otherwise \end{cases} \tag{B2}$$

The mean μ and variance σ^2 of the trapezoidal distribution are:

$$\mu = \frac{[(b_2+a_2)^2 - b_2a_2] - [(b_1+a_1)^2 - a_1b_1]}{3(b_2+a_2-a_1-b_1)} \tag{B3}$$

$$\sigma^2 = \frac{(b_2^2+a_2^2)(b_2+a_2) - (a_1^2+b_1^2)(a_1+b_1)}{6(b_2+a_2-a_1-b_1)} - \mu^2$$